SYNTHESIS AND CHARACTERIZATION OF HYBRID ORGANIC COATING SYSTEM TO REDUCE THERMAL DEGRADATION OF SOLAR CELLS

FARAH KHALEDA BINTI MOHD ZAINI

INSTITUTE FOR ADVANCED STUDIES
UNIVERSITY OF MALAYA
KUALA LUMPUR

2020

University of Malaya

SYNTHESIS AND CHARACTERIZATION OF HYBRID ORGANIC COATING SYSTEM TO REDUCE THERMAL DEGRADATION OF SOLAR CELLS

FARAH KHALEDA BINTI MOHD ZAINI

DISSERTATION SUBMITTED IN FULFILMENT OF
THE REQUIREMENTS FOR THE DEGREE OF MASTER
OF PHILOSOPHY

INSTITUTE FOR ADVANCED STUDIES
UNIVERSITY OF MALAYA
KUALA LUMPUR

2020

University of Malaya

UNIVERSITY OF MALAYA
ORIGINAL LITERARY WORK DECLARATION

Name of Candidate: Farah Khaleda binti Mohd Zaini

Matric No: HGF150011

Name of Degree: Master of Philosophy

Title of Dissertation ("this Work"): Synthesis and Characterization of Hybrid Organic Coating System to Reduce Thermal Degradation of Solar Cells

Field of Study: Renewable Energy (Solar Energy)

I do solemnly and sincerely declare that:

(1) I am the sole author/writer of this Work;
(2) This Work is original;
(3) Any use of any work in which copyright exists was done by way of fair dealing and for permitted purposes and any excerpt or extract from, or reference to or reproduction of any copyright work has been disclosed expressly and sufficiently and the title of the Work and its authorship have been acknowledged in this Work;
(4) I do not have any actual knowledge nor do I ought reasonably to know that the making of this work constitutes an infringement of any copyright work;
(5) I hereby assign all and every right in the copyright to this Work to the University of Malaya ("UM"), who henceforth shall be owner of the copyright in this Work and that any reproduction or use in any form or by any means whatsoever is prohibited without the written consent of UM having been first had and obtained;
(6) I am fully aware that if in the course of making this Work I have infringed any copyright whether intentionally or otherwise, I may be subject to legal action or any other action as may be determined by UM.

Candidate's Signature Date:

Subscribed and solemnly declared before,

Witness's Signature Date:

Name:

Designation:

University of Malaya

Synthesis and Characterization of Hybrid Organic Coating System to Reduce Thermal Degradation of Solar Cells

ABSTRACT

Thermal-decreasing hybrid organic coatings were developed for crystalline solar cells by using two types of binder systems; namely Aminopropyltriethoxysolution (APTES) / Methyltrimethoxysilane (MTMS) binder system (labelled as B1) and Methyltrimethoxysilane (MTMS) / nitric acid (HNO_3) binder system (labelled as B2). Three types of nanoparticles; Titanium dioxide, TiO_2 (Anatase), Zinc oxide, ZnO and Tin dioxide, SnO_2 nanoparticles with different weight percentage were introduced inside each binder system namely; 20 wt%, TiO_2 (T1B1 coating), 60 wt% TiO_2 (T2B1 coating), 20 wt% ZnO (Z1B1 coating), 60 wt% ZnO (T2B1 coating), 20 wt% SnO_2 (S1B1 coating) and 60 wt% SnO_2 (S2B1 coating) for B1 binder system and 20 wt%, TiO_2 (T1B2 coating), 60 wt% TiO_2 (T2B2 coating), 20 wt% ZnO (Z1B2 coating), 60 wt% ZnO (Z2B2 coating), 20 wt% SnO_2 (S1B2 coating) and 60 wt% SnO_2 (S2B2 coating) for B2 binder system. This work highlights the effects of nanoparticle coating systems on the surface temperature of solar cells along with several structural and electrical studies. It is found that B1 coating systems showed a better performance in decreasing the surface temperature of solar cells compared to B2 coating systems. The introduction of nanoparticles inside the binder systems further reduced the surface temperature of solar cells from 55.75 °C (non-coated solar cell) at 60th minute of exposure under standard test condition (STD) of 1000 W/m^2 irradiation and room temperature of 25°C. Under the same condition, S1B1 nanoparticle coating records the lowest temperature of 42.66°C for B1 binder system and Z1B2 coating system records a reduced temperature of 48.82°C for B2 binder system. Furthermore, the fill factor of solar cells was also improved by approximately 0.1 or 16.67% with binder coating systems (B1 and B2 coating systems)

University of Malaya

and about 0.2 or 33.33% with nanoparticle coating systems (T1B1, T2B1, Z1B1, T2B1, S1B1, S2B1, T1B2, T2B2, Z1B2, Z2B2, S1B2, S2B2 coating systems).

Keywords: Solar cell, silicon, nanoparticles coatings, temperature, fill factor

University of Malaya

Sintesis dan Pencirian Sistem Salutan Organik Hibrid bagi Mengurangkan Degradasi Termal Sel Solar

ABSTRAK

Tiga Salutan hibrida kekurangan haba organik telah dikajikan untuk sel solar kristal dengan menggunakan dua jenis sistem bahan pengikat; iaitu sistem pengikat Aminopropyltriethoxysolution (APTES) / Methyltrimethoxysilane (MTMS) (bertanda sebagai B1) dan sistem pengikat Methyltrimethoxysilane (MTMS) / asid nitrik (HNO_3) (dilabelkan sebagai B2). Tiga jenis nanopartikel; Titanium dioksida, TiO_2 (Anatase), Zink oksida, ZnO dan Tin dioksida, SnO_2 nanopartikel dengan peratusan berat yang berbeza diperkenalkan di dalam setiap sistem pengikat iaitu; 20 wt%, TiO_2 (salutan T1B1), 60 wt% TiO_2 (salutan T2B1), 20 wt% ZnO (salutan Z1B1), 60 wt% ZnO (salutan Z2B1), 20 wt% SnO_2 (salutan S1B1) dan 60 wt% SnO_2 (Salutan S2B1) untuk sistem pengikat B1 dan 20 wt% TiO_2 (salutan T1B2), 60% TiO_2 (salutan T2B2), 20 wt% ZnO (salutan Z1B2), 60 wt% ZnO (salutan Z2B2), 20 wt% SnO_2 (salutan S1B2) dan 60 wt% SnO_2 (salutan S2B2) untuk sistem pengikat B2. Kerja ini menyerlahkan kesan sistem salutan nanopartikel pada suhu permukaan sel suria bersama dengan beberapa kajian struktur dan elektrik yang lain. Kajian mendapati bahawa sistem salutan B1 menggambarkan prestasi yang lebih baik dalam mengurangkan suhu permukaan sel solar berbanding dengan sistem salutan B2. Pengenalan nanopartikel di dalam sistem pengikat terus mengurangkan suhu permukaan sel solar daripada 55.75 ° C (sel suria tidak bersalut) pada minit ke-60 setelah didedahkan di bawah penyinaran keadaan ujian standard (STD) 1000 W / m^2 dan suhu bilik 25 ° C. Dalam keadaan yang sama, salutan nanopartikel S1B1 merekodkan suhu terendah 42.66 ° C untuk sistem pengikat B1 dan sistem salutan Z1B2 merekodkan suhu berkurang pada 48.82 ° C untuk sistem pengikat B2. Selain itu, faktor pengisian sel suria juga meningkat sebanyak kira-kira 0.1 atau 16.67% dengan sistem salutan pengikat (sistem salutan B1 dan B2) dan kira-kira 0.2 atau 33.33% dengan sistem lapisan

University of Malaya

nanopartikel (T1B1, T2B1, Z1B1, T2B1, S1B1, S2B1, Sistem salutan T1B2, T2B2, Z1B2, Z2B2, S1B2, S2B2).

Kata kunci: sel suria, silikon, salutan nanopartikel, suhu, faktor pengisi

University of Malaya

ACKNOWLEDGEMENTS

Firstly, I would like to express my sincere gratitude to God for giving me the patience and perseverance to complete my research beautifully. Not to forget my supervisor and also advisor, Prof. Ir. Dr. Nasrudin Abdul Rahim for the continuous support of my study and for his patience, motivation, and immense knowledge. His guidance helped me in my direction of research. I could not have imagined having a better advisor and mentor for my MPhil. works.

Besides my supervisor, I would like to thank the rest of my thesis committee: Dr Vengadaesvaran Balakrisnan, Dr Adarsh Kumar Pandey, and Amirul Syafiq, for their insightful comments and encouragement. A special thanks to Dr Vengadaesvaran for his time and effort towards perfecting my research work, checking my progress from time to time as well as checking my thesis line by line for many days.

My sincere thanks also goes to Dr. Saipul, Dr. Azimah, and Dr.Akmaliah, who helped me a lot to progress in area of materials research. Besides supporting me during the solar simulation training, they gave a lot of useful advises and support during CEAT 2018 conference that I have participated as a presenter.

I thank my fellow labmates and my friends in UMPEDAC for their continuous support which keeps me going. In particular, I am grateful to Dr. Che Han Seng for helping and enlightening me on many things towards completing my first paper.

Last but not the least, I would like to thank my family, especially my father, Mohd Zaini bin Yunus and my mother, Suhaiza binti Hamid Khan, for the endless trust and motivation, and always be there to listen to my ups and downs stories throughout my research and my life in general.

University of Malaya

TABLE OF CONTENTS

University of Malaya

University of Malaya

University of Malaya

LIST OF FIGURES

University of Malaya

University of Malaya

University of Malaya

University of Malaya

LIST OF TABLES

University of Malaya

LIST OF SYMBOLS AND ABBREVIATIONS

E_{gap}	:	Bandgap energy
$R_{specular,solar}$	:	Specular reflectance of spectral
R_s	:	S-polarization reflection coefficient
R_p	:	P-polarization reflection coefficients
T_s	:	Transmission coefficients for s-polarization
T_p	:	Transmission coefficients for p-polarization
I_{sc}	:	Short-circuit current
V_{oc}	:	Open-circuit voltage
J_{sc}	:	Current density
E_P	:	Energy of the photons
n	:	Number of charge carriers
I	:	Light that passes through sample
I_o	:	Incident intensity
dT	:	Temperature difference
E_S	:	Seebeck voltage
ZnO	:	Zinc Oxide
TiO_2	:	Titanium dioxide
SnO_2	:	Tin dioxide
HNO_3	:	Nitric acid

University of Malaya

Abbreviations and acronyms:

PCE	:	Power conversion efficiency
PV	:	Photovoltaic
APE	:	Average photon energy
SSIM	:	Solar spectral irradiance meter
DNI	:	Direct normal irradiance
AM	:	Air mass
R	:	Reflectance
T	:	Transmittance
UV	:	Ultraviolet
IR	:	Infrared
FF	:	Fill factor
STPV	:	Solar thermophotovoltaic
TPV	:	Thermophotovoltaic
ARC	:	Anti-reflection coating
PECVD	:	Plasma enhanced chemical vapor deposition
PSC	:	Perovskite solar cells
NCA	:	Nanocone array
JCPDS	:	Joint Committee on Powder Diffraction Standards
APTES	:	Aminopropyltriethoxysilane
MTMS	:	Methyltrimethoxysilane
FESEM	:	Field emission scanning electron microscopy
EDX	:	Energy Dispersive X-ray Spectroscopy
CA	:	Contact angle
FTIR	:	Fourier Transform Infrared Spectroscopy

University of Malaya

XRD : X-ray diffraction

Greek symbols

θ_i : Angle of incidence

θ_t : Angle of refraction

Ɵ : Contact angle

α : The coefficient of proportionality

University of Malaya

CHAPTER 1: INTRODUCTION

1.1 Introduction

The pressing need for carbon-free energy and high energy demand for sustainable development paved the way for the diffusion and deployment of renewable technologies. It is said that solar energy is the most abundant renewable energy available and not to mention, the cleanest. While conventional sources of energy such as petroleum, coal and natural gas are being depleted, scientists are searching for the solutions on ways to meet the ever-increasing energy demands and solar energy the most promising renewable energy source. As of now, there are two main techniques that generate electricity from solar energy namely, solar thermal and photovoltaic (PV). Solar cells due to their simplicity in operation and maintenance have attracted a number of researchers to improve the performance and operability of solar panels. Various approaches have been tried to improve the conversion efficiency and reduce the manufacturing cost. Besides its manufacturing and installation cost (H Aberlin & Eppel, 2012), there are various factors such as shading, availability of sunlight, heat, humidity (Visoly-Fisher et al., 2003) and others which affects its efficiency. After applying a number of modifications on the PVs , the highest reported efficiency is 46% which is achieved through multi-junction silicon based solar cell (Green et al., 2017). Over the past few years, power conversion efficiency (PCE) has been reported to be steadily improving as shown as Figure 1.1 below.

University of Malaya

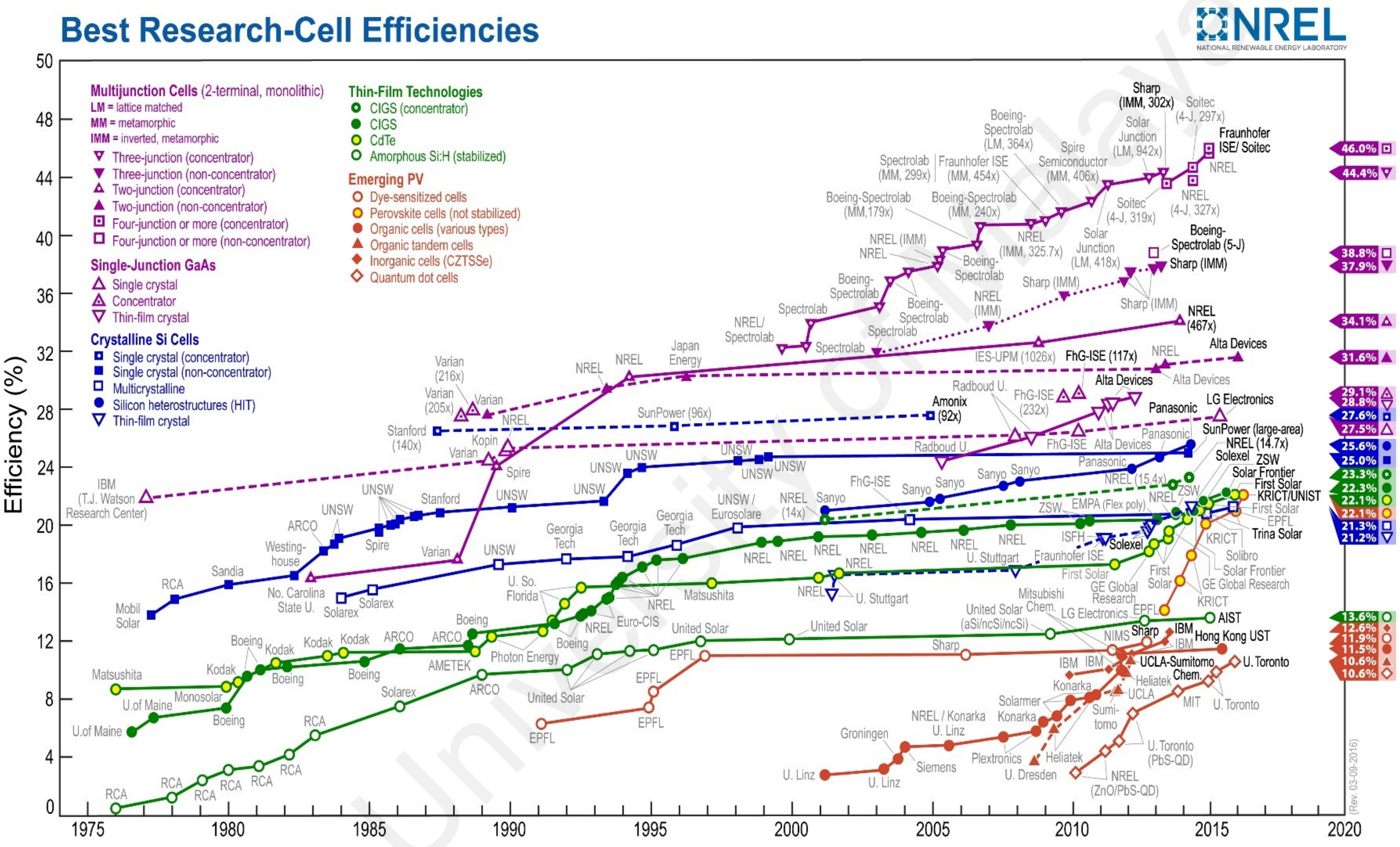

University of Malaya

Figure 1.1: The efficiency of different types of solar devices over time (M. S. Ahmad, Pandey, & Rahim, 2017; Green, Emery, Hishikawa, Warta, & Dunlop, 2015a; Pandey et al., 2016)

1.2 Fundamental aspects

There are many aspects that need to be taken into account, specifically the spectral distribution of the total radiation. Only some wavelengths in the spectrum contributes to the efficiency and lifetime of photovoltaic devices. In this section, some important measurement quantities are outlined for the purpose of determining the concept of experiment and properties of materials for reducing the surface temperature of solar cells without affecting their efficiencies or better, improving them.

1.2.1 Light conversion process

A photovoltaic solar cells work like a semiconductor diode where the material of semiconductor absorbs the incident photons and turn them into electron-hole pairs or excitons (Shah, Torres, Tscharner, Wyrsch, & Keppner, 1999). Those excitons exploit photovoltaic effect which exists at semiconductor junctions (Smestad, 1998; Zweibel & Singh, 1993). With the correct wavelength of an incident photon with energy more than the bandgap's energy (E_{gap}), an electron from valence band can be excited to conduction band, leaving a hole in the valence band. For that stage, due to uneven distribution of charge carriers (Neville, 1995), it leads to the formation of forward bias by in-built voltage that sweeps away these carriers from across p-n junction forming as the basic feature of PV energy conversion as shown in Figure 1.2.

University of Malaya

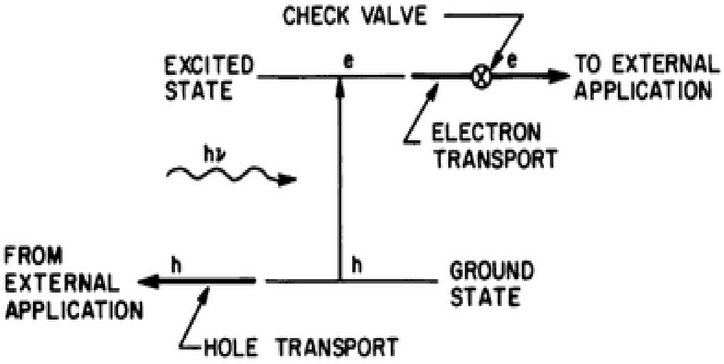

Figure 1.2: Basic characteristic of PV energy conversion (Fonash, 2012)

The check valve as in the Figure 1.2 is to prevent back flow of excited photogenerated electrons and recombine (Fonash, 2012). As further note, no photons with energy below than the E_{gap} can excite the electrons to the conduction band. Nevertheless, due to thermalization, excess energy will be lost rapidly during the process (Shah et al., 1999). Eventually, at some point, some electrons from the conduction band will lose energy and go back to recombine with a hole in the valence band which is known as recombination.

1.2.2 Source spectrum

Solar spectrum gives crucial influence on photovoltaic performance which affects it terms of its temporal and geographic conditions (Tatsiankou et al., 2016). The right amount of light source is important to ensure the optimum conversion efficiency is achieved. This relates to the distribution of solar irradiance with an average photon energy (APE) at the site and affects the amount of electrical energy loss to spectral mismatch of a device over its lifetime(Reynolds & Smirnov, 2015). This means different sites or places have different solar spectrum or solar irradiance which in return, affects for the performance of solar cell. It is however difficult to decouple several variables such as

University of Malaya

temperature, APE, irradiance, light-induced degradation and annealing cycles for spectral matching studies (Reynolds & Smirnov, 2015; Alessandro Virtuani & Fanni, 2014). Nonetheless, for the outdoor applications or standard test conditions, the standard global AM 1.5G spectrum is used as reported by several researchers (He et al., 2012; Liang et al., 2010; Peet et al., 2007). A device such as solar spectral irradiance meter (SSIM) is also useful to measure direct normal irradiance (DNI) in several wavelength bands (Tatsiankou et al., 2016). Combining with certain models, the resulting spectral irradiance distribution as well as the key atmospheric transmittances under all sky conditions can be obtained.

On the other hand, there is no standardize light source for indoor application as mentioned by Minnaert et al. (Minnaert & Veelaert, 2014). That is the reason why Minnaert et al. (Minnaert & Veelaert, 2014) designed an experiment and suggests a proposal to characterize indoor light sources in different categories. As such, different types of solar technologies respond to those fluctuations differently. It is said that multi junction solar devices are more influenced by the change in solar spectral compared to single junction devices (Tatsiankou et al., 2016).

Zero air mass radiation spectrum of spectral distribution is referred to as Air Mass Zero (AM0), whereby the Air Mass is the measure of the absorption in the atmosphere that affects the intensity of solar radiation and their spectral content that reaches the surface of the Earth. The Air Mass (AM) calculation is given by Equation 1.1:

$$\text{AM} = {}^{1}/_{\cos \Theta} \qquad (1.1)$$

University of Malaya

1.2.3 Reflectance and transmittance

The reflection is a process where a portion of the radiant flux from incident rays on a surface is being returned back into the same hemisphere which contains incident radiation (Palmer, 1995). Hence, the spectral reflectance can be defined as the ratio of the reflected radiant flux over the incident radiant flux (Palmer, 1995). It is a fraction of light reflected from a surface as a function of wavelength. Anti-reflective coating or film plays an important role in reducing the reflection of sunlight from solar cells as well as increasing the light coupling into active region of PV devices, leading to its efficiency (Lee, Ruby, Peters, McKenzie, & Hsu, 2008). Reflectance can be measured with instruments such as reflectance spectrometry. However, effects such as particle size, scatter and multi-collinearity affects the performance in reflectance spectrometry diffusion (Barnes, Dhanoa, & Lister, 1989).

Figure 1.3 shows the specular reflectance of spectral, $R_{specular,solar}$ at incident angle of 15° of five solar reflective materials samples. As can be seen from Figure 1.3, aluminized aluminum sheet (AlSheet) has the lowest reflectance of 0.860 while silvered sheet (AgSheet#2) achieved the highest reflectance of 0.948 as compared to others (AgGlass4mm, AgFilm#1 and AlFilm) in the wavelength range between 0 to 2500 nm (Good et al., 2016).

University of Malaya

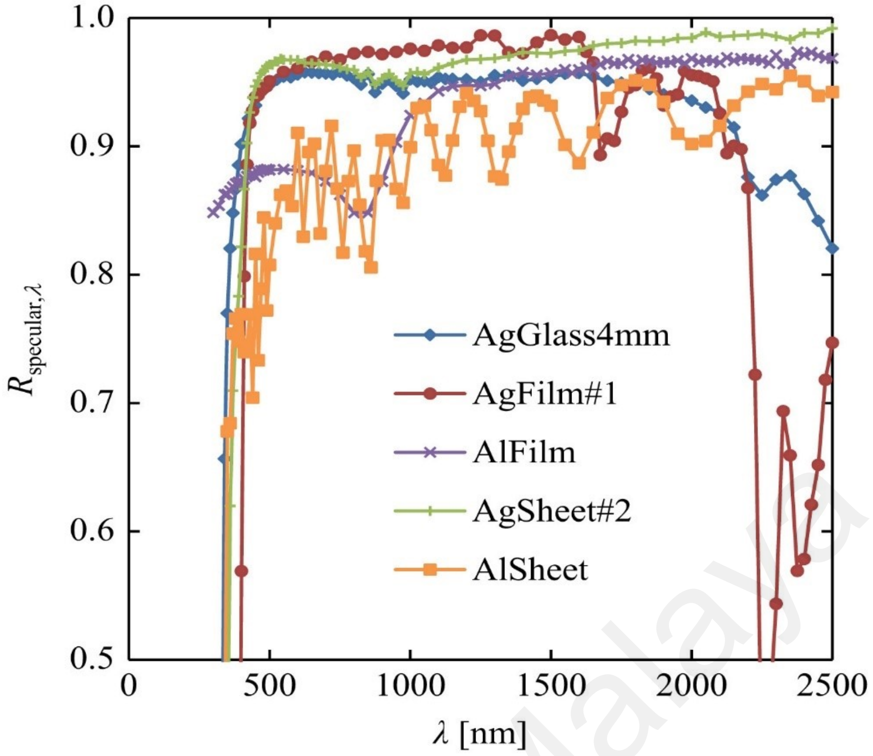

Figure 1.3: Specular reflectance spectra of back-silvered glass, silvered and aluminized polymer films, and silvered and aluminized aluminum sheets (Good et al., 2016)

University of Malaya

Similarly, the transmittance is defined as the ratio of solar energy falling on a cell that transmitted through it. It is the ratio of transmitted light intensity to the incident light intensity (Y.-C. Jiang, Liu, Zhang, & Kong, 2015). In a case where all light pass through a cell without any absorption, it is said that the absorbance is zero, and the transmittance is 100%. Besides reflectance, light intensity can be multiplied by transmittance at a given wavelength to determine the radiant energy (Palmer, 1995; Woolley, 1971). Filter with spectrally varying optical properties has better transmittance as compared to normal clear glasses which has flat transmittance (Gueymard, 2009). Figure 1.4 indicates the optical transmission indicates the optical transmission curve of $NiCO_2O_4$ films under various gas atmospheres.

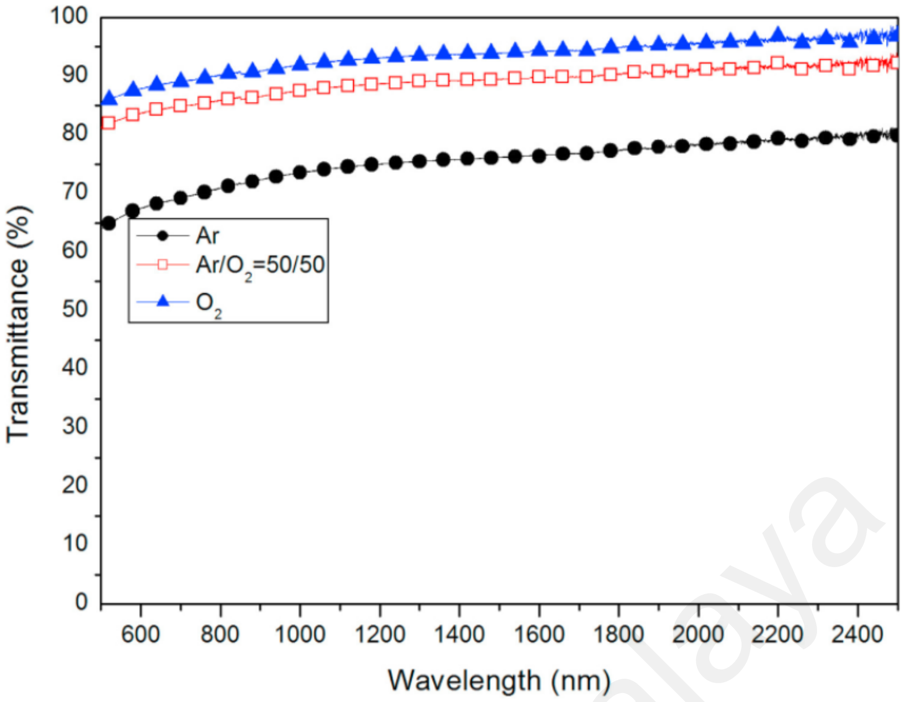

Figure 1.4: Optical transmittance for $NiCO_2O_4$ films under influence of different gasses at 300°C (Tsai, Ni, & Fung, 2017)

Observing from Figure 1.4, in the wavelength range of 600 to 2400 nm, the highest optical transmittance of light is displayed by the $NiCo_2O_4$ thin film deposition in the oxygen ambient atmosphere (O_2) which is approximately 90%. This proves that the oxygen ambient atmosphere leads to a remarkable improvement of the transmittance of the infrared $NiCo_2O_4$ films. According to the law of conservation of energy, the sum of the reflection coefficient (R) and the transmission coefficient (T) is (Born & Wolf, 2013; le Reinders, Verlinden, & Freundlich, 2017) given in Equation 1.2:

$$R + T = 1 \qquad (1.2)$$

Depending on the polarization of the irradiance, whether it is perpendicular or parallel to the plane, the values of R and T can be determined (Born & Wolf, 2013). S-polarization happens when the vector of electric field is perpendicular to the plane that contains the

University of Malaya

incident irradiance, both refracted and reflected. In this case, the reflection coefficient denotes by R$_s$. On the other hand, for the case where the vector of the electric field is in line with the incident plane, it is called p-polarization (R$_p$). By using the law of conservation of energy, their respective transmission coefficients can be calculated from Equation 1.3 and Equation 1.4 (le Reinders et al., 2017).

$$R_s + T_s = 1 \tag{1.3}$$

$$R_p + T_p = 1 \tag{1.4}$$

where T_s and T_p are transmission coefficients for s-polarization and p-polarization respectively. From Fresnel's equations, R$_s$ and R$_p$ can be determined as shown in Equation 1.5 to Equation 1.8 (Valenzuela, 1978). They are often used to determine the values of reflectance and transmittance at the interface between two mediums with different refractive indexes at various incident angles (le Reinders et al., 2017) (Hecht, 2002):

$$R_s = [\frac{\sin(\theta_t - \theta_i)}{\sin(\theta_t + \theta_i)}] = [\frac{n_1\cos(\theta_i) - n_2\cos(\theta_t)}{n_1\cos(\theta_i) + n_2\cos(\theta_t)}]^2 \tag{1.5}$$

$$R_s = [\frac{n_1\cos(\theta_i) - n_2\sqrt{1 - (\frac{n_1}{n_2}\sin\theta_i)^{\,2}}}{n_1\cos(\theta_i) + n_2\sqrt{1 - (\frac{n_1}{n_2}\sin\theta_i)^{\,2}}}]^2 \tag{1.6}$$

$$R_p = [\frac{\tan(\theta_t - \theta_i)}{\tan(\theta_t + \theta_i)}] = [\frac{n_1\cos(\theta_t) - n_2\cos(\theta_i)}{n_1\cos(\theta_t) + n_2\cos(\theta_i)}]^2 \tag{1.7}$$

$$R_p = [\frac{n_1\sqrt{1 - (\frac{n_1}{n_2}\sin\theta_i)^{\,2}} - n_2\cos(\theta_i)}{n_1\sqrt{1 - (\frac{n_1}{n_2}\sin\theta_i)^{\,2}} + n_2\cos(\theta_i)}]^2 \tag{1.8}$$

University of Malaya

where n_1 and n_2 are mediums with different refractive indexes while θ_i and θ_t are angle of incidence (towards the normal of the surface) and angle of refraction (the outgoing beam) respectively (le Reinders et al., 2017).

1.2.4 Heat loss mechanisms

The operating temperature of solar cell is one of the concerns in solar cell researches whereby it leads to the loss in electrical efficiency of solar cells. Generally, only 15% of radiation is converted into electricity and the rest is loss as heat (Teo, Lee, & Hawlader, 2012). Therefore, some of the heat is trapped inside the solar cell, increasing the temperature of the cell, leading to the decrease in the electrical efficiency of the overall system. There are three mechanisms that causes heat loss in solar cells, namely conduction, convection and radiation (Harris & Lenz, 1985). Conduction is a heat transfer mode from high temperature to low temperature area caused by the temperature gradient in an object (solid or fluids at rest) (Ã–zisik, Özısık, & Özışık, 1993). The ability of solar cells to transfer heat to the environment depends on thermal resistance and properties of materials used to encapsulate of solar cells. On the other hand, convective heat transfer (convection) is the transport of heat which is affected by the flow of adjacent moving fluids (Bejan, 2013; Jiji & Jiji, 2006). In solar cells, convection is caused by the blowing wind across the solar cells. Another form of heat transfer mode is thermal radiation, whereby it is defined as the radiant energy which is emitted by an object that is caused by solely to the temperature of the object. It is a transfer of heat energy by electromagnetic waves or photons whereby a medium emits radiation based on its temperature. Figure 1.5 is an illustration of heat loss mechanisms in flat-plate collector. In transparent coatings, heat is loss from the transparent cover to the environment is often caused by the exchange of radiation and convection modes (Agbo & Okoroigwe, 2007). These modes are

University of Malaya

influenced by surrounding conditions such as wind velocity, grounds and wavelength radiation from sunlight.

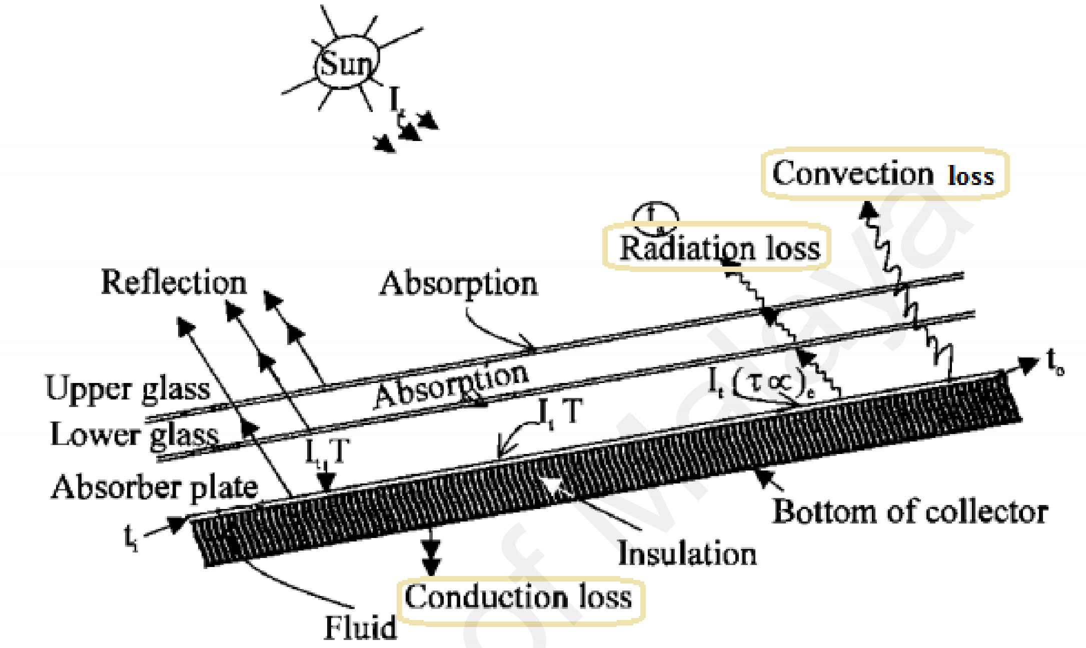

Figure 1.5: Modes of heat loss (Agbo & Okoroigwe, 2007)

University of Malaya

1.3 Problem statement

Under current researches in solar industries, scientists often faced setbacks in maximizing the performance of solar panels. Often, under developed methods, the efficiencies of solar panels increase but degradations occurred due to rapid temperature increase occur, leading to decreased in the lifetime of solar panels (Green et al., 2017) (N. Ahmad, Ota, & Nishioka, 2017). In some cases, the development of method to lengthen the lifetime of solar panels were successful however, the efficiencies obtained from solar energy are still far from the conventional energy due to many factors such as low transparency of coated glass covers or the degradation of materials used (Park, Grätzel, Miyasaka, Zhu, & Emery, 2016). Therefore, this leads to the work which aims to provide the best method for improving the performance of solar cell in terms of both decreasing the temperature of solar cell and increasing its efficiency. Since the use of nanotechnology is popular nowadays due to the flexibility and tunability of nanomaterials (Otanicar et al., 2016), several nanoparticle powders, namely, zinc oxide (ZnO) titanium dioxide (TiO_2) and tin dioxide (SnO_2) are selected in this study to be introduced in the developed binder combinations, APTES/MTMS and MTMS/HNO_3 separately.

1.4 Objective of the thesis

A novel approach for nanoparticle coating systems are developed in this study by using three types of nanoparticles, ZnO, TiO_2 and SnO_2 by using two types of hybrid binder systems, namely APTES/MTMS and MTMS/HNO_3. The main focus of this study is to find out which organic coating system is the best one for reducing the temperature of solar cells without affecting the efficiency solar cells. Hence, the objectives of this work are as follows:

1. To develop a simple and cost-effective method for the synthesis of nanoparticle coatings on substrates.
2. To determine the suitable organic binder system for the selected nanoparticle coating systems.
3. To determine the best nanoparticle coating system for reducing the temperature of solar cells while maintaining or improving fill factor.

1.5 Scope of research

The nanoparticles coating systems only involves three types of nanoparticles, ZnO, TiO_2 and SnO_2 and are introduced in two types of binder combinations, APTES/MTMS and MTMS/HNO_3. All nanoparticle coating systems are developed by using the same method which is time and cost effective. The nanoparticle coating systems are cured in

University of Malaya

room temperature for approximately 20 minutes. The nanoparticle coatings which are coated on glass substrates are only tested on monocrystalline solar cells and the experiment is limited under the laboratory conditions. This work is intended to produce best performing nanoparticle coatings which can reduce the temperature of solar cells without affecting their efficiencies.

1.6 Significant of study

The main aim for this work is to use coating method with introduction of nanoparticles for temperature reduction of solar cells without decreasing the efficiencies. The method used for the nanoparticle coating system is an attractive one for many industries as it is time-efficient and economically viable. Those nanoparticle coatings can potentially be produced in bulks in a short time. By introducing the selected nanoparticles, ZnO, TiO_2 and SnO_2 into two types of binder systems APTES/MTMS and MTMS/HNO_3 separately, the best coating system that meets the objectives of this study can be determined and used for further development. The positive result of this work can be applied on solar panels for the increase in the lifetime of solar panels while maintaining their electrical performance, or better, improving them. This work also includes the several structural studies to support understanding behind the physical results obtained and hence eases for the work to be further expanded in the future.

University of Malaya

1.7 Thesis structure

The thesis consists of five chapters and the outline for each chapter is summarized as follows:

Chapter 1 shows a brief introduction of the fundamental background along with problem statement, objective of this study, scope of research and significance of study to understand the results better.

Chapter 2 presents comprehensive past studies on the factors that influence the performance of solar cells, followed by various methods used by researchers to control the temperature of solar cells. The chapter is wrapped up with recent studies on nanoparticle coatings for solar cells to prevent degradation caused by temperature.

Chapter 3 highlights the fabrication and method of nanoparticle coatings used in this work. Besides all characterizations used in this experiment are explained in detail in this section along with their basic working principle for better understanding of the outcomes.

Chapter 4 presents all the results obtained by the characterizations in this study and followed by discussions on the outcomes. The chapter is divided into four subsections, namely, physical properties, structural properties, electrical properties and lastly temperature analysis. The best binder system and overall coating system are also determined in this chapter which focuses on the temperature decrease of the solar cells.

Chapter 5 concludes the overall work for this study. Suggestions for further work and recent trends statistics are also included in the final chapter.

University of Malaya

CHAPTER 2: LITERATURE REVIEW

2.1 Introduction

This chapter is divided by three main sections and is started off with the main factors which affect the performance of solar cells in terms of the efficiency and the lifetime of the cells. It is then followed by current methods used by researchers to improve the temperature and efficiency of solar cells. Finally, this chapter focuses on the recent works on nanoparticle coatings involving types of nanoparticles that are chosen for this study.

2.2 Factors affecting the performance of solar devices

There is a number of factors that affect the spectral response of solar cells. One of the main factors is solar irradiance, which is defined as the radiance flux received from the sun in form of electromagnetic radiation in terms of wavelength on a surface per unit area of the cell (W/m^2) and it projects power density at a given wavelength. Also, there are several parameters such as incident angle of the sun, clouds in hazy weather as well as air pollution which affect irradiance level at any particular location at a given time. The spectral distribution of radiance that arrives on Earth's surface is another important parameter that influences the efficiency of photovoltaic cells (PV) (Iqbal, 2012). Previous research showed that irradiance varies throughout within a certain duration of time (Green, 1982; Willson, Gulkis, Janssen, Hudson, & Chapman, 1981). Figure 2.1 shows the I-V characteristics for a clean PV at different solar irradiance by using a variable resistor (Goossens & Van Kerschaever, 1999). The graph shows that the output voltage increases with increasing the solar irradiance. The result shows that at maximum solar intensity of 773 Wm^{-2}, the output voltage obtained was 1138 mA.

University of Malaya

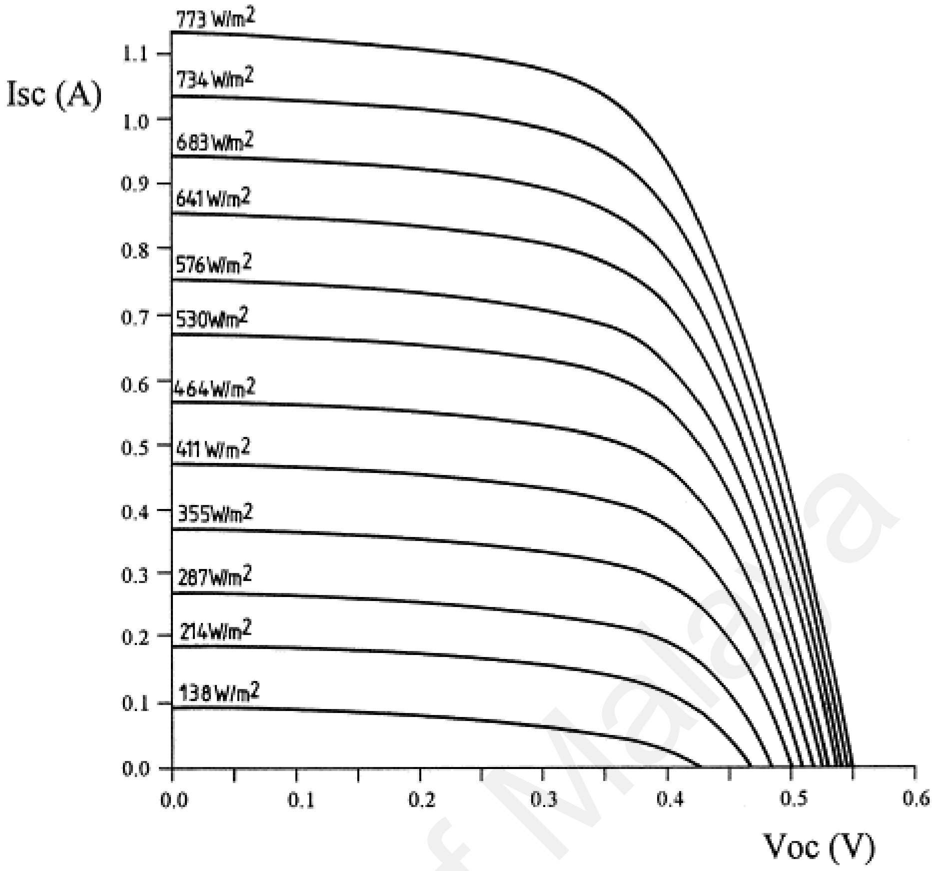

Figure 2.1: The I-V curve of a PV cell at different solar intensities (Goossens & Van Kerschaever, 1999)

University of Malaya

Another main factor that influences the spectral response of solar cells is a phenomenon called photoaging, which contributes in speeding up the deterioration process in solar cells. Photoaging or photodegradation is a type of deterioration which involves chemical reactions that is caused by exposure to UV (ultraviolet) rays (Yousif & Haddad, 2013). Photoaging is influenced by several factors such as air, solar UV radiation and other pollutants whereby parameters such as temperature, mechanical stresses as well as presence of organic solvents and water fastens the process (Rabek, 2012). This phenomenon gives an impact on the mechanical properties of some materials such as Polystyrene (Yousif & Haddad, 2013), Polycarbonate (Pryde, 1985) and several other polymers, which causing the materials to become useless over a certain period of time. Hence, careful calculations in terms of weight percentage used need to be made when including materials such as polystyrene-modified TiO_2 film in quantum dot-sensitized solar cell (Chou, Lee, Vittal, & Ho, 2011) or micro-porous polycarbonate film in dye-sensitized solar cells (DSSCs) (Lue, Lo, Hung, & Tung, 2010) as they could degrade in a short time due to photodegradation. Photodegradation happens when there is activation of polymer macromolecule upon photon absorption by the polymers. Figure 2.2 shows the basic illustration of formation of microcracks and weak centers caused by UV radiation and mechanical stress.

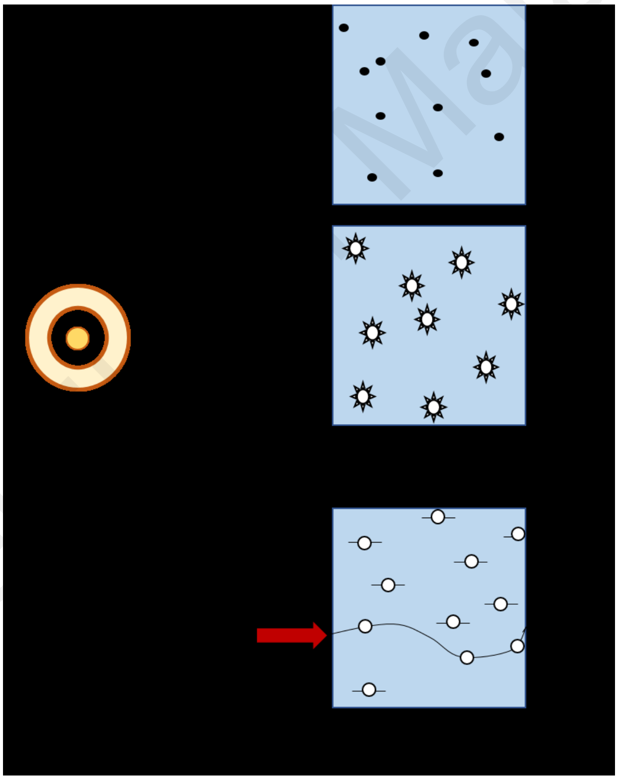

Figure 2.2: a) Initial chemical heterogeinities b) Subsequent effects of UV radiation and c) Mechanical stress on the formation of weak centers and microcracks (Rabek, 2012)

University of Malaya

Photo-degradation is a serious aspect that needs to be taken into account to bring the performance of polymer-based solar cells to another level. Generally, it disturbs the mechanical, physical and chemical properties of most polymers (Ghasemi-Kahrizsangi, Neshati, Shariatpanahi, & Akbarinezhad, 2015; Yousif & Haddad, 2013; Z. Zhang, Wang, & Zhang, 2014). For solar cells such as thin film and organic types, photodegradation needs to be avoided to prolong the lifetime of the cells. Therefore, there are several methods which can be followed to overcome these drawbacks for example, by mixing certain polymers with fullerenes which has proven to show positive result for plastic solar cells (Neugebauer, Brabec, Hummelen, & Sariciftci, 2000). The analysis indicates that the rate of degradation of conjugated polymers which is high under influence of light and oxygen is remarkably decreased by adding fullerenes as used in plastic solar cells.

Photoaging can be considered as reason why various solutions such as nanofilters and anti-reflective coatings for improving efficiency of solar cells ended up as failures. This is because of the fact that this particular phenomenon gives negative impacts on the barrier and the optical properties of many coatings which could damage the target applications (Topolniak et al., 2017). The presence of some impurities also affects the rate of degradation (Rabek, 2012). Most of the pure polymers do not absorb light at wavelengths of more than 200 nm, however photodegradation of polymers can even occur at wavelengths of more than 300 nm. This means that the polymers contain impurities that are most likely to contain conjugated double bonds or carbonyl groups which are responsible for the absorption of radiation over 220 nm (Rabek, 2012). The durability of materials is the key element in progression of solar cells other than the primary type (crystalline) application specifically for those involving polymeric materials.

Researchers have developed many ways for photostabilization of polymers. One of their exceptional works is by using well-selected stabilizers. Using preventive stabilizer such as UV absorbers which functions to absorb and transform the detrimental radiation

University of Malaya

into harmless thermal energy is one of a popular method for photostabilisation (Pospíšil et al., 2006). Figure 2.3 shows that in a sample labelled A, yellow coloration started to appear after UV radiation of 500 hours and it reached the highest intensity after 800 hours. On the other hand, in sample labelled B which contains organic UV absorbers (Tinuvin 1130), only a fade yellowing is spotted, showing a low intensity of coloration after 800 hours of UV. This proves that Tinuvin 1130 works as a very effective protection against UV light in sample B (Nikafshar et al., 2017).

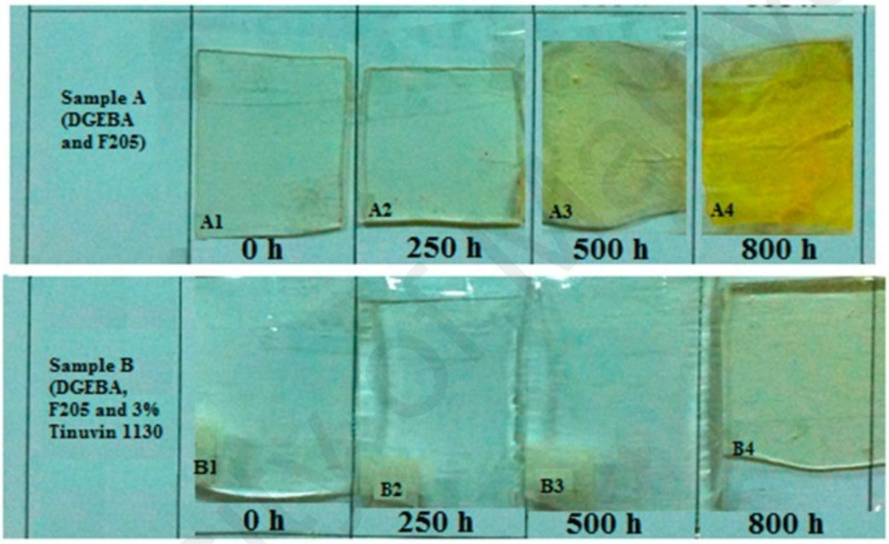

Figure 2.3: Optical image of coloration of sample A and B after 0, 250, 500 and 800 h of UV radiation exposure (Nikafshar et al., 2017)

The performance of solar cells is also affected by environmental condition. Temperature has an impact on all solar cell module parameters, such as short circuit current, open circuit voltage, efficiency and many other important parameters (Karki, 2016; Luque & Hegedus, 2003). Different from irradiance, short-circuit current (I_{sc}) and open-circuit voltage (V_{oc}) increases when irradiance increases, while the temperature has the reverse effect as the temperature is a function of irradiance. This shows that when the temperature of a solar cell increases, V_{oc} decreases and I_{sc} increases under standard test

University of Malaya

condition (a global AM 1.5 spectrum, 25°C ambient air temperature, and 1000 Wm^{-2}) (Mekhilef, Saidur, & Kamalisarvestani, 2012; A Virtuani, Lotter, & Powalla, 2006). This is due to the fact that as the temperature of the solar cell increases, the resistance also increases and the electrons move slowly through it. This leads to another situation where the quality of solar panels becomes another significant factor. High quality solar panels are designed to withstand extreme heat and lower quality panels lose efficiency and produce lesser energy (Amelia et al., 2016). Figure 2.4 shows the power-voltage curve (P-V) of a PV panel at a constant solar irradiance of 1000 Wm^{-2} with different temperatures of the PV panel (Amelia et al., 2016). It is clear from Figure 2.4 that as the panel temperature increases, the output power decreases gradually. The graph shows that by increasing the temperature of the PV panel by 10°C, the output power is decreased by about 5 W or 5%. As clearly seen from Figure 2.4, the minimum output power obtained was 79.5 W at temperature of 65°C while the maximum power of 100 W was achieved when the temperature of the panel is 25°C.

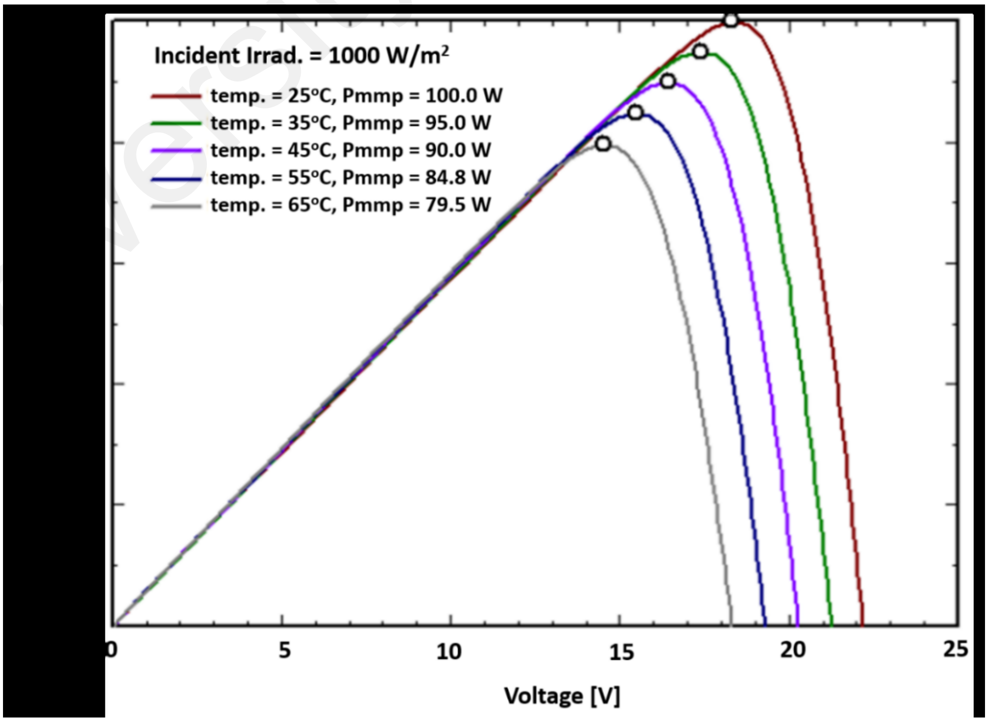

Figure 2.4: P-V curve of PV panel at constant solar irradiance with distinct PV panel temperatures (Amelia et al., 2016)

University of Malaya

The bandgap of a cell’s material is another parameter that affects the efficiency of a solar cell significantly. Materials with large bandgap such as GaN will result in insufficient energy absorption, while materials with narrow bandgap such as PbS and Ge will result in insufficient photovoltage. With low bandgap polymers, the lights absorbed can be extended into the red and infrared region, causing the cell to harvest more solar energy, leading to higher efficiency of solar panels (K. Colladet, 2004; Perzon et al., 2005; X. Wang, 2004). Figure 2.5 shows performance of solar cells as a function of bandgap with 1000 W/m^2 irradiation and spectrum of AM1.5. The lines demonstrate the empirical trends as well as physical limits of these parameters. From Figure 2.5, it is known that even though V_{oc} and J_{sc} could potentially improve, fill factor (FF) contributes the most in terms of difference between device’s performance and potential, showing that FF determines the quality of solar cells (Stuckelberger, Biron, Wyrsch, Haug, & Ballif, 2017).

University of Malaya

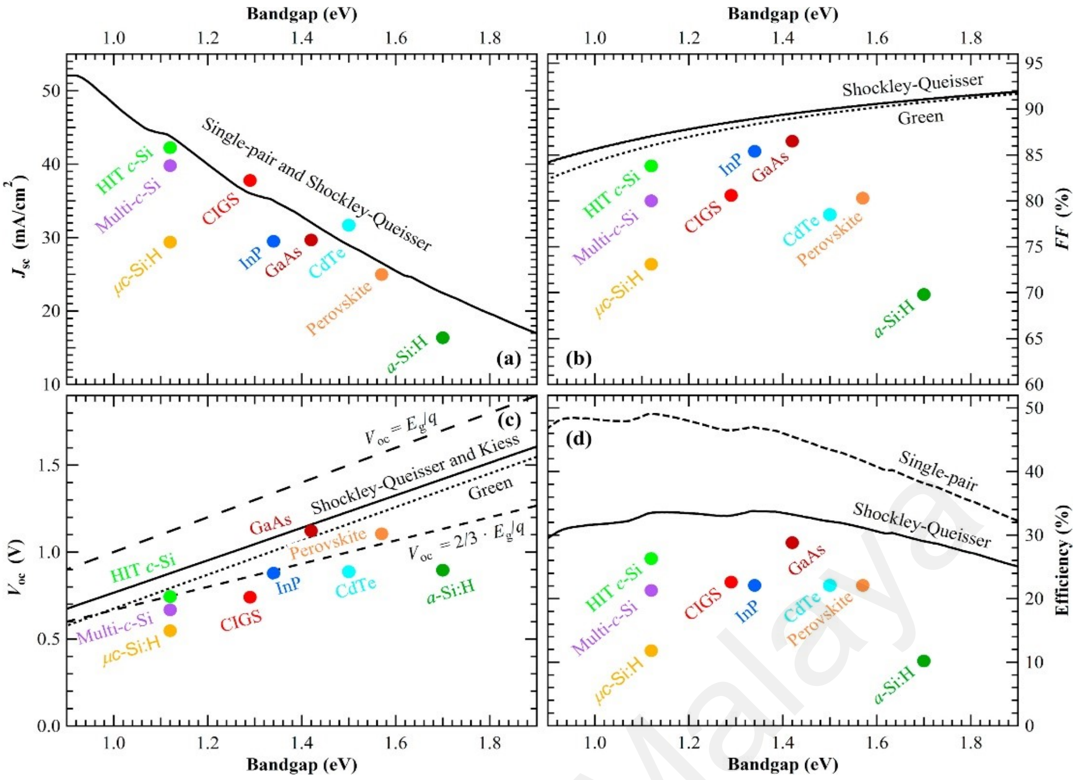

Figure 2.5: The performance and theoretical limits of single-junction solar cells of distinct classes; (a) short-circuit current density, (b) fill factor, (c) open-circuit voltage and (d) conversion efficiency (Stuckelberger et al., 2017)

The architecture and insulation of PV systems should also be taken into consideration for an optimum power output. The good choice of construction and the design of solar PV panels can potentially minimize the negative environmental impacts on the performance of the PV panels (Cimmino et al., 2017). Introduction of innovative approaches such as adiabatic cooling system, light-directing elements, switchable glass and vacuum insulating panels leads to solar smart architecture which will bring rise to modern solar technologies (Schittich, 2003). Shading issues due to trees, size, height, and proximity of surrounding barriers can be minimized or eliminated with proper and suitable designs of the system (Patel & Agarwal, 2008). Shaded solar panels contribute to ununiform solar radiation hence produces less power (Chowdhury & Saha, 2010). Besides, unclean or soiled solar panel due to soiling also produces less electricity. The

University of Malaya

term “soiling” refers to foreign substances which settles on the surface of solar panels such as dusts, dirt and other debris (García, Marroyo, Lorenzo, & Pérez, 2011; Pavan, Mellit, & De Pieri, 2011). This causes the partially blocking of sunlight from reaching the solar system properly and affects its overall performance and the desired efficiency could not be obtained (Zorrilla-Casanova et al., 2013). In places with frequent rain, soiling does not affect much in the power output as the soiling contributors tend to be washed away naturally. The regions which experience a long period of dry and hot weather like California as well as south of Navarre (Spain), are more likely to experience more soiling compared to other countries with high humidity especially during the summer (Caron & Littmann, 2012) (García et al., 2011). Soiling can also be occurred in a short time near construction sites or besides beaches whereby the dust deposits on solar panel more frequently and rapidly, therefore cleaning the systems regularly may be the solution for this matter but to keep up with the maintenance is quite costly and time consuming. Hence, self-cleaning system is creatively proposed with various materials and methods as the best problem solver in this case as of now (Verma et al., 2011).

Furthermore, the wind speed also affects the performance of solar cells, significantly. In a study made by Goossens et al. (Goossens & Van Kerschaever, 1999), wind velocity has an impact on the cell’s performance. The high winds affect the sedimentological structure of dust coatings on the surface of solar cells, which in return creating a higher transmittance of light for coatings. The wind speed affects the temperature of the PV cell (Mekhilef et al., 2012; Nann & Emery, 1992). Mekhilef et al. (Mekhilef et al., 2012) stated that increasing the wind velocity reduces the heat and humidity on the surface of the PV cell which leads to the increase in overall efficiency of a PV system.

All of these factors should be taken into account seriously when fabricating systems for improved solar technologies. These might be the core reasons of why efficiencies of

University of Malaya

the solar PV could not be levelled up significantly over the time. In our opinion, to eliminate factors contributing to inefficiency of solar devices, it is also important to study thoroughly other effects of combining different methods into one system as it might influence the lifetime of the devices. In other word, the efficiencies of solar cells could have some vast improvements with the newly invented system architectures but the materials could not be used for a long period of time. While increasing the efficiency of those cells, researchers should design systems that can adapt to the to the degradation of the cell’s materials at the same time such as using vacuum encapsulation of solar panels or by using transparent insulating materials (Schittich, 2003).

University of Malaya

2.3 Methods for improving the performance of solar devices

In this modern era, solar cell technology is evolving and developing at an astounding rate due to a number of factors including environmental issues. In order to achieve perfection in solar cells, there are certain variables that should be considered which can potentially affect the output significantly (Tada, Carter Jr, Anspaugh, & Downing, 1982). The prime improvement of solar cells can be seen from its efficiency as well as its durability. Today, there are various types of solar cells which have been developed with improved efficiency such as solar cells with some modification such as incorporation of foreign elements, transparent solar cells, encapsulation of solar cells and many more. Each of these solar cells has their own uniqueness and contributed to some advantages.

2.3.1 Solar filter / coatings

One of methods to improve the performance of solar cells is by using a filter (Gunawan & Lei, 2017). Solar filter or solar cell coatings has grabbed attention of many scientists.

Astronomically, a solar filter functions to block off some sunlight that can cause harm to the eyes. Often, they are made of a highly durable glass or film which transmits 1/100000th of light. Depending on materials used for solar filters, solar filters can eliminate certain unwanted wavelength that degrades solar cells. Long term exposure to UV rays might induce photocatalytic activity in some materials, which leads to the degradation of solar devices. Park et al. (Park et al., 2016) stated that the UV excitation can largely be prevented by the use of FTO conducting glass support as well as TiO_2 or SnO_2 layer to filter out UV photons.

There was a research made by Kazem et al. (Kazem & Chaichan, 2016) to find the best wavelength or colour for a filter that gives the best performance of solar cells. The result of the study proved that the sunlight spectrum colors affect the output of solar photovoltaic cells. One way to determine the total irradiance of artificial light from solar simulator upon different types of solar filters is by normalization of the chronoamperometry measurement as shown in Figure 2.6 (Tavella et al., 2017). From the graph below, the UV B/C blocking filter that cuts below 350 nm and above 500 nm of wavelength, shows an improved normalized current density compared to open spectrum. This indicates that light portion in the range of 350 – 500 nm range is indeed effective in photocurrent production (Tavella et al., 2017).

University of Malaya

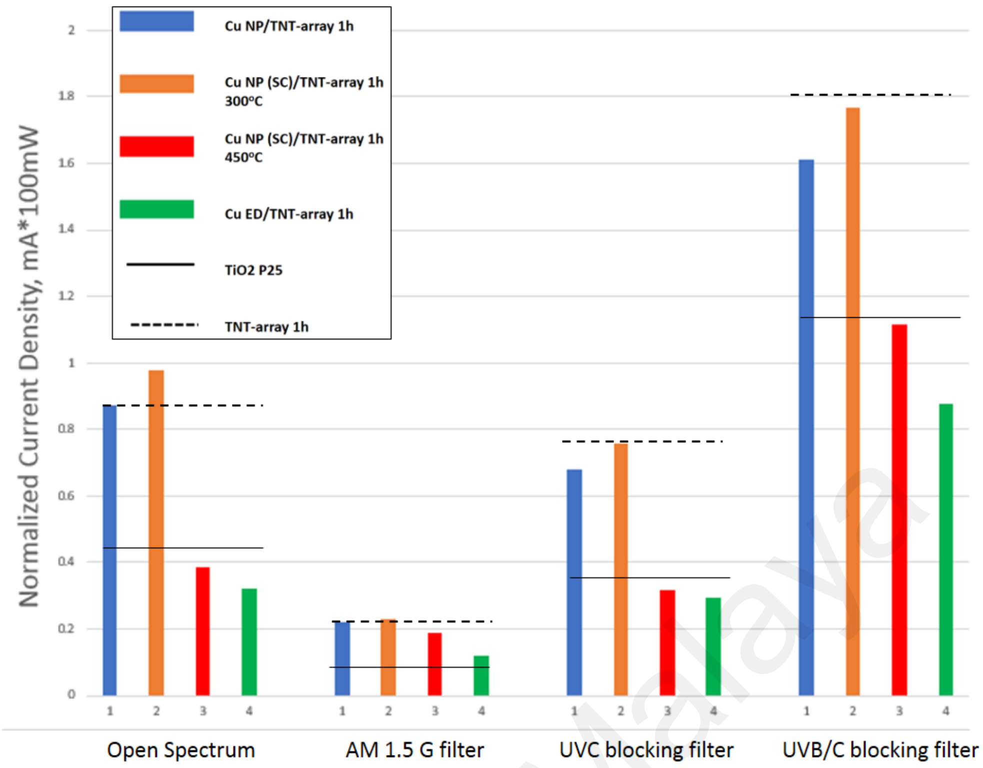

Figure 2.6: Measurement of normalized chronoamperometry for different filters to solar simulator light (Tavella et al., 2017)

Nanoparticles in the fluid enable the absorption and transmission of specific wavelengths. Its flexibility is one of advantages of using nanoparticles whereby it can be grown into distinct shapes, materials and sizes, which makes it convenient to tune and scale up the spectral properties up to massive volume production. Nanoparticles can also be used for achieving selective spectral filtration for solar cells which is attractively cost-effective. In a study made by Otanicar et al. (Otanicar et al., 2016), an efficient solar energy conversion can be achieved with a hybrid system composed of selective solar filter by using a suspended nanoparticle fluid to absorb non-PV photons directly. In the study, indium tin oxide (ITO) and gold (Au) nanoparticles were chosen for a well-blended atomic mixture.

University of Malaya

An optical filter is proven to be useful in solar thermophotovoltaic (STPV) system (Mbakop, Djongyang, Ejuh, Raïdandi, & Woafo, 2017). Referring to Figure 2.7, in the STPV system, the absorption and emission of solar radiation occur as thermal radiation takes place before illumination of solar cells. The thermophotovoltaic (TPV) enables the utilization of selective filter as well as sub-banding gap photon reflection to the emitter, in order to increase the efficiency (Ismail, 2011). Mbakop et al. (Mbakop et al., 2017) uses the emitter and spectral filter of a 1-dimensional (1D) photonic crystal which are applied to a STPV system to study its thermal efficiencies. A titanium dioxide (TiO_2) / silicon dioxide (SiO_2) photonic crystal filter was chosen towards making the filter structure to match well with the spectral distribution of the emitter with high temperature within the corresponding transmission band.

University of Malaya

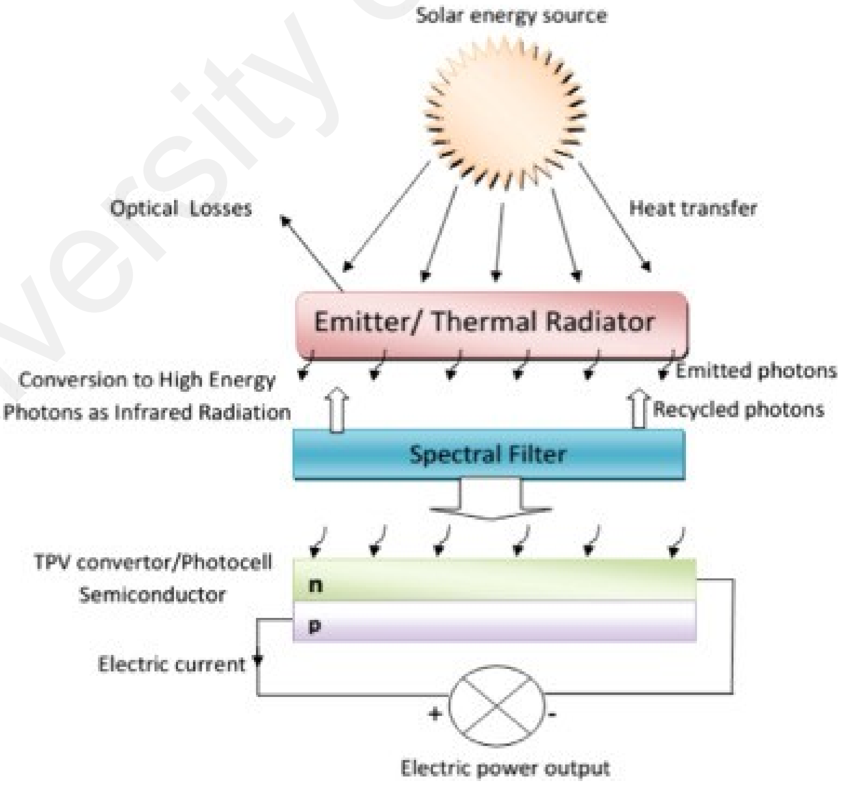

Figure 2.7: An illustration of the basic concept of the STPV (Mbakop et al., 2017)

The application of liquid filters for hybrid photovoltaic-thermal (PVT) solar systems have also been proven to be effective in making solar cells operate with higher efficiency as stated by Chemisana et al. (Chemisana, Fernandez, Riverola, & Moreno, 2018). In the study, the direct immersion of the PV cell in the liquid improved the temperature control of the PV system. Photons with low frequency which contributes to the heating of the PV cell are absorbed by the liquid leading to the stable temperature of the cell. Among the few liquids that were tested for the application, a promising candidate which could benefits in terms of electrical, thermal, optical and operational aspect is a mixture of isopropyl alcohol and deionized water. The less expensive and suitable liquids that were proposed by Joshi et al. (Joshi & Dhoble, 2017) in PV thermal system are the tap water, silicone oil and coconut oil which offer good transparency. From spectroscopy analysis, these liquids also match with the range of response in crystalline silicon solar cells and showed excellent absorption in the UV and IR regions. As comparison for the three selected liquids, coconut oil showed the most outstanding performance with a recorded percentage of 12.53% of average electrical efficiency and 47% of thermal efficiency.

University of Malaya

2.3.2 Solar concentrator

Another method of collecting solar energy and concentrating it on solar panel is by using solar concentrators (Winston, 1974). They harvest sunlight over large area and focus them on photovoltaics or solar cells (Bradshaw, Knowles, McDowall, & Gamelin, 2015). In spite of the fact that many types of solar concentrators have been invented for quite some time since solar cell evolution, this type of solar technology have been overlooked up until recently. Researchers have started developing new materials for enhancing solar concentrators again. One type of solar concentrators that have been recently invented was organic solar concentrators (Currie, Mapel, Heidel, Goffri, &

Baldo, 2008). Not only it portrayed high quantum efficiency of more than 50%, but the cost of photovoltaic (PV) power can also be lessened with organic solar concentrators.

One recent work for solar concentrators is by using the V-trough booster reflector mirrors (Michael, Iqbal, Iniyan, & Goic, 2018) where higher incident irradiation was observed which also led to severe thermal stress to the laminated layer the PV module. Hence, an efficient cooling system was absolutely necessary in this system. According to Michael et al. (Michael et al., 2018), for one mirror arrangement the electrical power increased for a duration of 90 to 120 minutes around solar noon while for two mirror arrangements, the electrical power was increased for 60 minutes. In the method of using the V-trough concentrator using cheap reflector mirrors, it is said that the fixed tilt is appropriate for residential application and the periodic tilt suits for the commercial application.

A recent work proposed that solar cell's temperature can be decreased by combining the methods of solar concentrator and a filter. Solar concentrator was used to optimize the solar radiation and a long-wavelength cut filter is used to reduce the cell's temperature. Through this study, Ahmad et al. (N. Ahmad et al., 2017) has proved that the lifetime of a solar cell can be extended with an increase of increase of 1.9×10^5 h with Fresnel lens optical concentration system which can reduce the solar cell's temperature. The transmittance curve for the system in Figure 2.8 shows that more than 90% transmittance was obtained in a wavelength range of 400 – 1300 nm. The range of the long-length of over 1300 nm was successfully cut out.

University of Malaya

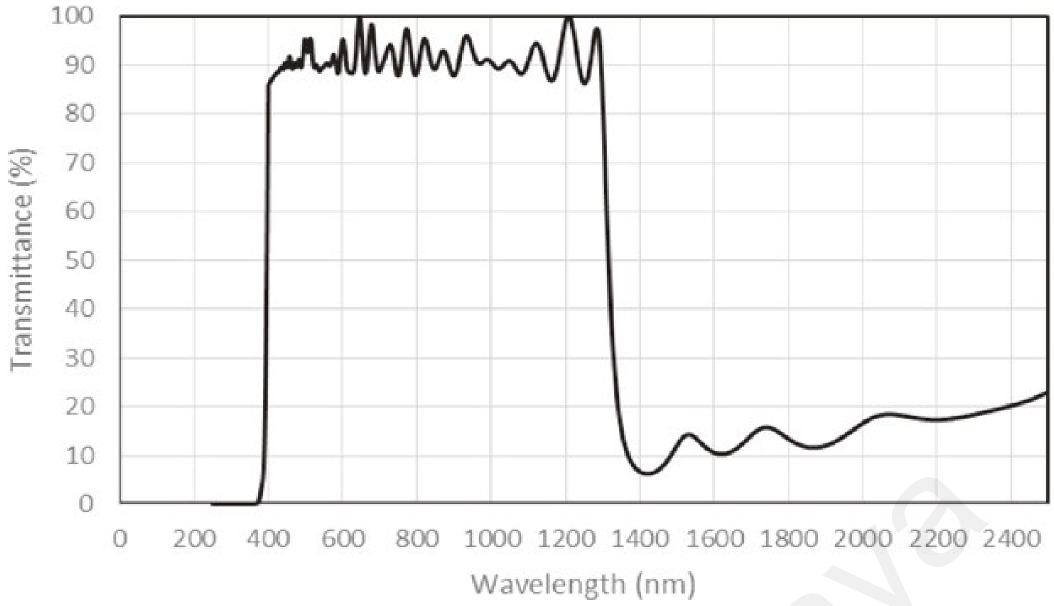

Figure 2.8: Transmittance curve as a function of wavelength for the solar cell system (N. Ahmad et al., 2017)

Recently, nanotechnology was introduced in this combination of concentrator-filtration method, whereby a nanoparticle fluid filter, which consists of gold with nano-sized particles and indium tin oxide nanocrystal were fabricated and the system is combined with a solar concentrator (DeJarnette et al., 2016). The filter efficiency was 62% for thin-film solar cell (GaAs) and 56% for crystalline silicon solar cell (c-Si). The installation of filter fluid which is placed directly in front of PV receiver creates an advantage to recollect the light that go through the filter and reflects off the PV cell. A schematic diagram on the system is shown in Figure 2.9.

University of Malaya

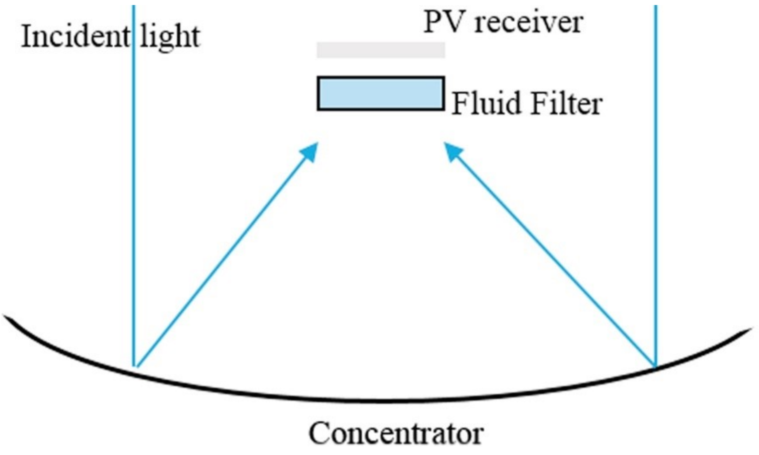

Figure 2.9: A concentrator system with PV receiver and fluid filter in the direction of the concentrated light (DeJarnette et al., 2016)

2.3.3 Anti-reflection coatings

Coating is defined as a substance (normally in liquid from) that is applied onto the exterior and appears as a continuous or discontinuous form of film after it dries (S. K. Ghosh, 2006). A popular all-time alternative to improve solar technologies performance is by using anti-reflection coating (ARC). It is a coating that is used for reducing a reflection off from a surface ("Three layer anti-reflection coating," 1965). This is an efficienct method to improve since loss of light. It is an old technology which still undergoes into modern development to match the efficiency target. Some of the useful techniques used in fabricating ARCs are sputtering (Ali, Khan, & Jafri, 2014), plasma-enhanced chemical vapor deposition (PECVD) (Wan, McIntosh, & Thomson, 2013), dip-coating (Uzum et al., 2017), spin-coating (Lien, Wuu, Yeh, & Liu, 2006), spray pyrolysis (Uzum et al., 2017) and liquid-phase deposition (LPD) (J.-J. Huang & Lee, 2013).

According to Jiang Y. et al. (Y. Jiang et al., 2016), in the attempt to increase the performance of colourful perovskite solar cells, it is proved that the power conversion efficiency managed to reach up to 13 to 15% by modifying the device’s structure with the use of transparent conducting polymer poly (3,4-ethylenedioxythiophene: poly

University of Malaya

(styrenesulfonate) (PEDOT:PSS^T) top electrode as shown in Figure 2.10. The conducting polymer serves as anti-reflection coating, whereby its thickness variation leads to the reflectance's suppression at certain wavelength, instead of a whole visible spectral wavelength (Y. Jiang et al., 2016). A recent technique was introduced towards improvising the performance of solar cells whereby a multilayer ARC with optimal design was fabricated for III-V quadruple junction (4J) solar cells (S. Dong et al., 2018). In the study by Dong et al. (S. Dong et al., 2018), it is proven that the oxide layer of the fabricated ARC played a crucial role to enhance the spectrum.

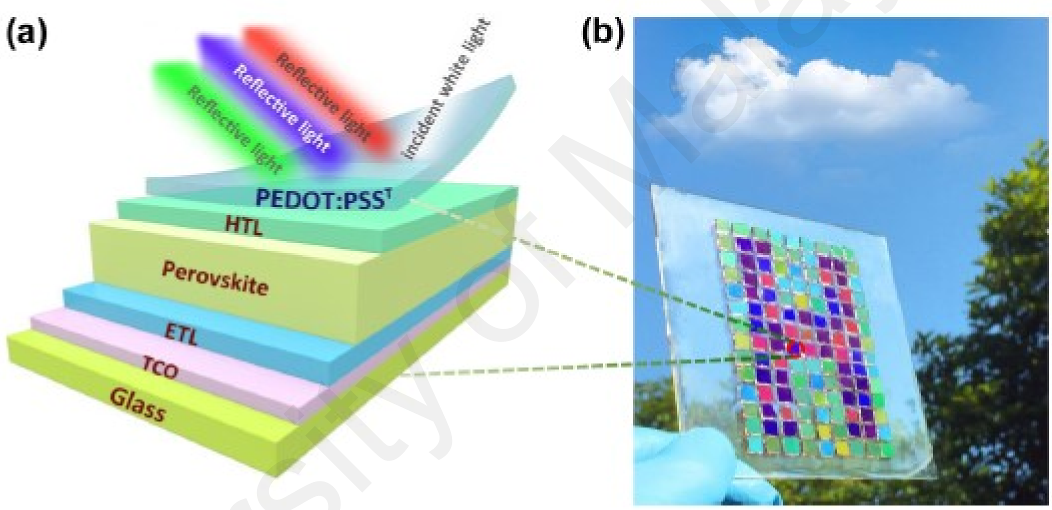

Figure 2.10: a) The cell's architecture layer with conducting polymer PEDOT:PSS^T as top electrode and b) A photographic coloured image of letter H collected by colourful perovskite solar cells whereby the size of each pixel substrate is approximately 5 x 5 mm^2 (Y. Jiang et al., 2016)

Uzum et al. (Uzum et al., 2017)stated that the key factor to enhance the efficiency of silicon solar cells, optical losses should be reduced and the absorption properties of the solar cell must be improved. Therefore, Uzum et al. (Uzum et al., 2017) introduced an alternative for anti-reflection coating layers for silicon solar cell by using TiO_2^- compact as well as ZrO_2^- polymer composite coating layers. It is proved that reflectance further decreased with ZrO_2^- polymer composite/ TiO_2^- compact layer compared to a single TiO_2^-

University of Malaya

compact film in a range of spectra, around 550-1050 nm. Figure 2.11 shows the reflectance curve for both cases. From the graph below, the average reflectance was lowered with the addition of ZrO_2^- polymer composite to the TiO_2^- compact film with 5 to 12% reflectance gain in a wavelength range of 300-450 nm. A steady low reflectance can also be found in a wavelength range of around 700-1000 nm.

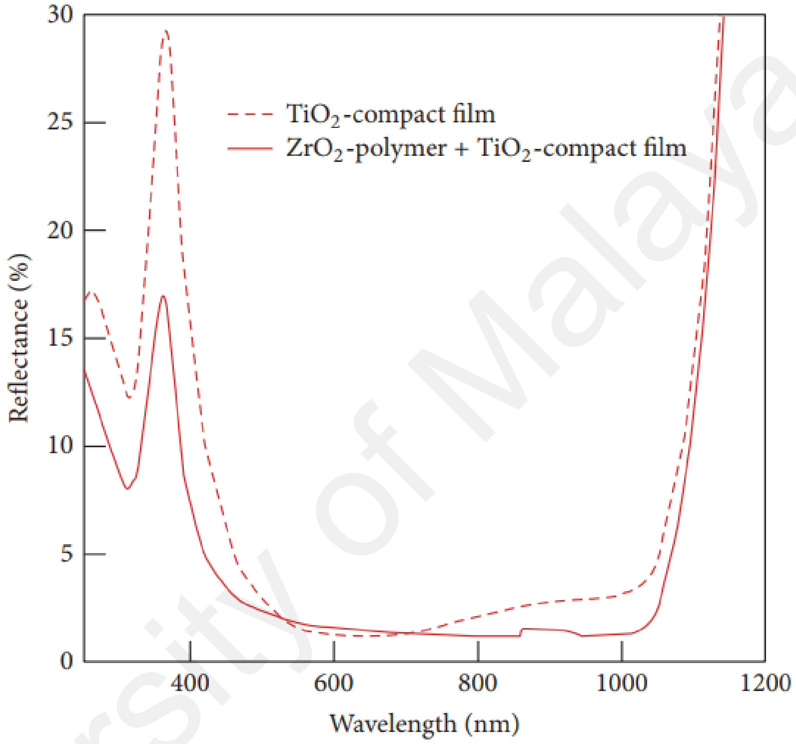

Figure 2.11: The reflectivity comparison of the textured silicon wafers with single TiO_2^- compact film and ZrO_2^- polymer composite/ TiO_2^- compact layer (Uzum et al., 2017)

University of Malaya

In addition, an improved version of anti-reflective coatings on crystalline silicon solar cells is also developed by implementing argon plasma treatment of silicon nitride (SiN) which results in lower reflectance (H. Ghosh, Mitra, Saha, Datta, & Banerjee, 2017). By using plasma-enhanced chemical vapor deposition (PECVD) technique, Hydrogenated silicon nitride (a-SiN:H) was deposited on a silicon substrate with mixture of ammonia (NH_3) and hydrogen (H_2) gasses, and consequently with argon plasma treatment. The

EQE from this study showed a relative increase of 2.72% and 4.46% in current density and conversion efficiency respectively.

Like in many other methods, nanotechnology is also suitable to be applied in order to improve the performance of anti-reflection coatings with simple preparation and economically viable (Elshorbagy, Abdel-Hady, Kamal, & Alda, 2017). In a work made by Elshorbagy et al. (Elshorbagy et al., 2017), short circuit current managed to be enhanced by 15.2% with a reference flat solar cell and a lower reflectivity was achieved with a particular design of anti-reflection coating in the form of Si_3N_4 subwavelength nanostructured dielectric layers. This study utilizes the light-trapping mechanism in the amorphous silicon hydrogenated (aSi-H) solar cells by using the Si_3N_4 nanostructured layers which traps light towards the aSi-H active layer. Duan et al. (Duan, Li, Mwenya, Li, & Song, 2017) has also done similar research on utilizing light-trapping mechanism by using silver nanoparticle and managed to enhance the light absorption of c-Si cell by 26%. A high quality, tunable and scratch resistance ARCs can be yielded with an enhanced layer-by-layer ionic of self-assembled silica nanoparticle which was introduced by Metzman et al. (Metzman, Wang, Morris, & Heflin, 2018).

For a practical antireflective application, the ultra-low refractive index thin films must have good transparency, economical with high durability against harsh temperature and weather condition. Karthik et al. (Karthik, Pendse, Sakthivel, Ramasamy, & Joshi, 2017) introduced the application of a facile synthesis of Ink-Bottle mesoporous MgF_2 nanoparticles with excellent crystallinity and dispersible properties in anti-reflective coatings. With the coatings, an outstanding result was achieved whereby a nearly 100% transmittance was observed in the wavelength range of 615-660 nm (visible range) as well as average transmittance of 99% and 97% in wavelength range of 400-800 nm (visible range) and 300-1500 nm (active solar range) respectively.

University of Malaya

A novel bionic ARC which managed to increase the light harvesting efficiency to promote a better spectral response of solar cells was proposed by Huang et al. (Z. Huang et al., 2018). It is believed that by imprinting the microstructures of the leaves on the polymer-silicon system, the light reflection of the surface will be reduced. When the lotus leaf surface structures were imprinted on the Si-based PV, a maximum power gain of 10.9% was reached on top of having a durable, hydrophobic, antireflective and self-cleaning properties. The hydrophobic surface and low rolling angle gave the self-cleaning properties to the coatings. Figure 2.12 shows the snapshot photographs of a rolling water droplet angle of the coated silicon surface with photopolymer replica of the lotus leaf master. From Figure 2.12 (d), it is shown that the water droplet started rolling at an angle of at 20° (± 0.5).

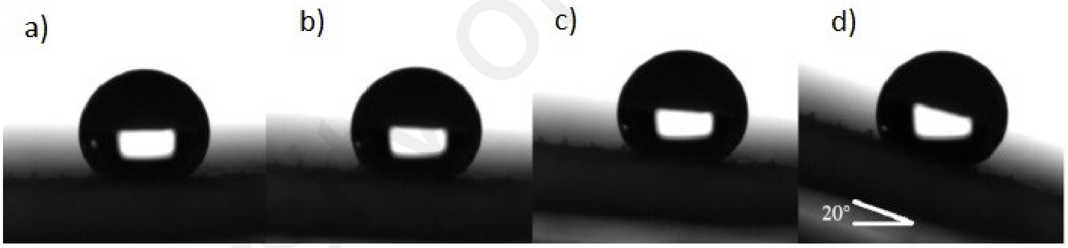

Figure 2.12: Photographs of rolling angle tests of water droplet dripped on coated silicon surface covered by biomimicking surface of lotus leaf master (Z. Huang et al., 2018)

2.3.4 Solar cell encapsulation

Solar cell encapsulation is also a promising method to further boost solar PV's output and avoid degradation. Without encapsulation, the devices will commonly exhibit a formidable degradation under hours of continuous illumination whereas encapsulated devices will have a longer lifetime (Q. Dong et al., 2016). Encapsulation is a crucial component for solar modules to ensure stability in terms of mechanical and environmental

University of Malaya

aspect (Cheacharoen et al., 2018). This method is specifically beneficial to organic solar cells which have high degradation rate and cells which are exposed to high humidity condition. Basically, a complete solar cell encapsulants should consist of an adhesive layer, a weather-resistant layer and a pottant (Gupta, Ingham, & Yavrouian, 1983). The pottant acts as insulator which also protects the fragile electrical as well as mechanical elements from external forces in the environment. Weather-resistant layer is needed to prevent solar cell from being exposed to rains, dusts and other debris while adhesive layer is to connect the solid outer weather-resistant layer to the shock-proof pottant layer.

According to Bryant et al. (Bryant et al., 2016), degradation caused by light and oxygen is the main reason of the low-operational stability of perovskite solar cells that were exposed in ambient environment. It is found that those without encapsulated cells went through a speedy degradation on time scales of minutes to several hours when they are exposed to light and dry air. A successful encapsulation as well as effective barrier layers will contribute to the long-term stability (Bryant et al., 2016). From a study by Dennler et al. (Dennler et al., 2006), an extended lifetime of solar cells was achieved by using a new type of transparent, flexible ultra-high barrier material produced by plasma enhanced chemical vapor deposition(PECVD) to encapsulate the cells. As the result from this study, the shelf lifetime of the 30 x 57 mm^2 of encapsulated solar cell was increased from a few hours into more than 3000 hours or more than 4 months.

Rizzo et al. (Rizzo et al., 2017) further investigated the effect of temperature, moisture as well as humidity on the degradation of perovskite solar cells (PSC) and applied different sealing techniques while encapsulating the devices, in order to analyse the differences during experiment. Two different glass to glass sealing methods were used: without (GS-PSC) and with (ES-PSC) to study the intrinsic stability of PSC. Figure 2.13 shows two strategies of encapsulations with and without addition of a light-curable glue.

University of Malaya

It is proven that the one with light-curable glue edge sealing managed to reduce moisture percolation as well as mechanisms of oxidation at stress temperature of below 80°. Consequently, it results in a prolonged lifetime of the cell (Rizzo et al., 2017).

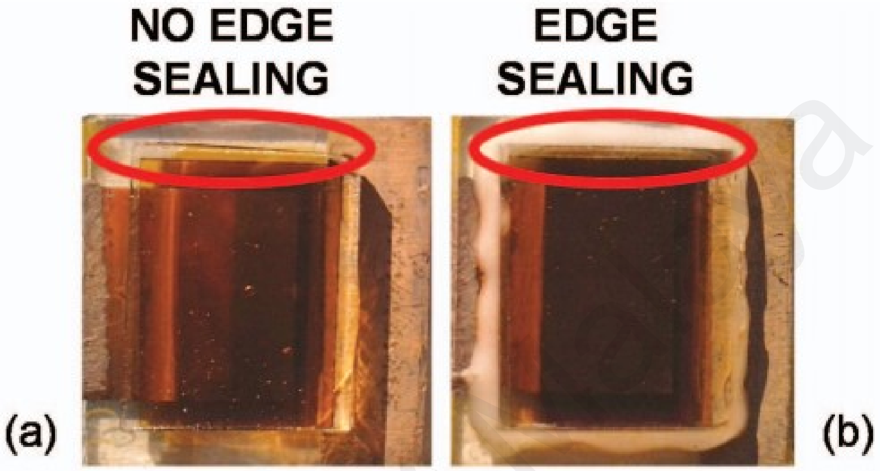

Figure 2.13: Images of samples a) non-sealed edge and b) sealed edge (Rizzo et al., 2017)

Ethylene vinyl acetate (EVA) has been reported to be a popular pick for majority solar module manufacturer and will probably be dominating the encapsulation material in the future years (Metz et al., 2015; Witteck et al., 2017). The stability of EVA has remarkably improved with the addition of UV absorbing agents (Griffini & Turri, 2016; Jentsch, Eichhorn, & Voit, 2015). The result in a study made by Witteck et al. (Witteck et al., 2017) shows that UV transparent encapsulation polymers might produce UV unstable modules, hence, a stable UV passivation layers are proposed to further improve the performance of UV-encapsulation materials for solar modules.

Microencapsulation is another innovative idea for solar cell encapsulation. Among the advantages of using microencapsulation method are the self-life enhancement by

University of Malaya

blocking degradative reactions such as oxidation and dehydration, better processability and excellent protection of materials which are sensitive towards their environment (S. K. Ghosh, 2006). In a study by Döğüşcü et al (Kahraman Döğüşcü, Kızıl, Biçer, Sarı, & Alkan, 2018), thermal stability of microencapsulated eutectic mixtures (MEEMs) was demonstrated by 5000 times accelerated heating-cooling cycles and its thermal conductivity was proven to be better than Polystyrene (PS). Hence, MEEMs are found to be a potential material candidate for latent heat thermal energy storage for solar heating and cooling applications.

Nanotechnology has also been implemented in the attempt of making improved encapsulations. Polyvinyl butyral (PVB) which has good attribution for possessing excellent adhesiveness for the surface of glass laminates, was successfully fabricated with graphene nanoplates (GN) to strengthen the heat transfer rate (X. Huang, Lin, & Fang, 2018). The composites result in suitable ionic conductivity as encapsulation materials for solar cell, on top of having remarkable thermal conductivity, thermal stability and insulation. The use of 30 (Wt%) of GN as thermal conductivity enhancement filler managed to further improve heating and cooling rates of 28% to 37% respectively. Furthermore, the fabrication of nanocone arrays (NCAs) as anti-reflection coating on the encapsulated cover glass also drives up the power conversion efficiency of solar cells (Leem et al., 2014). Figure 2.14 shows that over a broad wavelength of 330 - 1800 nm, NCAs ARC glass exhibited highest transmittance spectrum due to its conical nanostructures with small periods of < 200 nm.

University of Malaya

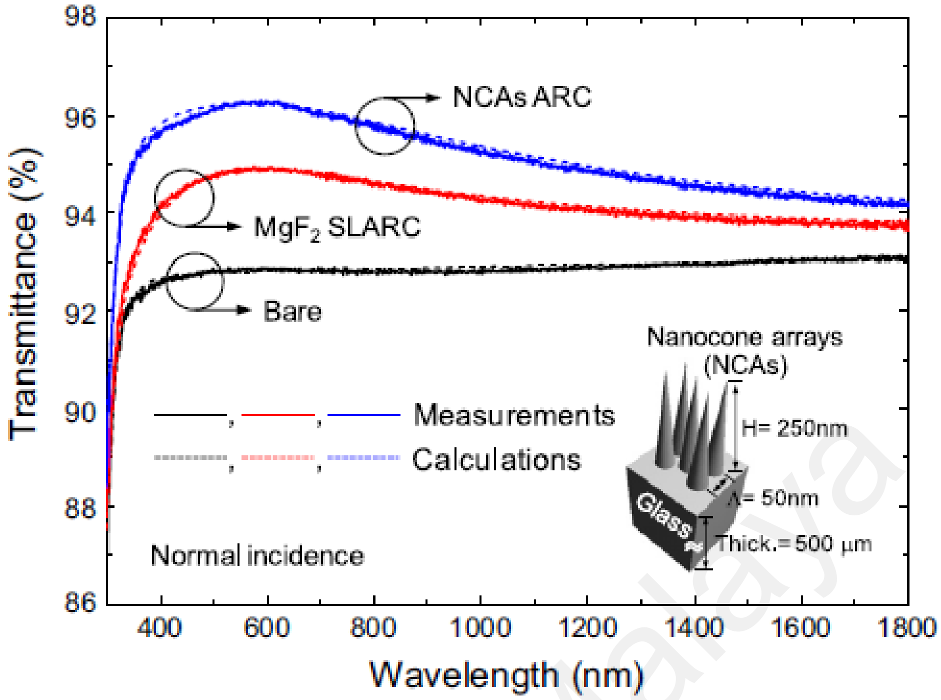

Figure 2.14: A graph of measured (solid lines) and calculated (dotted lines) transmittance spectra at normal incidence of the bare, MgF$_2$ SLARC and NCAs ARC (Leem et al., 2014)

In organic-inorganic solar cells, Formamidinium (FA)-based lead iodide perovskite solar cells (PSC) has shown a promising light absorber and low-cost solar cells with excellent optoelectronic properties (Liu et al., 2018). Nonetheless, this technology suffers from phase-instability problem in the ambient environment, which limits the full potential of the FA-PSCs. Hence, Liu et al. (Liu et al., 2018) introduced the in-situ grain encapsulation method whereby the perovskite grains are encapsulated by amorphous silica layers which are cultivated at the nano-scale. The silica functions to protect the PSC from elements that are contributing towards degradation and to improve charge-carrier dynamics of the perovskite films. Impressively, the result of this study showed an enhanced efficiency, showing an efficiency of approximately 20% as well as retention of 97% after 1000 hours storage under ambient environment.

University of Malaya

2.3.5 Spectral splitting

The efficiency in a single-bandgap solar cell is restricted by the inability to convert photon energy in a broad range of solar spectrum efficiently. One suggested way to overcome this problem is to split the wide solar spectrum into ranges of smaller energy (Sarswat, Jagannathan, & Free, 2017). Then, utilization of each energy range can take place on the appropriately tuned bandgap of PV cell. The concept of spectral splitting was introduced in 1960's (Nelson, 2003) (Rabady, 2017). It is a technique of separating sunlight spectrally into various wavelength bands with the use of spectral beam splitter and targeting each band at most efficient receiver. Distribution of incident angles on wavelengths interference filter can be created by concentrating spectral splitting systems which results in diverged transmission or reflection characteristics (Mojiri, Taylor, Thomsen, & Rosengarten, 2013). Theoretically, photons with energy that are near to the bandgap of solar cells are more efficient in producing electricity and the non-utilised energy is often dissipated as heat (Ju et al., 2017). This problem leads to the discovery of the spectral beam approach.

There are few attempts for introducing methods for spectral splitting. Among primary technology for spectral splitting are by using a thin-film interference filter and a selective absorbing or transmitting filter as shown in Figure 2.15 with small graphs portraying the spectrum range presents at each stage (Mojiri et al., 2013). For the filter's composition, a number of thin layers ranging from a few nanometres to hundreds of nanometres thick of high refractive index (HRI) contrast non-absorbing dielectric materials, are deposited on a transparent substrate. The centre of the research made by Macleod et al. (Macleod, 2017) is the filter, whereby it functions like an edge-filter, band-stop or band pass. Similarly, Widyolar et al. (Widyolar, Jiang, & Winston, 2018) also managed to demonstrate higher conversion efficiencies with the use of typical interference (dichroic) filter systems rather than semi-transparent and back-reflecting beam splitters.

University of Malaya

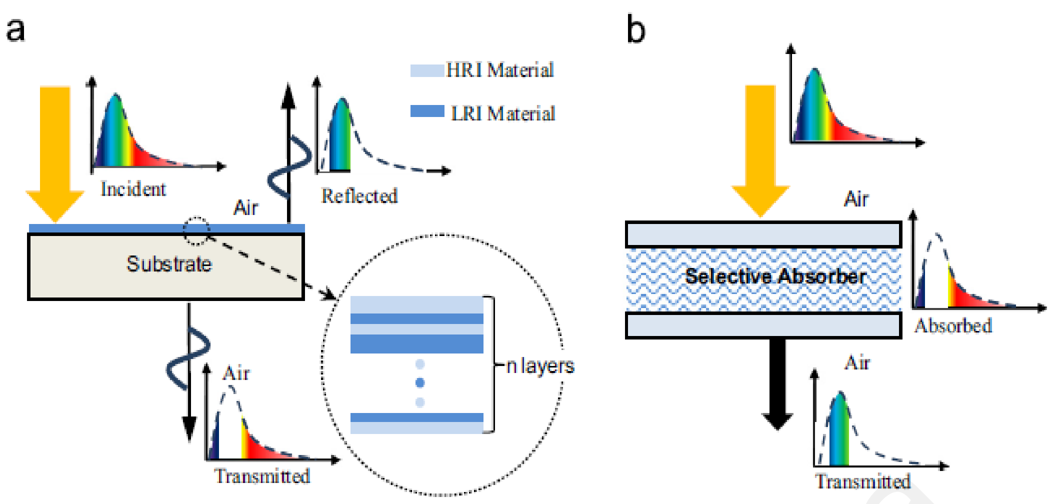

Figure 2.15: Mechanisms of spectral splitting by using a) Thin film interference filter with layers of High Refractive Index (HRI) and Low Refractive Index (LRI) materials and b) Selective absorber (solid or liquid) (Mojiri et al., 2013)

University of Malaya

It is known that ultraviolet (UV) and infrared (IR) parts of spectrum contributes to the heating of the solar cell therefore by utilizing visible region of spectral response, spectral beam splitting could eliminate excessive heating problem. In a study made by Kandilli et al. (Kandilli & Külahlı, 2017), concentrated solar irradiance can be divided into 'light' and 'heat' part by implementing the spectral beam splitting approach with a system assembled by cold mirror, fibre optic bundle, paraboloidal dish, dual axes tracking system and Stirling engine on a lighting-power generation combined system (LIPGECOS). The setup of the experiment is as shown in Figure 2.16. The cold mirror is the core element to experimentally separate the full solar spectra into distinct wavelengths. An average lighting efficiency of 14% ± 0.03 was achieved (Rizzo et al., 2017). Bicer et al. (Bicer, Sprotte, & Dincer, 2017) also done a similar work on a PV panel by utilizing cold mirrors in spectral splitting system and has increased the power output from 3.50W to 6.75W.

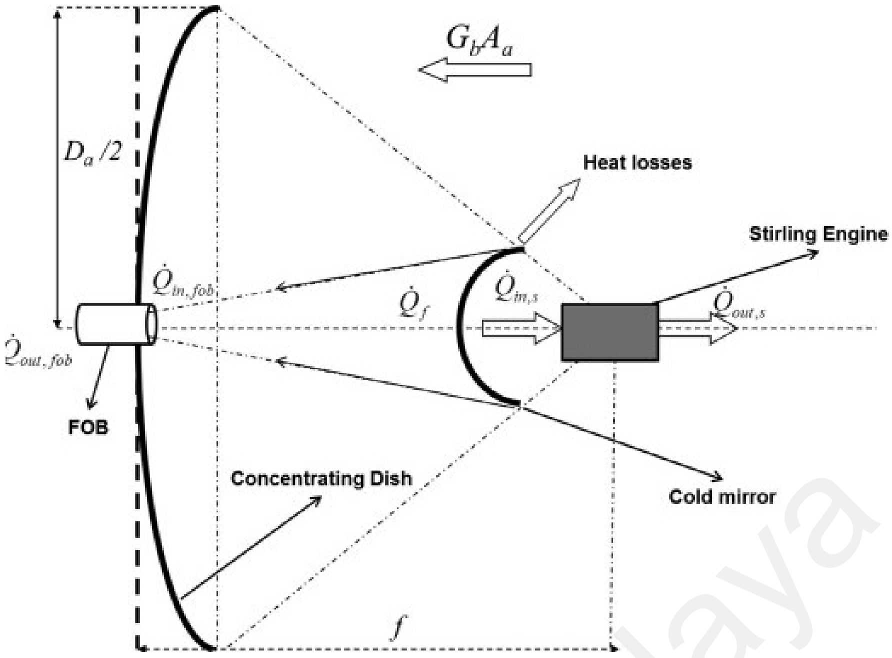

Figure 2.16: Illustration for the LIPGECOS setup (Rizzo et al., 2017)

Sarswat et al. (Sarswat et al., 2017) also proved that energy conversion efficiency of solar cells (GaAs and c-Si solar cells) can be improved by 10% with the use of prism-cylindrical lens combination method for spectral splitting of white light. Towards achieving the subdivision of a broad spectrum into several energy ranges, the setup is rather simple, which consists of a dispersive equilateral prism, a cylindrical lens, sample solar cells mounted on a scanning stage and lastly, a light source as shown in Figure 2.17. For this experiment, the prism and the lens are the key component whereby their positions were chosen as the setup below to maximize the dispersion. When the white light from the collimated fibre source, it is dispersed by the prism. Every colour in the dispersed beam is then portrayed to a laterally separated line by the lens (Sarswat et al., 2017).

University of Malaya

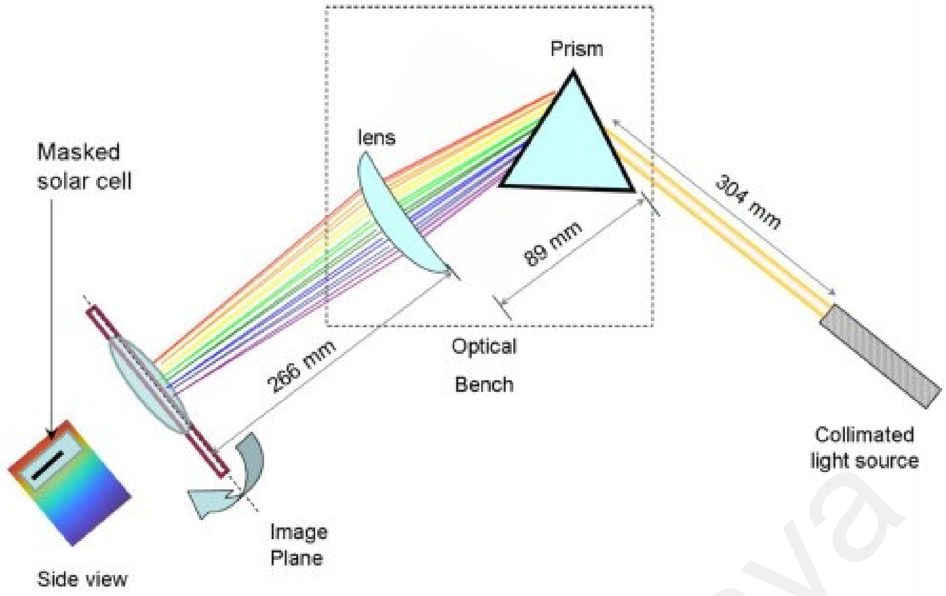

Figure 2.17: Schematic view of spectral splitting setup (Sarswat et al., 2017)

Another approach for the spectral splitting is by implementing a liquid-based spectral splitting method. A research by Ni et al. (Ni, Li, An, & Zhu, 2018) showed that by using nanofluid-based spectral splitting technique on photovoltaic/thermal system (NSS-PV/T), the overall efficiency can be further enhanced and proven to be higher than the conventional hybrid system. The merit becomes more apparent when the heat-to-electricity ratio was increased, whereas the value of overall efficiency of the NSS-PV/T system reached up to 16.2% with the aid of cell waste heat collection.

In concentrator photovoltaic system, the overall efficiency of the system often drops due to problems such as current mismatch and hotspots in solar cells which is caused by illumination non-uniformity (Yeh & Yeh, 2018). However, these problems are tackled by Yeh et al. (Yeh & Yeh, 2018) in a remarkable research which exploited a spectrum control method to enhance the concentration flux uniformity as well as redirects energy which could lead to the increase in temperature by utilizing Fresnel lens. By using the correctly positioned dichroic mirrors and the right dimension of second stage reflectors, this study

University of Malaya

resulted reallocation of temperature propelling energy and desired spectrum being directed in the targeted areas with the use of spectrum splitters.

2.3.6 Tandem system

Another concept for improving solar devices is by creating ‘tandem junction’, by placing a wide-band gap ‘top-cell’ on top of a silicon cell known as ‘bottom-cell’ (McMeekin et al., 2016). Generally, tandem cells ca be fabricated in either 2-terminal (2-T) or 4-terminal (4-T) configurations, representing distinct extremums in the optical and electronic coupling space (Adhyaksa, Johlin, & Garnett, 2017). The difference between these two terminals is the 2-T design is monolithic and series of interconnected cells are needed whereas the 4-T design consists of cells being stacked mechanically and the design allows those cells to be connected independently. Both designs have some drawbacks which could cause some efficiency losses about 10-11% (Mailoa et al., 2016; Rowell & McGehee, 2011). Therefore, the 3-terminal (3-T) configuration was introduced with possibilities for picking up the advantages of both standard configurations on top of avoiding their downsides (Bahro et al., 2015; Martí & Luque, 2015).

With tandem system approach, the efficiency of silicon solar cell can increase from 25.6 to above 30% (Green, Emery, Hishikawa, Warta, & Dunlop, 2015b; Sivaram, Stranks, & Snaith, 2015). An example of the device architecture of the planar heterojunction of the solar cell using tandem approach is shown in Figure 2.18 by using scanning electron microscope (SEM). McMeekin et al. (McMeekin et al., 2016) stated that metal halide perovskite PV cell has the potential to increase the efficiency of commercial silicon PV cells by about 20-30% when tandem architecture is introduced into the system. Nonetheless, this system faces many difficulties of finding the ideal wide-band gap materials that offers stability, cost-effective with high performance for

University of Malaya

crystalline and thin film solar technologies (McMeekin et al., 2016). To tackle such issues, Sahli et al. (Sahli et al., 2018) proposed a tandem cells featuring a nanocrystalline silicon recombination junction as well as silicon heterojunction cell by using a top cell deposition technique. As a result, a steady-state efficiency of 25.2% and current density of 19.5 mAcm^{-2} were attained due to the pyramidal texture of the silicon(Sahli et al., 2018).

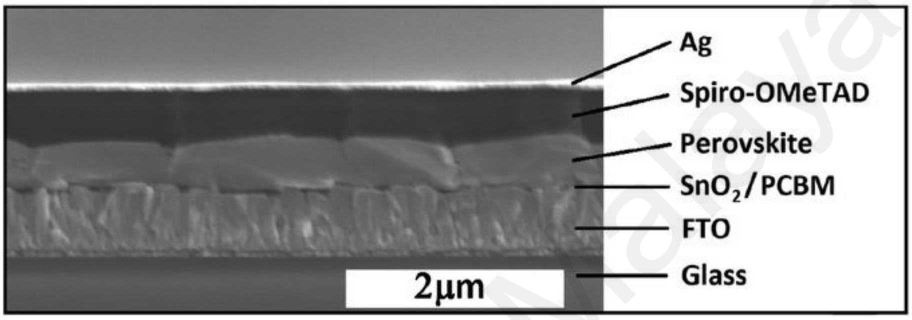

Figure 2.18: SEM image of the cross-section of a planar heterojunction of solar cell system (McMeekin et al., 2016)

In hybrid tandem solar cell technology, Blanker et al. (Blanker et al., 2018) has developed two-terminal hybrid tandem solar cells which contributed towards an efficient light management without damaging the electrical performance (Blanker et al., 2018). By compromising copper-indium-gallium-di-selenide (CIGS) with amorphous silicon (a:Si) absorber along with surface morphology manipulation, reflectance of the device managed to be reduced with optical optimum of $11.59 \pm 2.61\%$ reflection under a range of wavelength of 300-1000 nm (Blanker et al., 2018). The use of haze managed to improve the efficiency by using tandem systems has also been proven in a similar work made by Bush et al. (Bush et al., 2016), whereby a mechanically stacked perovskite/silicon tandem performance is studied as shown in Figure 2.19. From the J-V curve below, the efficiency of mono-Si alone is 17%. However, with the semi-transparent perovskite solar cell

University of Malaya

stacked on top of the mono-Si cell, the efficiency went up to 18% (12.3% + 5.7%) in the tandem, with the J_{sc} of 13.3 mA cm^{-2} from the bottom filtered Si cell.

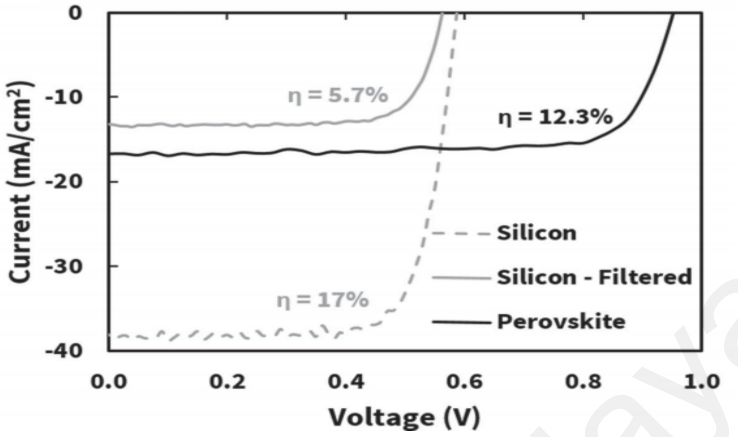

Figure 2.19: J-V curve of the tandem with maximum power of tandem that is calculated from the addition of silicon cells and perovskite (Bush et al., 2016)

A remarkable recent work has also been made whereby the power conversion efficiency is raised from 34% to 45% by using tandem systems. Pazos-Outón et al. (Pazos-Outón et al., 2017) promoted the use of this system for spectral stability by using voltage-matched tandem solar cells and taking into account its traditional series-connected counterparts. The study demonstrated how singlet fission can be used to produce simple voltage-matched tandems as shown in Figure 2.20 (a). The tandem cell demonstrates an efficient photo-current addition, leading to external quantum efficiency exceeding 100% at pentacene's main absorption peak as shown in Figure 2.20 (b).

University of Malaya

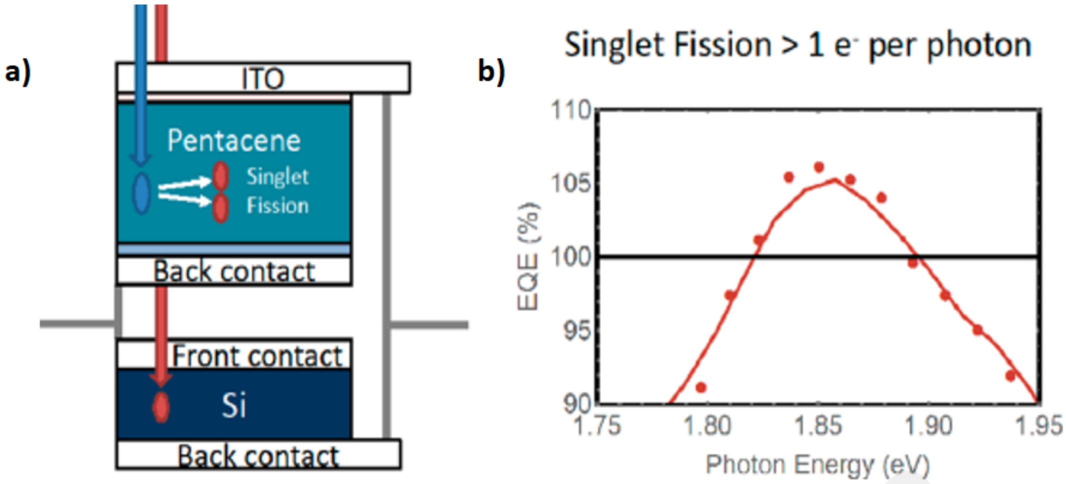

Figure 2.20: a) A mechanism of the parallel tandem cell and b) EQE graph of the tandem (Pazos-Outón et al., 2017)

A recent study made by Wu et al. (Wu, Li, & Klimov, 2018) has opened the door of possibilities for a combination of several approaches into a single solar system whereas the new concept of solar spectrum splitting in tandem luminescence solar concentrator (LSC) was proposed. The LSC which serves as large-area sunlight collectors in a tandem architecture leads to the efficiency gains with increasing of LSC size. For the prototype device, it is reported that under sunlight illumination, a remarkably high optical quantum efficiency of 6.4% as well as solar-to-electrical power conversion efficiency of 3.1% were obtained in the research. Bi et al proposed that the implementation of PV absorbers into the perovskite and Si-based solar cells is a crucial point for creating tandem solar cells with cost-effective and remarkable efficiency (Bi et al., 2018). In the study, the application of hybrid organic-inorganic ligand exchange process in to quantum dot solar cell along with perovskite film has also proven to deliver an additional 3.3% of power conversion efficiency (PCE) by utilization of over 750 nm of light.

University of Malaya

Some advancements that have been made by researchers have obviously shown numerous improved results however, the increased efficiencies are yet to compete the conventional energy source that we are currently exploiting worldwide. From our standpoint, to replace the use of fossil fuels which are depleting over time, beside focusing on increasing the efficiencies of solar technologies, the costs for constructing contemporary solar engineering systems should also be considered since large-scale of highly efficient solar devices often require a lot of maintenance and space. It is however a difficult challenge to achieve both efficient and economic cost at the same time but with the right combination of technologies, it can be accomplished soon.

University of Malaya

2.4 Nanoparticle coatings

There are various methods that have been implemented in solar industry to improvise the performance of solar devices in the attempt to catch up with the efficiency of conventional energy sources. A recent and popular method is by using nanotechnology in the solar research which has been proven by recent findings to improve solar technologies. The use of nanoparticles for solar cells is an effective strategy and economically feasible method that leads to high efficiency of solar cells (McLeod, Hages, Carter, & Agrawal, 2015).

Ananthoju et al. (Ananthoju, Mohapatra, Bahadur, Medhekar, & Aslam, 2019) proposed a simple and cost-effective way to implement Cu_2ZnSnS_4 (CZTS) nanoparticles in absorber layer for solar cells. In order to replace the conventional toxic absorber layers, CZTS was used as it has numerous attractive properties such as non-toxic, abundant, has suitable bandgap, high electrical conductivity and absorption coefficient, making it an ideal choice for solar energy conversion systems. In the study, it was found that with the increasing sizes of CZTS nanoparticles, the power conversion efficiency were also increased from 3.6% to 4.8% under AM 1.5G solar illumination as seen from the J-V curve in Figure 2.21 (Ananthoju et al., 2019).

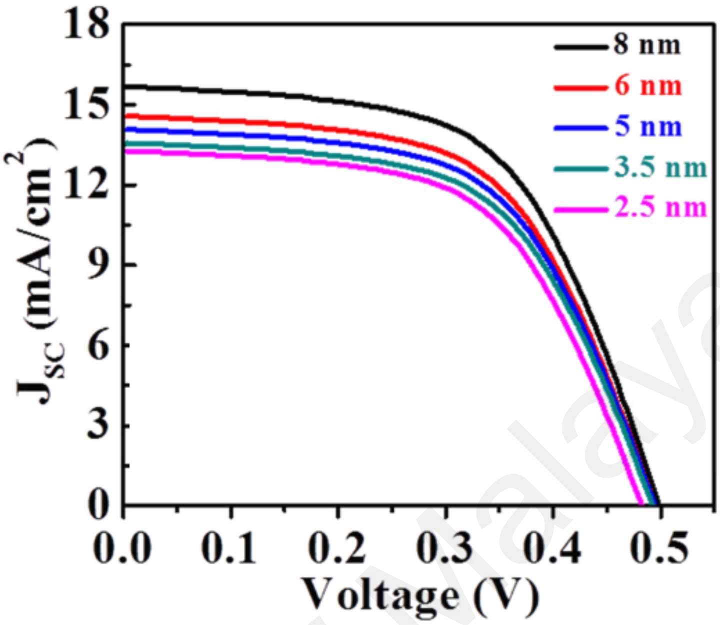

Figure 2.21: The J-V curve of solar cells with different sizes of CZTS nanoparticles (Ananthoju et al., 2019)

University of Malaya

The use of silicon (Si) nanoparticles as an active layer in a solar cell has been researched by Ichihara et al. (Ichihara et al., 2018) he has used spin-coating method to deposit i-type silicon nanoparticles (i-SiNPs) on a glass substrate forming a thin film. The overall result showed that the i-SiNP coating layer managed to aid the solar cells to achieve a high open circuit voltage (V_{OC}) of 140mV and V_{OC} is an important parameter to enhance the efficiency of solar cells (Green, 1984). Figure 2.22 below shows the position of i-SiNP film as an active layer that was sandwiched in between amorphous silicon (a-Si) layers.

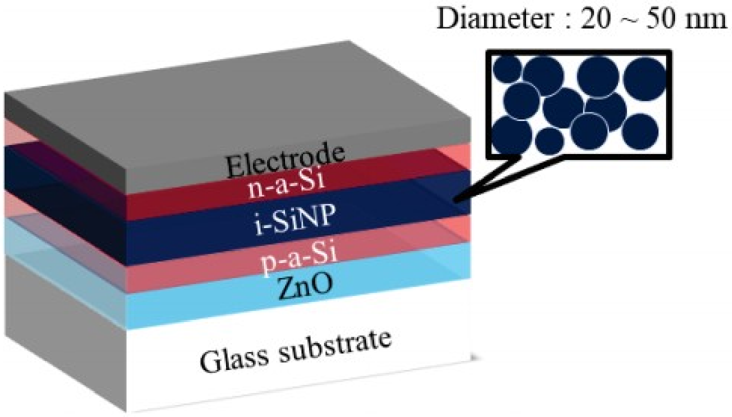

Figure 2.22: An illustration of solar cell structure with i-SiNP active layer (Ichihara et al., 2018)

University of Malaya

Researches on nanoparticle coatings for solar cells are growing and are being put into practice in various creative ways. Thirugnanasambandan et al. has reported on the use of silver nanoparticles as a thin film coating which was deposited on the solar cell itself and this work leads to an ongoing exploration on novel glass frits for future generation smart solar cells (Thirugnanasambandan et al., 2018). The efficiency of solar cells was multiplied with the implementation of silver nanoparticles ultra-thin film which was deposited on the silicon solar cells due to the reduced contact resistance of solar cells. This work has successfully shown the fabrication of hybrid composite solar cells with unique nature which separate the absorber layer by using silver nanoparticles as shown in Figure 2.23.

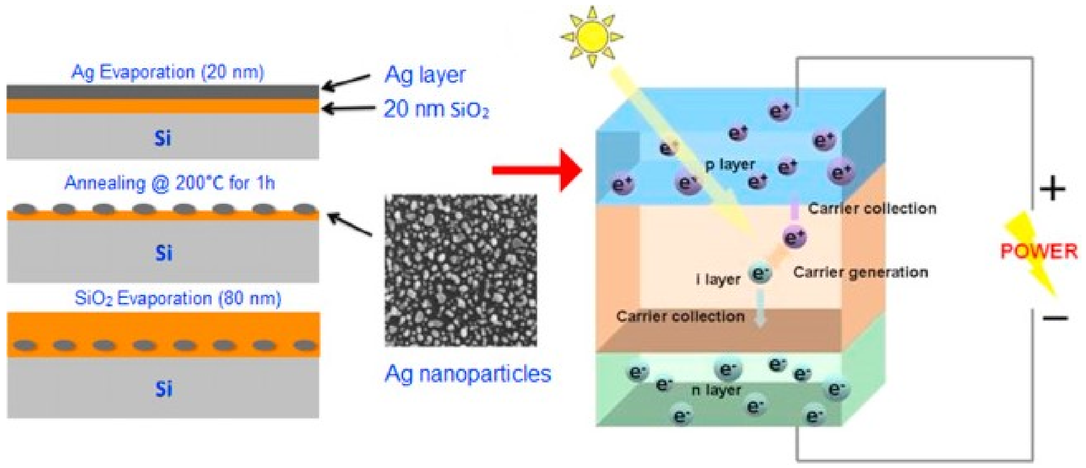

Figure 2.23: The schematic diagram showing the configuration of solar cell with a PN junction and silver nanoparticles (Ag) which are embedded with silicon dioxide layer SiO_2 (Thirugnanasambandan et al., 2018)

Nanoparticle coatings are also being implemented in a larger scale in solar energy industry. Solar absorbing coatings was used for concentrated solar power plant (CSP) by using various Cu(II) containing spinel oxide nanoparticles for improved optical properties and long term thermal properties of (Rubin, Chen, & Chen, 2019). The research focused on the optical characteristics and long-term thermal stability of solar absorbing coatings (SACs) which are made from many types of Cu(II) that contains spinel oxide nanoparticles ($CuCr_2O_4$, $Cu_{0\cdot5}Cr_{1\cdot1}Mn_{1\cdot4}O_4$, $CuFeMnO_4$) to be compared with Pyromark 2500 coating. Before thermal annealing, it was observed that the porous $Cu_{0\cdot5}Cr_{1\cdot1}Mn_{1\cdot4}O_4$ achieved the highest solar absorptance at 97.1% and hence, contributing to both nanostructuring and intrinsic solar absorptance properties leading to enhanced photothermal performance.

Nanotechnology in form of coatings which is specially engineered for the use of solar technologies has open new door of possibilities to ensure maximum amount of electricity is produced while having maximum lifetime at minimum cost. Therefore, it is convinced that with rapid developments of nanoparticle coatings in solar industries, solar energy can

University of Malaya

be the primary choice for source of energy in future, replacing the conventional ones which are getting depleted over time.

University of Malaya

CHAPTER 3: METHODOLOGY

3.1 Introduction

In this chapter, a complete detail on the materials, methods, characterizations and equipment used for producing the nanoparticle coatings in two types of binder systems are discussed. The methodology of the fabrication of coatings that uses three types of nanoparticles (TiO_2, SnO_2 and ZnO) is discussed extensively in this section. The section begins with the naming of coating systems, followed by the preparation of coatings and subsequently the characterization analysis in terms of structural, electrical as well as thermal properties.

3.2 Experimental works

3.2.1 Coating systems

The solar cells used in this study were purchased from H&N Total Resources Sdn. Bhd. Malaysia and the purchased solar cells have surface area of 15.6 cm^2, blue-colored and with thickness of 200µm. The chemicals ordered from suppliers were utilized without further purification. 3-Aminopropyltriethoxysilane (APTES), which is famous for its ability to give good electrical properties to a system (Hafeez et al., 2019) and to facilitate the sticking of coating mixture onto the substrates (Múgica-Vidal, Alba-Elías, Sainz-García, & Pantoja-Ruiz, 2015), was purchased from Shin-Etsu Chemical Co., Ltd. (USA) in liquid form. Methyltrimethoxysilane (MTMS) in liquid form, which is from Merck (Malaysia) is chosen as co-precursor in the coatings and it has been widely used in previous studies to increase thermal insulation property of a system (Pan et al., 2017; Ulhaq et al., 2017). Titanium dioxide, TiO_2 (Anatase), Zinc Oxide, ZnO and Tin dioxide, SnO_2 nanoparticle powders were also purchased from Merck (Malaysia). Isopropyl alcohol ($CH_3CHOHCH_3$) and nitric acid (HNO_3) were purchased from Sigma-Aldrich

University of Malaya

(Malaysia). Isopropyl alcohol is used as solvent for the coating mixture and HNO_3 is used to aid the monodispersion of nanoparticles in the coating system (Ito, Kitamura, Wada, & Yanagida, 2003). In this work, two types of binder systems were used namely; 3-Aminopropyltriethoxysolution (APTES)/Methyltrimethoxysilane (MTMS) binder and Methyltrimethoxysilane MTMS)/nitric acid (HNO_3) binder. Different weight ratios of nano-TiO_2, nano-ZnO and nano-SnO_2 were incorporated into both type of binders. The label and blending ratios and formulation of nanoparticle coating systems were tabulated in Table 3.1.

Table 3.1: Types of nanoparticles coating systems

Nanoparticles	**Weight percentage (wt%)**	**Coating Systems**	
		Binder 1 (B1): APTES/MTMS	**Binder 2 (B2): MTMS/HNO_3**
Titanium dioxide (TiO_2)	20 (T1)	T1B1	T1B2
	60 (T2)	T2B1	T2B2
Zinc dioxide (ZnO)	20 (Z1)	Z1B1	Z1B2
	60 (Z2)	Z2B1	Z2B2
Tin dioxide (SnO_2)	20 (S1)	S1B1	S1B2
	60 (S2)	S2B1	S2B2

3.2.2 Preparation of coatings

The synthesizing process of coating systems as illustrated in Figure 3.1 requires three steps including sonicating process, stirring process as well as coating application:

University of Malaya

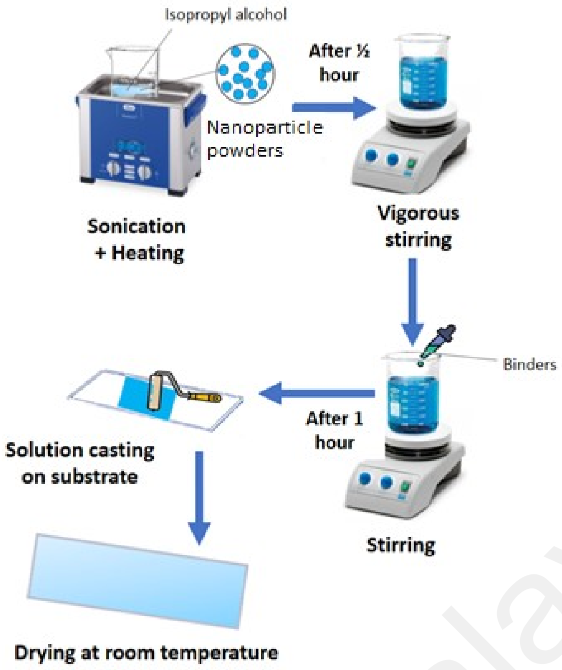

Figure 3.1: Fabrication of nanoparticle coating on glass substrate

1. **Sonication**: Firstly, nanoparticles was sonicated inside 90 ml of isopropyl alcohol by using ultra-sonicator bath for 30 minutes at 50°C in order to create a well-dispersed solution as shown in Figure 3.2.

Figure 3.2: Sonication of nanoparticle solution by using Ultra-sonicator

University of Malaya

2. **Stirring**: After that, the nanoparticles were stirred with isopropyl alcohol using a magnetic stirrer which was stirred at 400 rpm at room temperature for 1 hour as shown in Figure 3.3. During the stirring process, 5% of APTES and 5% of MTMS were added to the nanoparticles mixture and stirred again for another one more hour to produce an even and a well-mixed solution.

Figure 3.3: The stirring process of the nanoparticle solution

3. **Coating Application Method**: Finally, the solution was coated onto glass panels via dip-coating method. The coated glass panels were dried under room temperature room (approximately 25ºC) for 20 minutes before subjecting to further characterization.

University of Malaya

3.3 Characterization techniques

3.3.1 Field Emission Scanning Electron Microscopy (FESEM) analysis

Field emission scanning electron microscopy (FESEM) is a microscope that operates with electrons which are liberated by field emission force instead of using light. Researchers employed this characterization to observe tiny structures as small as one nanometer which is equals to around one billion of millimeter (Phillips, Horr, Huson, Turner, & Shanks, 1995) (Goldberg, 2008).

FESEM provides detailed particulars on elemental and topographic information of the samples with coatings whereby the magnification can be increased to 300,000x along with virtually infinity depth of field. FESEM has the ability to determine the structure uniformity of the coating samples and examine small-area contamination sites at electron accelerating voltages. Finest structural morphology of nanomaterials on the specimens can be obtained at low voltages with negligible electrical charging of the specimens, showing another feature of FESEM (Chandran, Begam, Padmanabhan, & Basu, 2014). Figure 3.4 shows an example of FESEM images of nanoparticle dispersions, whereby the white spots represents the nanoparticles (Jiao, Seraphin, Wang, & Withers, 1996).

University of Malaya

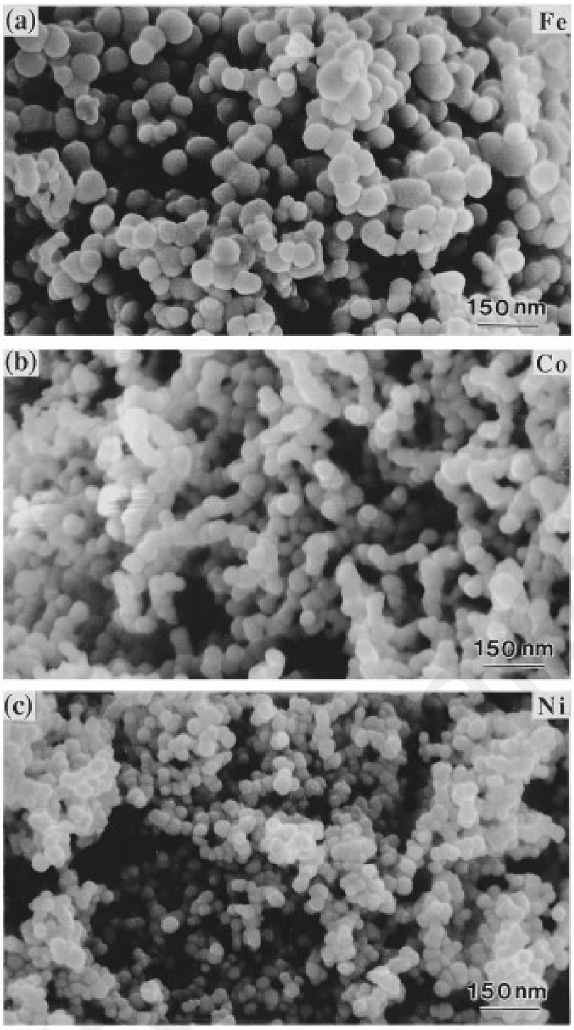

Figure 3.4: FESEM morphology of carbon-coated metal particles: a) iron, Fe particles, b) cobalt, Co particles and c) nickel, Ni particles. (Jiao et al., 1996)

3.3.2 Energy Dispersive X-ray Spectroscopy (EDX)

Energy Dispersive Spectroscopy (EDX) is a standard method to identify and quantify compositions of elements in a sample. EDX is a powerful tool to detect types of nanoparticles in many fields of studies (Ebnesajjad, 2011) (Scimeca, Bischetti, Lamsira, Bonfiglio, & Bonanno, 2018). It uses an analytical technique on the surface whereby the electron beam strikes on the coated sample, leading to an electron excitement in the inner shell, its injection as well as the formation of the electron hole within the elemental electronic structure. As energy of photon is transferred to the bound inner shell, atomic

University of Malaya

electron is then ejected with kinetic energy and reduces binding energy of atom. Consequently, the ejected photoelectron experience inelastic scattering in the Si crystal. Approximately, the charge generation process requires 3.6 eV per electron hole pair to make the number of charge carriers (n)proportional to the original energy of the photons(E_P) as shown in Equation 3.1 (Goldstein et al., 2017);

$$n = {}^{E_P}/_{3.6\ eV} \tag{3.1}$$

In nanoparticle coatings, EDX is used to obtain atomic compositions and percentage of the coating sample. Impurities can also be detected from EDX data patterns. Figure 3.5 shows an example of EDX mapping to highlight the presence of silicon (Si) and cupric oxide (CuO) particles in silicon nanoparticles doped cupric oxide (Si-NPs-CuO) pellet (Ahmmed, Aktar, Kuddus, & Ismail, 2018).

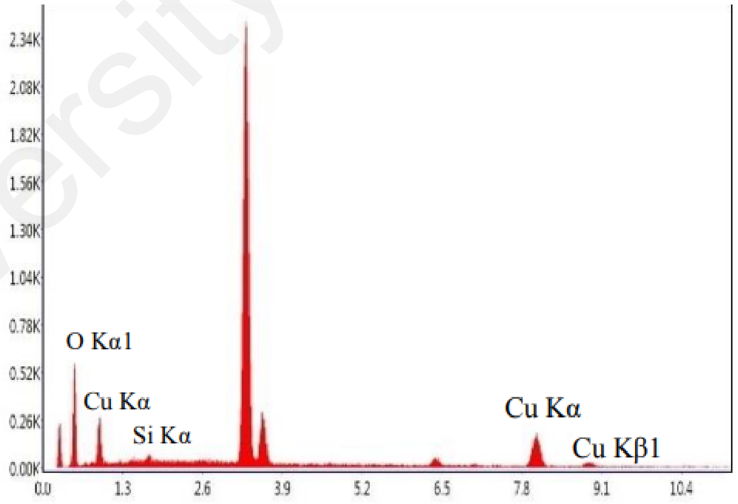

Figure 3.5: EDX mapping of Si-NPs-CuO pellet (Ahmmed et al., 2018)

University of Malaya

3.3.3 Contact Angle measurement

The contact angle, which is also known as the wetting angle, is a measure of wettability of a solid by a liquid. When a liquid touches the surface of a solid, the angle of the interface between the surface of the liquid and the surface of the solid is defined as contact angle, ϴ. Contact angle with one or more water droplets is used to determine free energy of the surface of a solid. Low contact angle value shows that the water is most likely to spread on the surface of the solid (hydrophilic)(Hirose, Zhou, & Nagai, 2000). Oppositely, high contact angle value demonstrates the tendency of the surface of the solid to repel water (hydrophobic) (Huhtamäki, Tian, Korhonen, & Ras, 2018). A complete spreading of water on the surface of a solid (complete wetting) is where the contact angle is 0° which is also called super-hydrophilicity (Wei et al., 2007) . When the contact angle is between 0° and 90°, the surface of the solid is considered wettable whereas the above 90°, the surface of the solid is not wettable (Drelich, Chibowski, Meng, & Terpilowski, 2011). As the contact angle reaches the theoretical limit of 180°, the surface of the solid experiences a phenomenon called the lotus effect, showing that the solid is ultra-hydrophobic materials (Gao & McCarthy, 2006; Marmur, 2004). Super hydrophilicity is when the contact angle is reaching 0°.

In coating and paint industries, contact angle measurement is important to determine the physical properties of the surface of a solid in terms of water repellent and absorbance (Osterhold & Armbruster, 1998). It highlights the wettability of the surface materials which can be achieved by coatings according to application preferences. An ideal coating for solar cells should be able of resist contamination whereby hydrophobicity of a material plays a part that leads to “self-cleaning” condition (Prevo, Hon, & Velev, 2007). Figure 3.6 shows an example of images of static water droplets with their respective contact angles on various surface conditions (Forrest et al., 2010).

University of Malaya

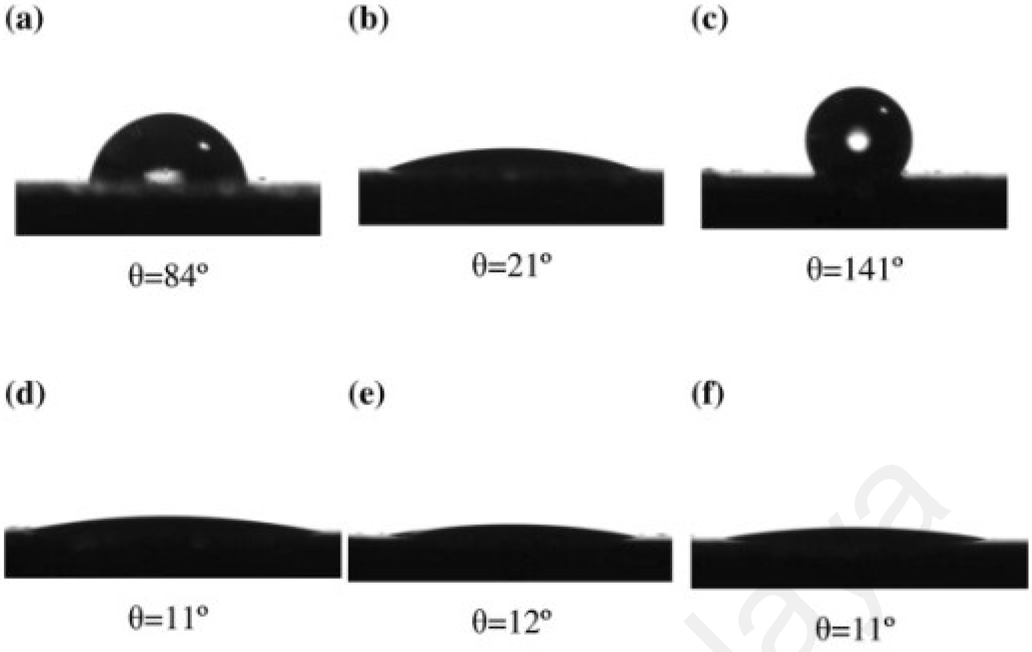

Figure 3.6: Images of static water droplets with their respective contact angles on different surface of coated samples (Forrest et al., 2010)

3.3.4 Ultraviolet Visible Spectroscopy (UV-Vis)

Ultraviolet-visible spectroscopy (UV-Vis) is a simple and low-cost method which is used widely in material or chemical analytical characterization and identification. It applies a quantitative analytical technique that involves absorption of near-infrared, IR with wavelength range of 180 nm to 390 nm and visible region with wavelength range of 390 nm to 780 radiation in organic and inorganic constituents in broad range of sample matrices. UV-Vis is used to measure transmittance, which is expressed in percentage (% T), is the energy of the light's ratio that falls on a body which transmitted through it as shown in Equation 3.2. A device which is called UV-Vis spectrophotometer is used in the UV-Vis to measure the light which passes through a sample, I. It is then compared to the intensity of the light before it passes through the same sample, I_o (Skoog, Holler, & Crouch, 2017).

University of Malaya

$$T = {}^{I}/_{I_o} \tag{3.2}$$

A improved efficiency of solar devices can be achieved with transparent coatings as it is proven that they can produce high energy conversion efficiency under 100 mW irradiance of AM 1.5 white light (Hong, Xu, Lu, Li, & Shi, 2008). From the UV-Vis transmission spectra, transparency of coatings can be measured whereby the higher the percentage of transmittance, the higher the transparency of the coatings (Li, Liu, & Sun, 2009). Also, a high transmittance also indicates that the coating has a low reflection. Figure 3.7 shows an example of transmission spectra of four types of coating films on quartz substrates (Li et al., 2009).

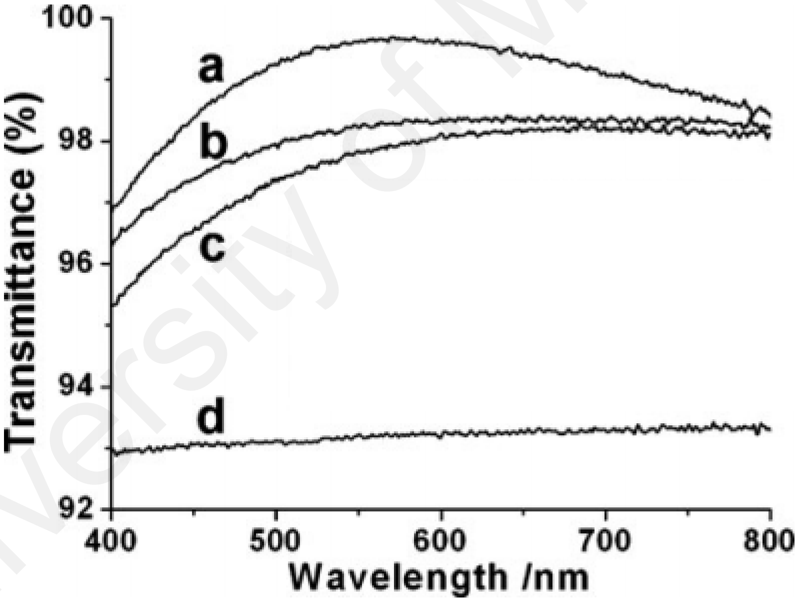

Figure 3.7: Transmission spectra of different bilayers of poly(allylamine hydrochloride) (PAH)/SiO_2 nanoparticle films on top of the poly(diallyldimethylammonium chloride) (PDDA)-sodium silicate and poly(acrylic acid) (PAA) film which are deposited on quartz substrates (Li et al., 2009)

3.3.5 Fourier-Transform Infrared Spectroscopy (FTIR)

Fourier Transform Infrared Spectroscopy, FTIR or FTIR Analysis is a non-destructive technique that uses infrared light to scan the experimental samples for the identification

University of Malaya

of various types of materials such as polymeric and organic materials. It is a useful instrument to obtain information on bonding mechanisms on surface of materials and in solids (Peak, 2005). FTIR uses spectral fingerprinting technique, whereby it is a comparison of the unknown samples to the spectra of the known samples for the determination of the unknown structures. Table 3 shows the classification of absorption peak range obtained from the coating samples through FTIR analysis with their respective bands.

Table 3.2: Classifications of absorption peak range with their respective bands

Bands	Range of wavenumber (cm^{-1})	References
Si-C	800 - 865	(Adamczyk & Długoń, 2012; Masson, Paquin, Poulin-Dandurand, Sacher, & Yelon, 1984)
Si-OH bending	900 - 950	(H. S. Mansur, R. L. Oréfice, & A. A. Mansur, 2004)
Si-O-Si stretching	1000 - 1200	(Kanemitsu & Okamoto, 1997; Herman S Mansur et al., 2004)
Si-CH_3 deformation	1254 - 1277	(Mhaisagar, Joshi, & Mahajan, 2012; Sun, Thomas, Crooks, & Ricco, 1991)
CH_3 deformation	1400 - 1420	(Depan, Shah, & Misra, 2011; Sagdinc & Bayari, 2004)
H-OH band	≈ 1648	(Yang et al., 2010)
Si-H_n bending	2049 - 2156	(Adjallah, 2010; Belogorokhov, Gavrilov, Kashkarov, & Belogorokhov, 2005; Masson et al., 1984)

University of Malaya

Si-OH stretching	3200 - 3600	(Burgos & Langlet, 1999; Herman S Mansur et al., 2004; Singh, Wu, & Williams, 2012)
CH_3 stretching	2800 - 3200	(Burgos & Langlet, 1999; Jang & Wilkie, 2004)

In thin film and coating field, FTIR is important to determine the modes of chemical bonding of the coating samples. The comparison of different coatings with similar precursor solution can determine new shifts or peaks in FTIR spectra which might indicate some important phenomenon such as aggregation, blending or cross-linking between the molecules in the coating systems. Figure 3.8 shows an example of FTIR spectra of silicon dioxide film which was deposited on silicon substrates by using chemical vapor deposition (PECVD) technique at different pressure of 1 and 0.1 mbar for sample A and sample B respectively (Shokri, Firouzjah, & Hosseini, 2009). The transmitted peaks are noted and labelled according to their wavenumbers (cm^{-1}). The peaks at 1085, 800 and 460 cm^{-1} are classified to the stretching, bending and out of plane of Si-O bands respectively. The FTIR spectra also shows that the deposited films contained a large amount of OH groups in the sample coatings at approximately 2500cm^{-1}. According to Shokri et al. (Shokri et al., 2009), this peaks will decrease if annealing method is applied.

University of Malaya

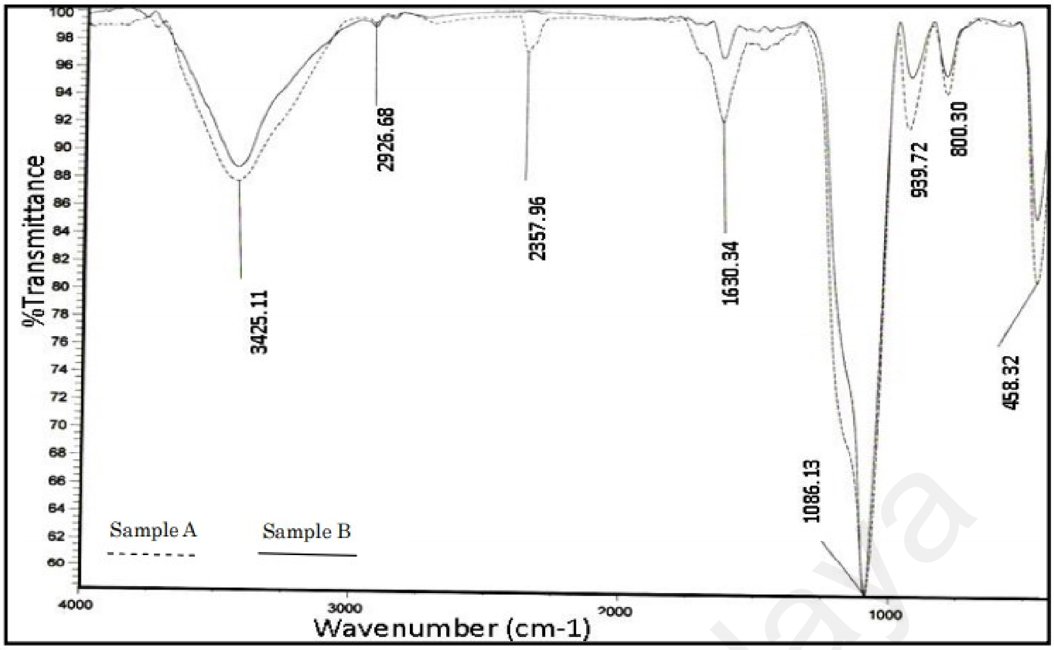

Figure 3.8: FTIR spectra of sample A and sample B (Shokri et al., 2009)

3.3.6 X-ray Powder Diffraction (XRD)

X-ray diffraction is a method that depends on dual wave particles on nature of the X-rays to acquire information on crystallinity of a compound (Nallusamy & Manoj Babu, 2016). Identification of unknown solids is crucial in material coating and paint studies for measurement of sample purity and characterization of crystalline materials. Based on the crystalline sample and constructive interference of monochromatic X-rays, XRD analysis generates a unique polymorphic forms, the “fingerprint” pattern of the crystals in the samples (Maurin, Pluciński, Mazurek, & Fijałek, 2007). After proper interpretation, by comparing with standard reference measurements and patterns, the “fingerprint” patterns give the recognition of the crystalline forms. Figure 3.9 shows an example of XRD pattern of a nanoparticle coating sample (Ma et al., 2003).

University of Malaya

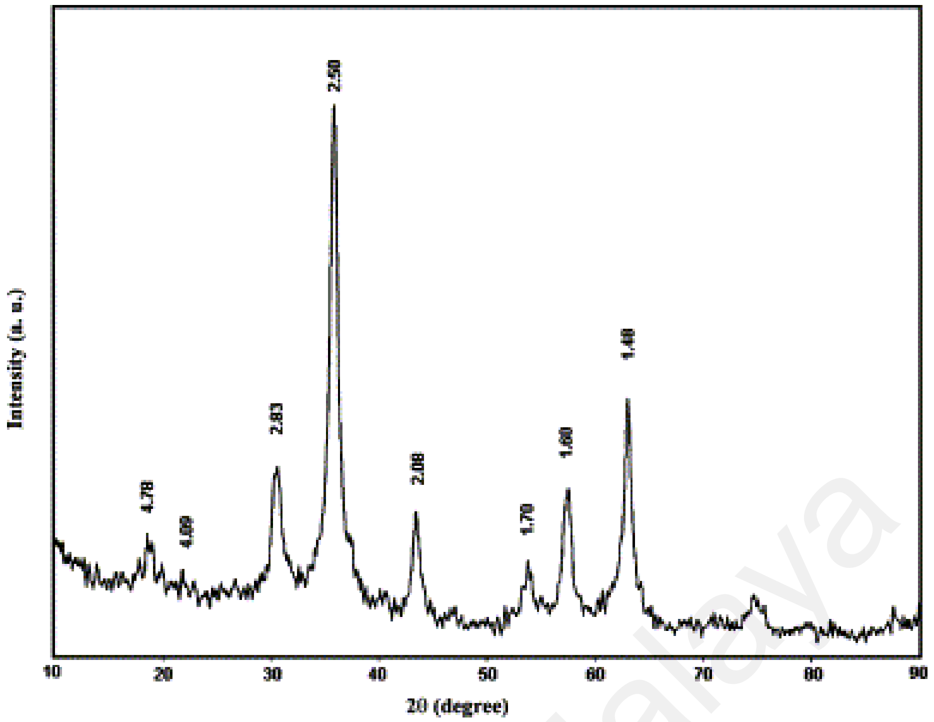

Figure 3.9: XRD pattern of a sample coating containing magnetite, Fe_3O_4 nanoparticles and aminopropyltriethoxysilane, APTS (Ma et al., 2003)

A polymorph refers to one of well-defined materials with same chemical composition with distinct crystal structures. Among polymorphs, the morphologies are different fundamentally because of a difference in crystal phase, leading to the difference in XRD pattern. Within the same polymorphs, XRD peak positions are identical despite having different crystal shapes and sizes due to the identical physical and chemical properties. Nonetheless, the diffraction peak intensities are different among the polymorphs due to the difference in total area of each crystal face following each crystal habit (Inoue & Hirasawa, 2013).

3.3.7 Solar Simulation

Solar simulator plays a crucial role in the testing of solar cells and devices which utilize solar radiation. Standard photovoltaic (PV) cells are used to place the intensity of the

University of Malaya

simulators to standard irradiation conditions for electrical characterizations of the PV cells (Lisbona, 2012). The Bentham ISR300, a single monochromator based on spectroradiometer along with integrated detection electronics is used in this work for electrical characterization of the coated and uncoated solar cells. It is enclosed with CL6-H standard of spectral irradiance and coupled with a D7 Cosine diffuser input optic for accurate and fast characterization of CW solar simulators for the range of 400 nm to 1100 nm irradiance, with an option for range extension until 2500 nm. Figure 3.10 illustrates the setup for the operation of solar simulation.

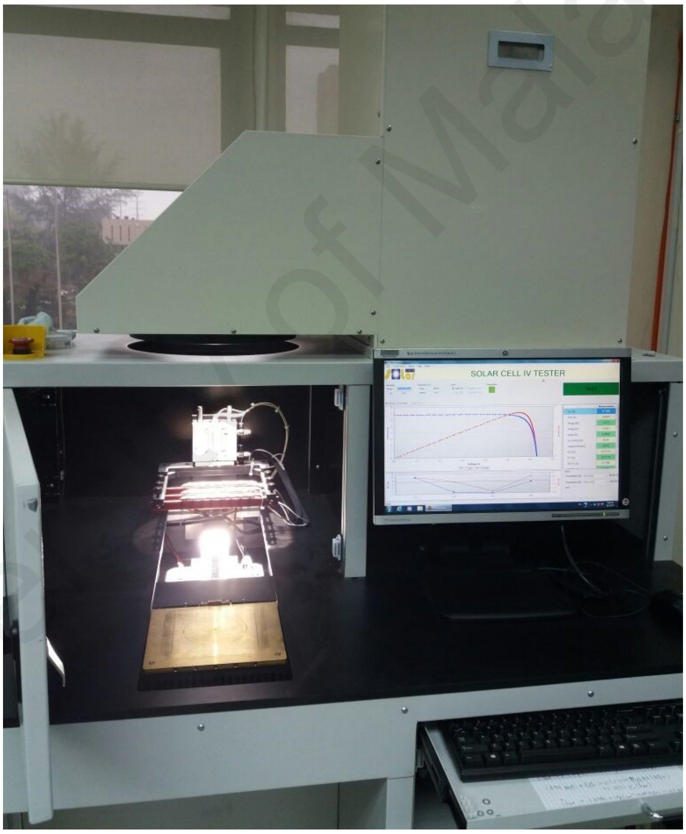

Figure 3.10: An overall setup for solar simulation

The Solar Cell IV-Tester provides wide range of information such as the current-voltage curve (I-V curve), power-voltage curve (P-V) curve, fill factor, efficiency, and many other electrical data on the solar cells under controlled parameters. It uses IVT-

University of Malaya

Solar as interface from the simulator to display the information obtained from the tested solar cells. There are many works that have been done by using solar simulators. A remarkable work was made by Shaheen et. al. (Shaheen et al., 2001) whereby 2.5% power conversion efficiency was achieved with organic plastic solar cells. In the study, measurements for electrical characterizations of solar devices such as power conversion efficiency, open circuit voltage, short circuit current density and fill factor were made under AM1.5 illumination by a solar simulator. Figure 3.11 is an example of J-V curve obtained from a solar simulator (Shaheen et al., 2001).

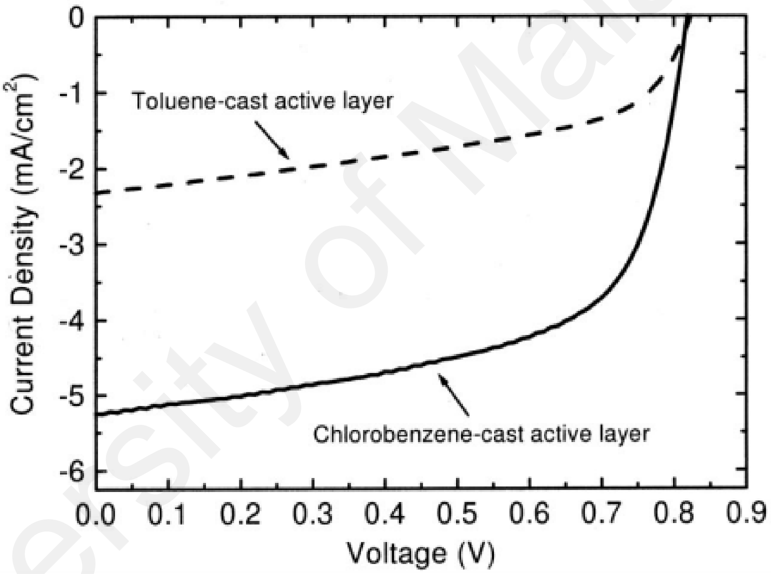

Figure 3.11: Electrical characterization for solar devices with an active layer from a toluene solution and from a chiorobenzene solution (Shaheen et al., 2001)

3.3.8 Thermal Analysis

For thermal characterization, lamp bulbs are used to illuminate solar irradiance which is measured by a pyranometer to obtain a standardize 1000 W/m^2 irradiance. The pyranometer is used to measure solar irradiance from all directions within a wavelength range of 0.3 μm to 3 μm from the hemisphere above. Moreover, type K thermocouple

University of Malaya

wires are used in this setup to measure the surface temperature of solar cells, as the thermocouples produces temperature-dependent voltages from the thermoelectric effect. The net conversion from thermal energy into electrical energy in form of electrical current is called Seebeck effect. As shown in Equation 3.3, for certain materials combination (A and B), a small temperature difference (dT) can be obtained (Measurement, 1993);

$$dE_S = \alpha_{AB} dT \tag{3.3}$$

where α_{AB} is the coefficient of proportionality (Seebeck coefficient), and E_S is the Seebeck voltage, which is the net thermal electromotive force that is set up in the thermocouples under zero-current condition.

The final step of the temperature characterization involves a data logger, an electronic device to record data over time as data acquisition system. With the thermocouples connected to it, the data logger is capable of recording temperatures over a certain period of time. The recorded digital data obtained from the data logger can then be saved and retrieved to be evaluated. Figure 3.12 shows the setup for the temperature characterization of the coated and uncoated solar cells for analyzation.

University of Malaya

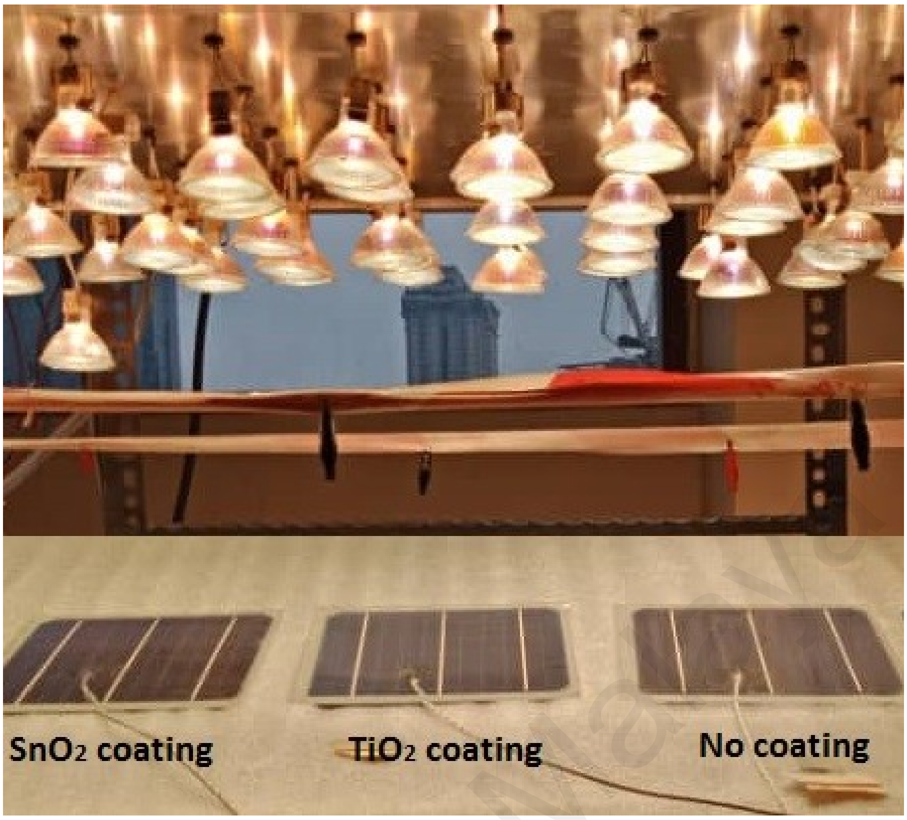

Figure 3.12: The physical setup for temperature characterization

The combination of thermocouples and data acquisition system for temperature studies in solar technologies was implemented in a work made by Sopian et. al. (Sopian, Liu, Kakac, & Veziroglu, 2000) for the performance of photovoltaic solar thermal collector. With a more defined architecture setup as shown in Figure 3.13, temperature rise and thermal efficiency at different mass flow rates were successfully measured (Sopian et al., 2000).

University of Malaya

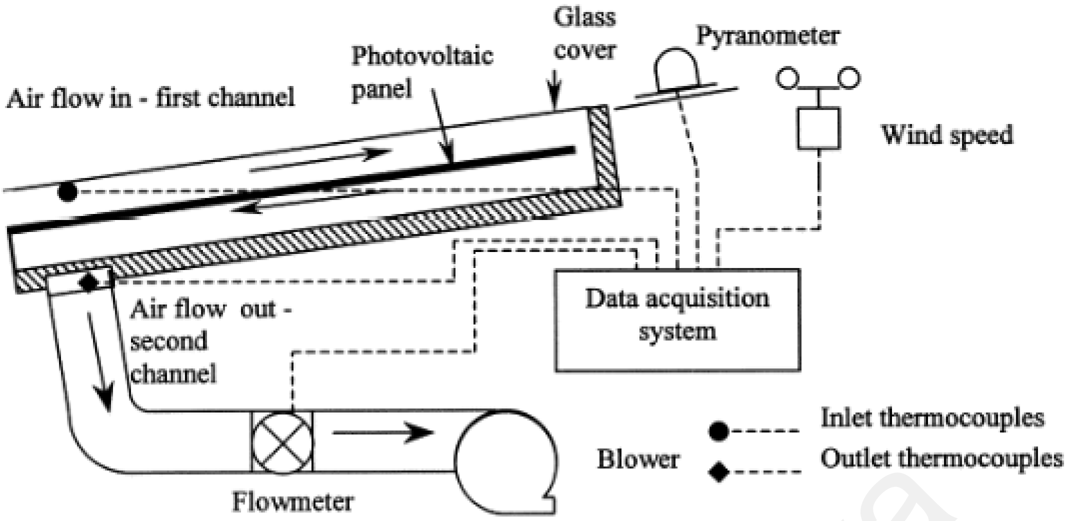

Figure 3.13: A setup for double pass photovoltaic thermal solar collector with the use of thermocouples and data acquisition system (Sopian et al., 2000)

University of Malaya

CHAPTER 4: RESULTS AND DISCUSSIONS

4.1 Introduction

This chapter presents the results of this work along with relevant explanation. Chapter 4 is divided into four main sections, whereby it is started off with the physical properties (contact angle and UV-Vis) of the nanoparticle coatings, followed by the structural (FESEM, EDX, FTIR and XRD) of the coated samples and electrical properties (solar simulation) of nanoparticle coating system on solar cells. The chapter is wrapped up with discussions on the main focus of the study, which is the thermal analysis of the nanoparticle coating systems on solar cells.

4.2 Physical Properties

4.2.1 Hydrophobicity of nanoparticle coatings

Water contact angle measurement is used to measure the hydrophobicity of nanoparticle coating systems in this study as shown Table 4.1.

University of Malaya

Table 4.1: The coating systems and their respective average water contact angles

	Nanoparticles (wt%)	Coating system	Contact angle (°)
No Coating	0	-	30 ± 0.27
Binder 1 (B1): APTES/MTMS	0	B1	69.25 ± 0.05
	20	T1B1	105.95 ± 0.45
	60	T2B1	107.55 ± 0.55
	20	Z1B1	92.35 ± 0.35
	60	Z2B1	102.85 ± 0.35
	20	S1B1	82.00 ± 0.50
	60	S2B1	125.00 ± 0.50
Binder 2 (B2): MTMS/HNO$_3$	0	B2	78.25 ± 0.25
	20	T1B2	90.65 ± 0.25
	60	T2B2	103.70 ± 0.05
	20	Z1B2	87.30 ± 0.30
	60	Z2B2	100.95 ± 0.15
	20	S1B2	89.25 ± 0.25
	60	S2B2	105.20 ± 0.20

University of Malaya

Table 4.1 shows that, in comparison with glass slide with no coating, the glass slides coated with binder solution managed to increase the contact angle value by approximately 40° for B1 binder coating system and 48° for B2 binder coating system. This proves that the binder solution managed to increase the surface roughness of the glass slides, leading to increased hydrophobicity of the binder-coated samples (Meiron, Marmur, & Saguy, 2004). The presence of MTMS in both binder systems act as a hydrophobic agent which has also been used in previous studies (Wheeler, Mendez-Vivar, & Fleming, 2003; Yokogawa, Yokoyama, Takahama, & Uegaki, 1996). B2 binder system has higher contact angle reading compared to B1 binder system as B2 binder system contains the right concentration of nitric acid which improves the adhesion of the coated samples, hence increasing the hydrophobicity of the coated glass slides (Bell & Ikeda, 2011; Wang et al., 2016).

Surface roughness of the coating samples was further increased as nanoparticles were introduced into the coating systems. S2B1 from B1 binder system and S2B2 from B2 binder system record the highest readings of 125.00 ± 0.50° and 105.20 ± 0.20° respectively. Compared to TiO_2 and ZnO nanoparticles, SnO_2 nanoparticles in the coating system increases the hydrophobicity of the nanoparticle coating samples better in both binder solutions. This is due to the large molecular structure of the SnO_2 nanoparticles inside the binder system which causes more air pockets between the atomic structures in the coating mixture, lowers the surface energy, causing the surface of the coating samples to become more porous and rough and hence, minimizes the contact area for the water droplet (Cassie, 1948; Nakae, Inui, Hirata, & Saito, 1998; Ogihara, Xie, Okagaki, & Saji, 2012).

It is also proven in this work that the higher the concentration of all nanoparticles in the binder solution, the higher the contact angle readings, leading to an improved hydrophobicity of the coated glass slides. This is because the concentration of nanoparticles in the binder system affect the wettability of the coated surface of the coated samples (Pilotek & Schmidt, 2003). Figure 4.1, Figure 4.2. and Figure 4.3 depict that different types of coated surface leads to changes in the shapes of static water droplet upon touching the nanoparticle coating samples. The shapes of the static water droplet lead to the various water contact angle readings (Forrest et al., 2010).

University of Malaya

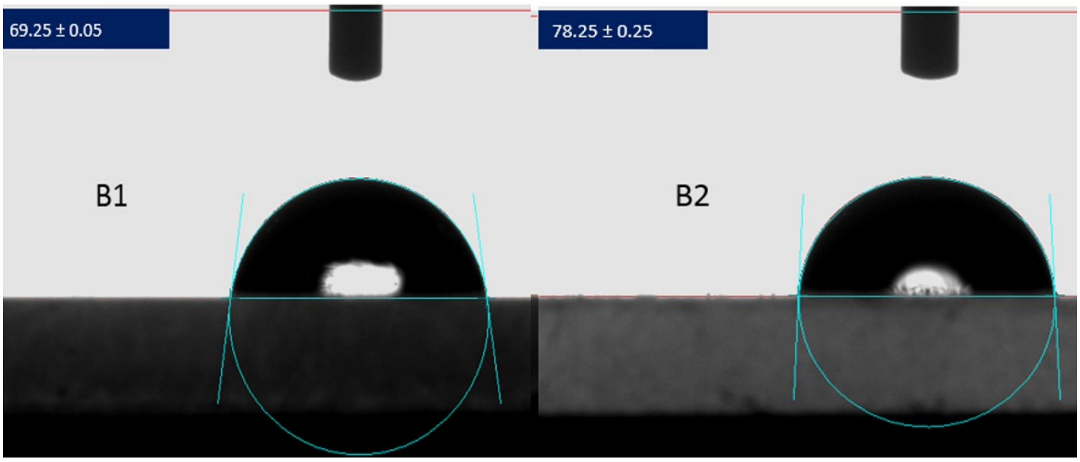

Figure 4.1: Contact angle measurements for glass slides coated with binder solution

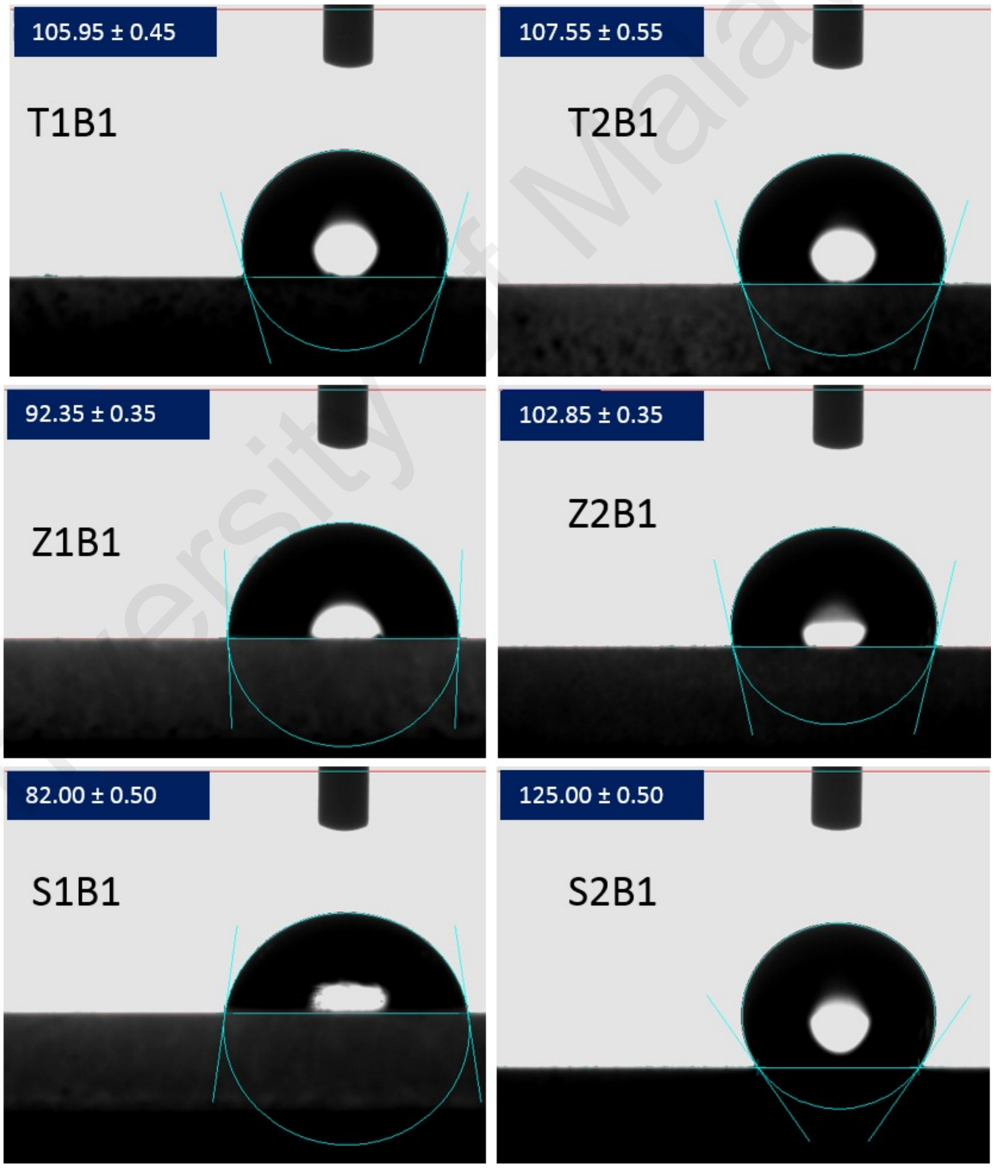

Figure 4.2: Contact angle measurements for nanoparticle coating systems in B1 binder

University of Malaya

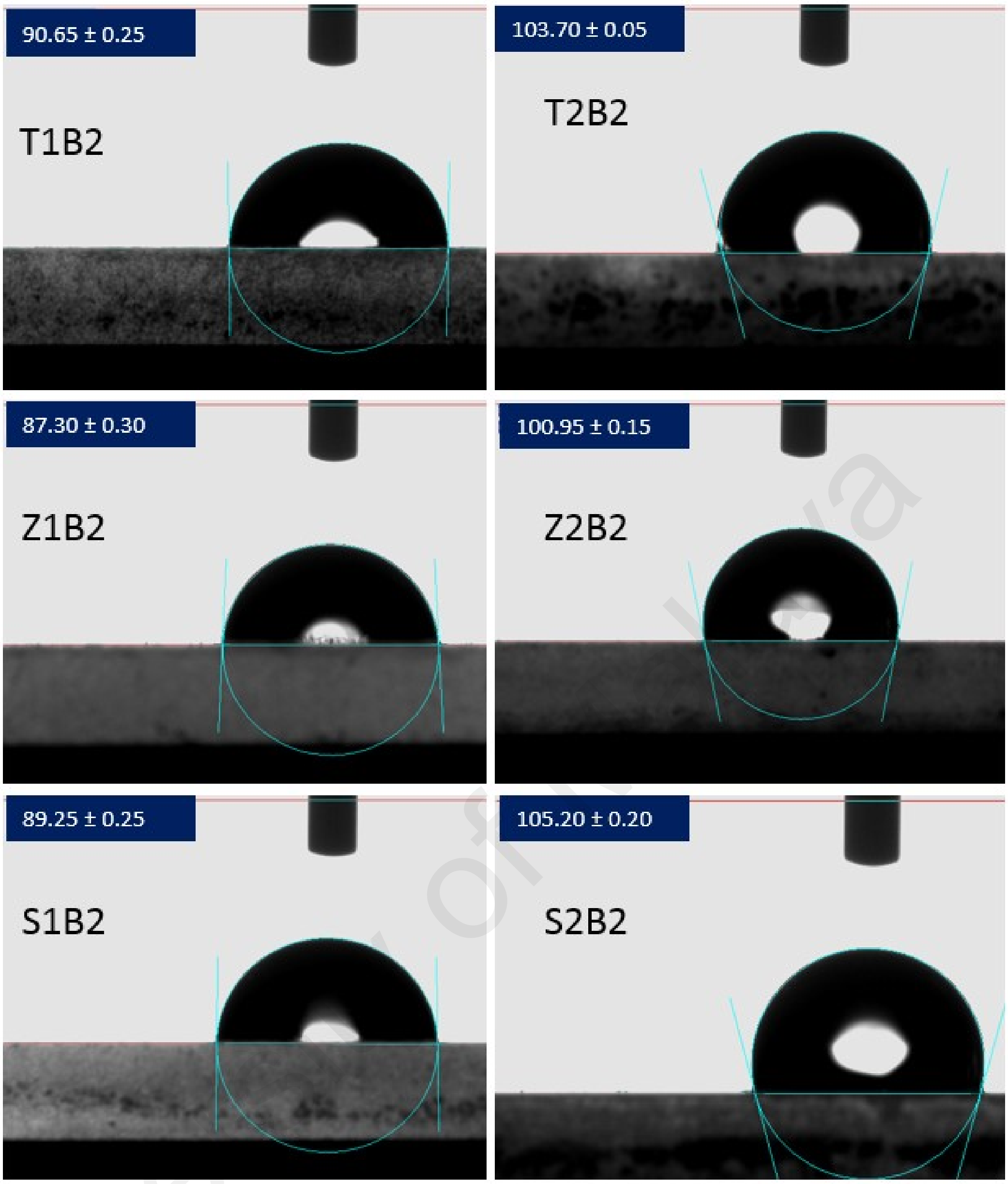

Figure 4.3: Contact angle measurements for nanoparticle coating systems in B2 binder

University of Malaya

4.2.2 Transparency of nanoparticle coatings

UV-Vis is a method chosen in this work to measure the transparency of the coating samples by measuring the transmittance of light across the ultraviolet and visible wavelengths through the samples (Workman Jr & Springsteen, 1998). Table 4.2 records average transmittance for all nanoparticle coating systems at two different ranges of wavelengths along with respective coating thickness.

Table 4.2: Average transmittance of all the nanoparticle coating systems at two ranges of wavelength

	Nanoparticles (wt%)	Coating System	Coating thickness (nm)	Average transmittance (%) at 400 – 550 nm	Average transmittance (%) at 600 - 800 nm
No Coating	0	-	-	90.06	91.2
Binder 1 (B1): APTES/ MTMS	0	B1	86.23 ± 0.63	87.76	88.9
	20	T1B1	153.03 ± 0.62	67.33	67.06
	60	T2B1	163.00 ± 1.01	61.58	59.26
	20	Z1B1	146.22 ± 1.11	78.35	78.34
	60	Z2B1	155.03 ± 1.07	62.32	63.21
	20	S1B1	127.07 ± 0.61	85.06	86.2
	60	S2B1	160.85 ± 0.97	36.23	52.83
Binder 2 (B2): MTMS/ HNO_3	0	B2	80.23 ± 0.59	81.8	83.77
	20	T1B2	157.45 ± 0.97	61.14	60.04
	60	T2B2	158.44 ± 1.04	58.72	57.43
	20	Z1B2	140.62 ± 1.13	75.46	77
	60	Z2B2	155.20 ± 1.05	71.44	73.55
	20	S1B2	133.54 ± 1.02	73.55	76.34
	60	S2B2	160.21 ± 1.15	46.47	45.77

From the Table 4.2, it is obvious that all coating systems have clear differences in average transmittance values ranging from approximately 30 – 80 %. At wavelength range of 600 – 800 nm, compared with the glass sample with no coating with average transmittance of 91.2%, both binder coating systems decrease the transmittance percentage with values of 88.9% (B1 binder coating system) and 83.77% (B2 binder coating system), indicating a decrease in transparency of the glass samples. This can be related with coating thickness, whereby from non-coated samples to the increasing thickness of the coatings layers, light scattering that occurs within the coating systems is

University of Malaya

increasing leading to a decreased in transmission of light through the samples (Abudula et al., 2014).

Figure 4.3 shows that in B1 binder system, S1B1 shows the highest transmittance and S2B1 show the lowest transmittance whereby addition of small amount of SnO_2 in APTES/MTMS matrix shows a great difference in transmittance. Similarly, from the Figure 4.3, it has been observed that the Z1B2 coated glass substrate shows the highest transmittance and S2B2 shows lowest transmittance among the nanoparticle coating systems in B2 binder system as small amount of ZnO is added into the MTMS/HNO_3 matrix portrayed a huge difference in transmittance. The overall result proves that as the amount of nanoparticle in the system increases, the transparency of the nanoparticle coating sample decreases because the light absorption by nanoparticles increases (Sukmanowski, Viguié, Nölting, & Royer, 2005). Therefore, to maintain or increase the transparency of the coatings, less nanoparticles should be used in the binder systems.

University of Malaya

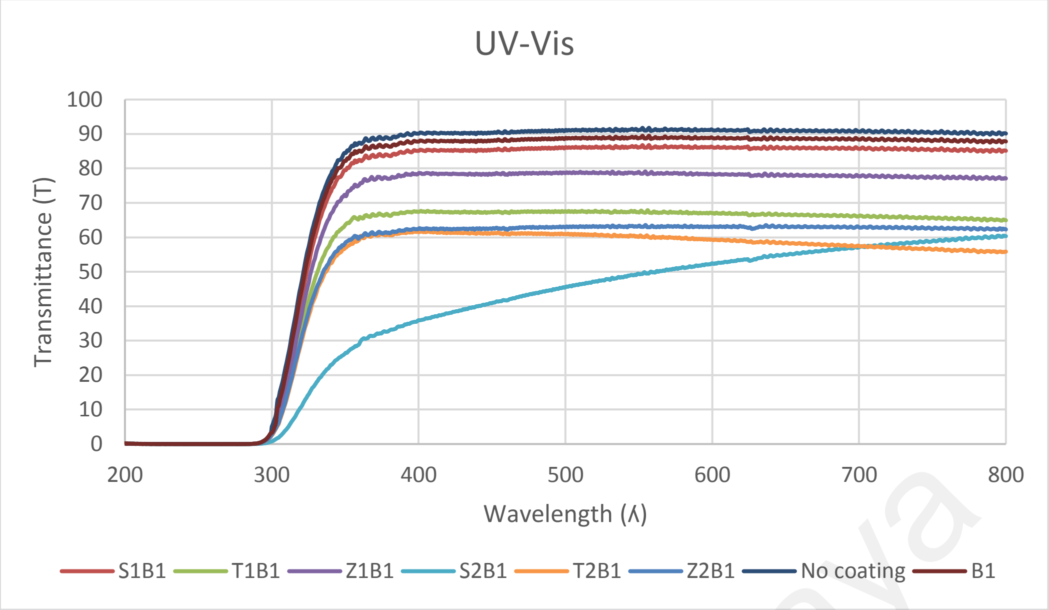

Figure 4.3: UV-Vis spectra for nanoparticle coating system with binder 1 (B1)

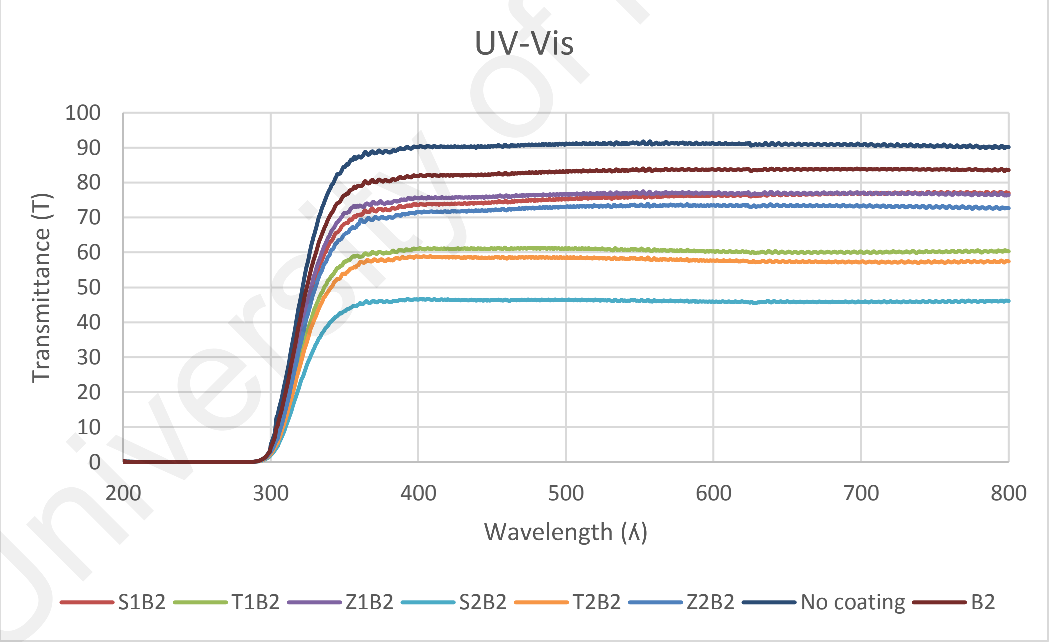

Figure 4.4: UV-Vis spectra for nanoparticle coating system with binder 2 (B2)

University of Malaya

4.3 Structural Properties

4.3.1 Surface morphology of nanoparticle coatings

The surface morphology of nanoparticle coating systems was characterized by using FESEM in low vacuum mode where the average diameter of nanoparticles observed from the study is between 30 nm to 90 nm as shown in Figure 4.5.

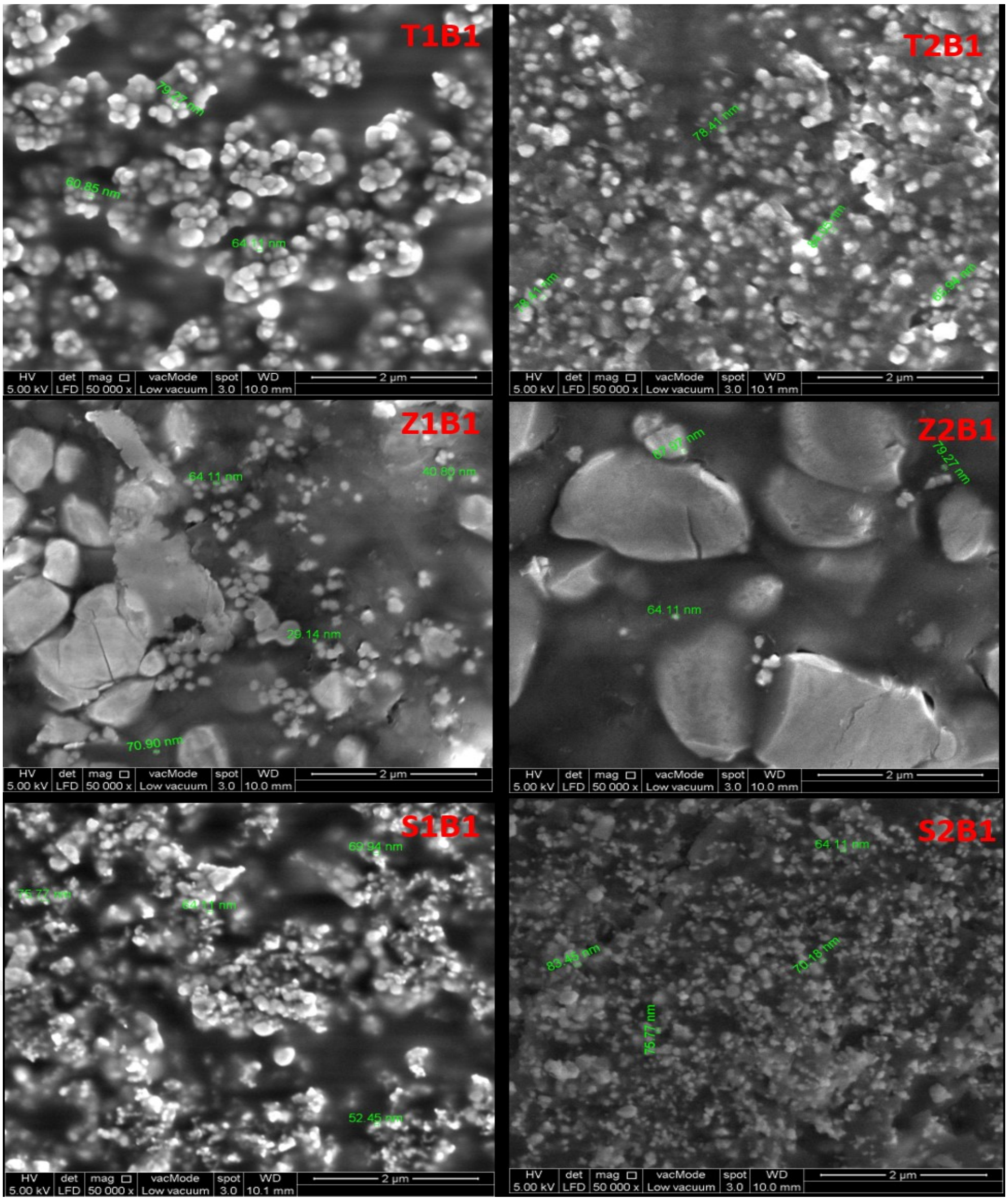

Figure 4.5: FESEM images of nanoparticle coating systems in B1 binder network

From Figure 4.5, the FESEM images shows that the nanoparticles in T1B1, T2B1, S1B1 and S2B1 are distributed uniformly throughout B1 binder system, indicating that the TiO_2 and SnO_2 are well-blended in APTES/MTMS matrix. The nanoparticles appear to be less packed in the coating systems for T1B1 and S1B1 as more pores (black areas) within the nanoparticles are observed. This shows that as the amount of SnO_2 and TiO_2 nanoparticles increases in B1 binder system, the distribution becomes more dispersed and randomly packed. The nanoparticles uneven packing manner which inside S2B1 coating system contributes to large air fractions on the coating surface, leading to high hydrophobicity of the coating film as proven by contact angle measurement (Xue, Li, Fu, & Han, 2009). However, the distribution of nanoparticles in Z1B1 and Z2B1 coating systems are not uniform and the morphologies are irregular because of large coating defects (Hou et al., 2017).

The presence of nanoparticles in B1 binder system has been further verified by EDX analysis as shown in Figure 4.6. EDX study also confirmed that there are no major contaminants on the coatings leading to better accuracy of the results. EDX study shows as the amount of TiO_2/ZnO/SnO_2 nanoparticles in the APTES/MTMS matrix increases, the percentage of Ti/Zn/Sn elements that are detected by EDX also increases respectively.

University of Malaya

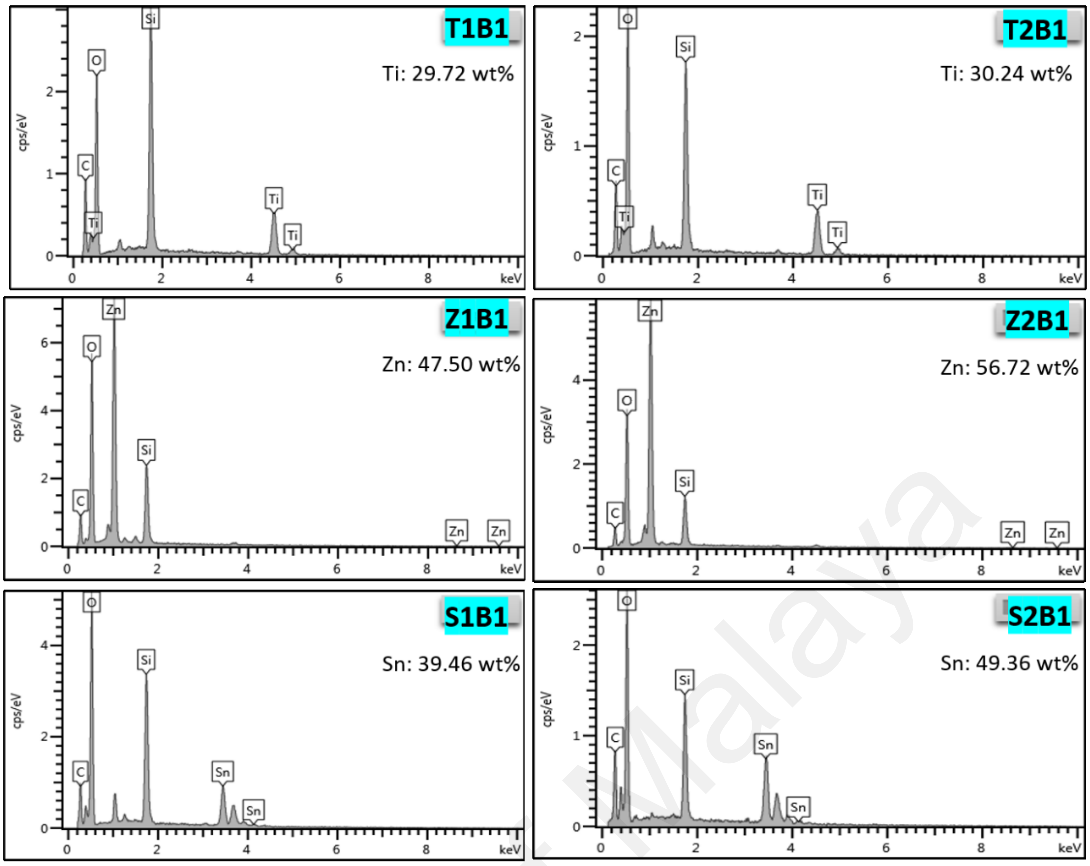

Figure 4.6: EDX spectra for nanoparticle coating systems in B1 binder network

Figure 4.7 shows surface morphology of nanoparticle coating systems by FESEM for binder 2 (B2) coating systems. From Figure 4.7, the FESEM images of T1B2, T2B2, S1B2 and S2B2 coating systems display a uniform distribution of nanostructures in B2 binder system, indicating that TiO_2 and SnO_2 nanoparticles managed to blend into the mesoporous network of the MTMS/HNO_3 matrix leading to enhanced structural characteristics of the coating mixtures. In Z1B2 and Z2B2 coating systems, deterioration of the uniformity is observed which is in similar case with Z1B1 and Z2B1 coating systems. Therefore, ZnO nanoparticles does not mix well in both B1 and B2 binder networks.

University of Malaya

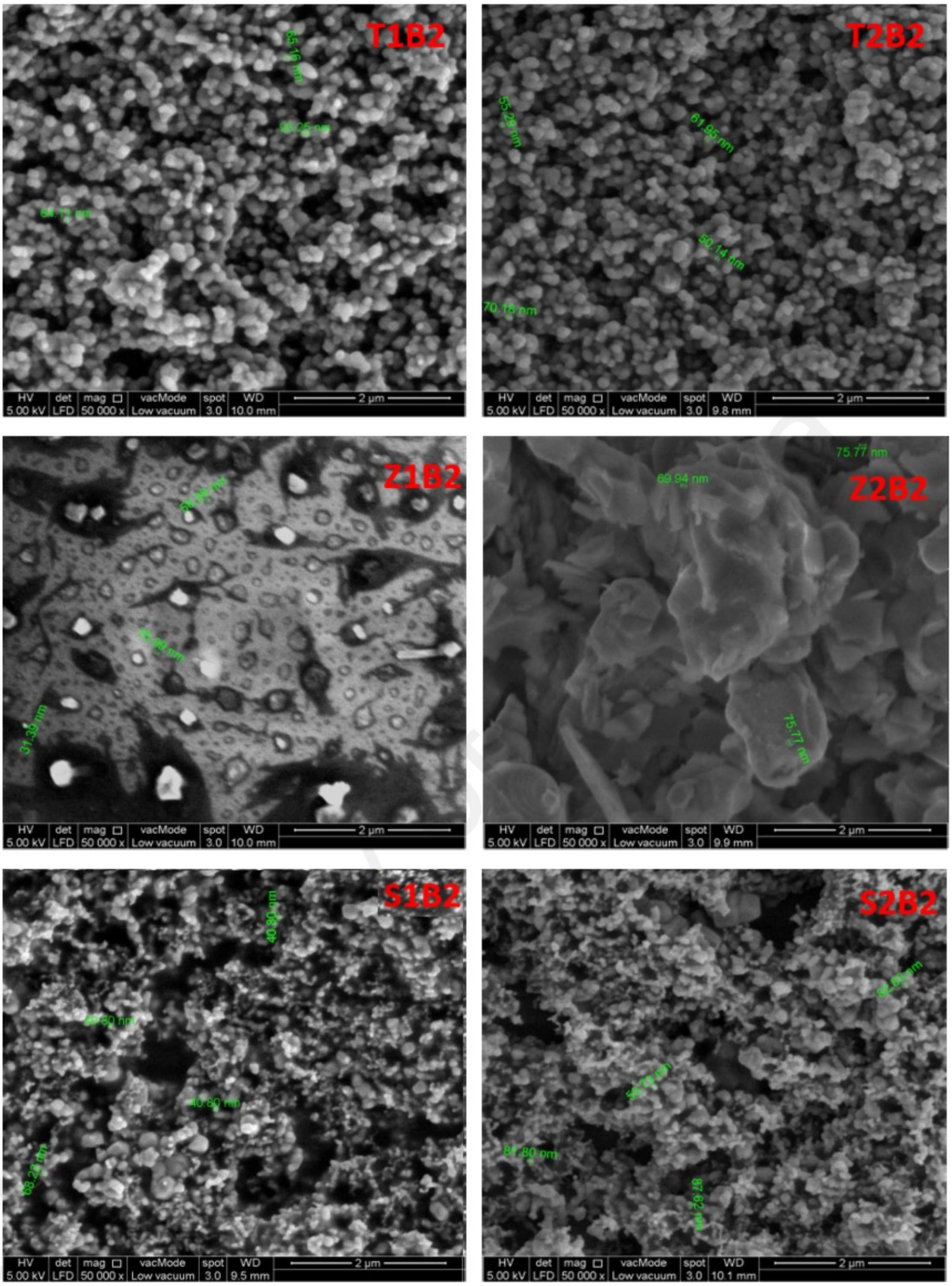

Figure 4.7: FESEM images of nanoparticles in B2 binder network

EDX study in Figure 4.8 further confirms the presence of nanoparticles in the binder network whereby as the amount of TiO_2/ZnO/SnO_2 nanoparticles in the MTMS/HNO_3 matrix (B2 binder system) increases, the percentage of Ti/Zn/Sn elements which are detected on the coated samples also increases. Figure 4.8 shows that there no major contaminant in the coating mixtures which results in a better accuracy of the outcomes.

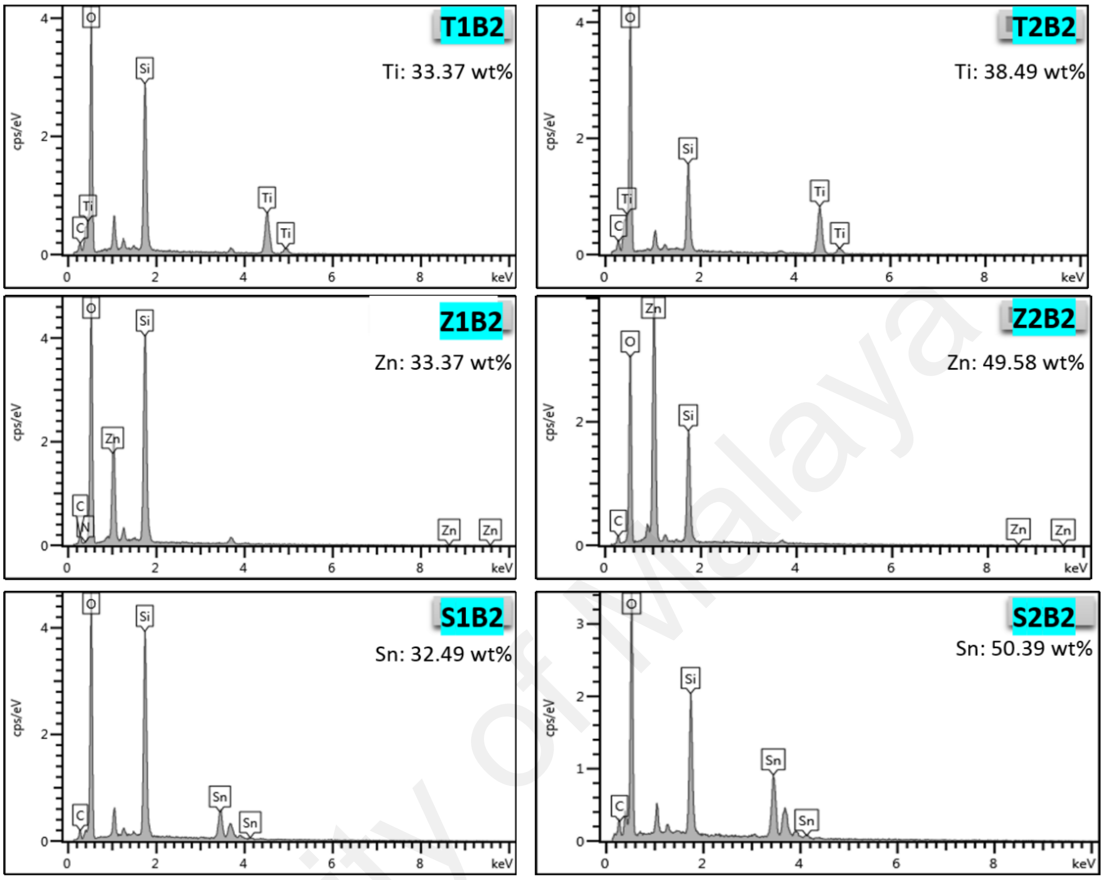

Figure 4.8: EDX spectra for nanoparticle coating systems in B2

4.3.2 FTIR analysis

Figure 4.9 shows the FTIR spectra obtained from all coating systems to obtain information on bonding mechanisms on surface of materials and in solids.

University of Malaya

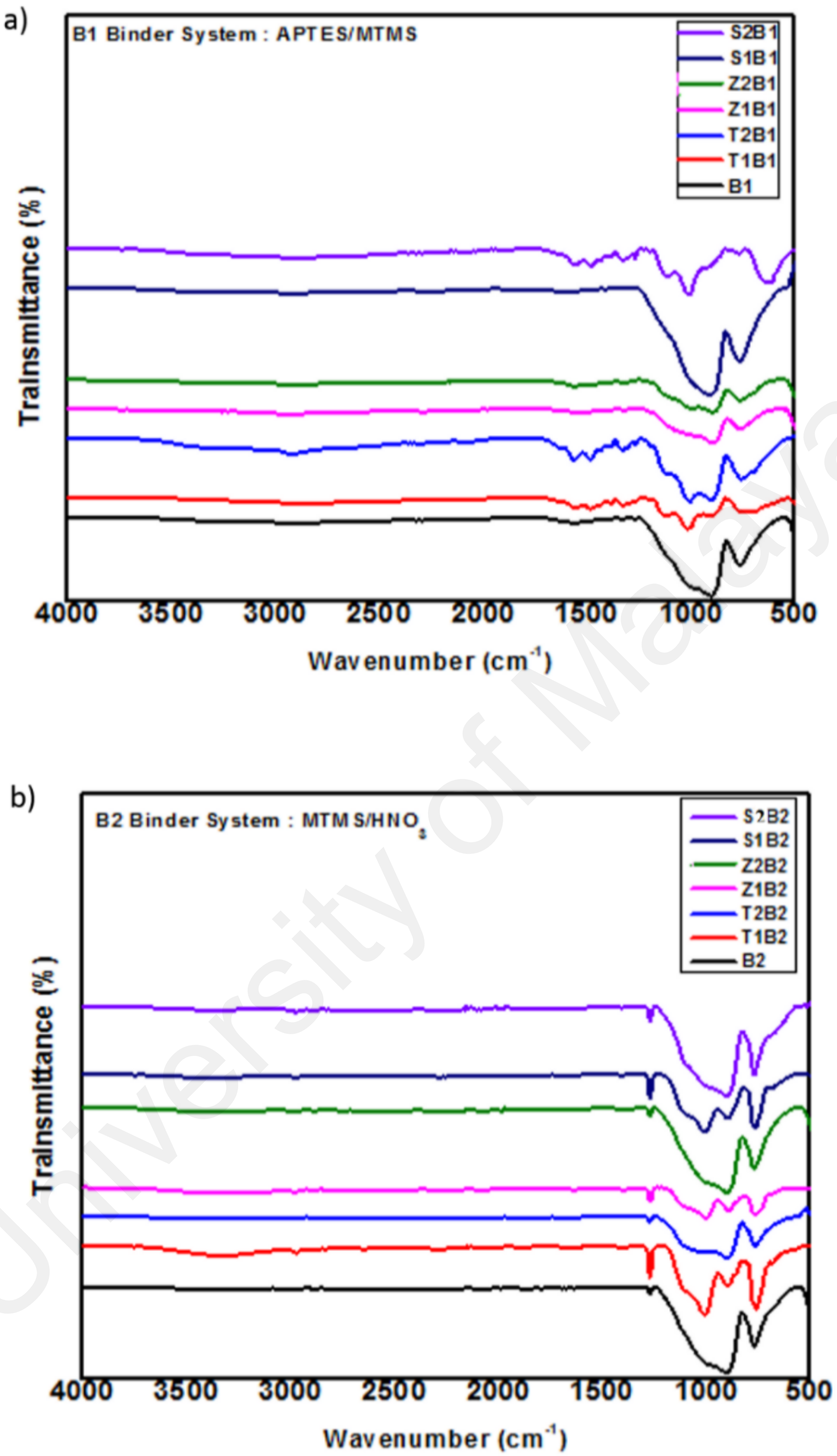

Figure 4.9: FTIR spectra for a) B1 coating systems and b) B2 coating systems

University of Malaya

From Figure 4.9, it is observed that the coating systems contained sharp peaks at Si-C band and the strongest peaks at Si-OH bending. High density of methyl group in all coatings can be observed from the peaks at wavenumber around 900 – 960 cm^{-1}. It is known that high density of methyl group leads to high hydrophobicity of the coatings (Rao, Rao, & Pajonk, 2007; Shewale, Rao, & Rao, 2008). This can be seen in S2B1 nanoparticle coating system in Figure 4.9 which produces the sharpest peak at 921.22 cm^{-1} and has the most hydrophobic surface as proven in contact angle measurement. The molecular entanglement as well as crystallinity of APTES/MTMS (B1 binder system) and MTMS/HNO_3 (B2 binder system) depend on hydrophilic or hydrophobic force balance of the coating systems (H. S. Mansur, R. L. Oréfice, & A. A. P. Mansur, 2004). The conformational configurations of the molecules created the hydrophobic-associated domains due to hydrogen bonds (Jenkins & Mills, 2005). Hence, the contribution of Si-OH group from MTMS in precursors leads to a positive modification in the crystalline structure of the coating systems as the peaks are broad and strong at Si-OH bending band. From Figure 4.9, more peaks are observed as nanoparticles are added into B1 and B2 binder systems. In B1 coating systems, all coatings formed peaks at $Si-H_n$ band. This indicates the coating films contain high atomic concentration of hydrogen (Pereyra, Carreno, Tabacniks, Prado, & Fantini, 1998; Ray et al., 2005). However, no peaks are found at CH_3 deformation, H-OH and Si-OH stretching bands. On the other hand, in B2 coating systems, there are weak peaks observed at CH_3 deformation, H-OH and Si-OH stretching bands after addition of 20 wt% of TiO_2 (T1B2 coating system) and ZnO nanoparticles (Z1B2 coating system) but the peaks disappeared as more nanoparticles were added. The weak bands at 1409.50 cm^{-1} (CH_3 deformation) for T1B2 coating system and 1403.49 cm^{-1} (CH_3 deformation) for Z1B2 coating system belong to the surface hydrocarbon which is formed on the coating surfaces (Mihály et al., 2006). The details of the peaks are presented in Table 4.3

University of Malaya

Table 4.3: The peak values obtained according to respective bands for all coating systems

Bands	Peak values for coating systems (cm^{-1})						
	B1	**T1B1**	**T2B1**	**Z1B1**	**Z2B1**	**S1B1**	**S2B1**
Si-C	763.94	725.39	754.64	762.14	761.12	766.55	772.17
Si-OH bending	928.46	914.62	906.35	900.46	957.22	923.63	921.22
Si-O-Si stretching	-	1014.59	1005.08	-	-	-	1010.94
Si-CH_3 deformation	1270.33	1269.77	1269.73	-	-	-	1269.96
CH_3 deformation	-	-	-	-	-	-	-
H-OH band	-	-	-	-	-	-	-
Si-H_n bending	2066.15	2070.11	2085.71	2083.07	2073.88	2081.38	2109.39
Si-OH stretching	-	-	-	-	-	-	-
CH_3 stretching	2917.84	2887.3	2913.85	2934.26	2907.47	2927.95	2901.03
	B2	**T1B2**	**T2B2**	**Z1B2**	**Z2B2**	**S1B2**	**S2B2**
Si-C	769.02	762.56	766.1	761.46	769.22	765.81	769.06
Si-OH bending	928.13	900.71	910.76	902.79	919.48	901.00	930.67
Si-O-Si stretching	-	1010.58	-	1003.45	-	1007.47	-
Si-CH_3 deformation	1272.19	1270.60	1272.29	1270.07	1272.45	1270.9	1270.41
CH_3 deformation	-	1409.50	-	1403.49	-	-	-
H-OH band	-	1638.85	-	1636.1	-	-	-
Si-H_n bending	-	-	-	2051.82	2069.02	2078.22	2077.72
Si-OH stretching	-	3325.48	-	3308.84	-	-	-
CH_3 stretching	2977.95	2972.38	2978.41	-	-	2973.29	2973.95

University of Malaya

4.3.3 XRD analysis

To understand the role of nanoparticles inside the binder coating systems, the nanoparticle coatings were characterized via XRD and the results are shown in Figure 4.10 and Table 4.4. With a change of nanoparticle shape, amount or size, the diffraction peaks observed in the XRD pattern indicates the change in crystal structure (Vorontsov & Tsybulya, 2018). Figure 4.10 shows that as the amount of nanoparticles increases in the coating systems, the peak intensities obtained by XRD also increases showing an increased in crystallinity of the coatings (Adnadjević, Vukićević, Filipović-Rojka, & Marković, 1990). Overall crystallinity improves around 20 – 50% upon addition of nanoparticles inside the binder system.

University of Malaya

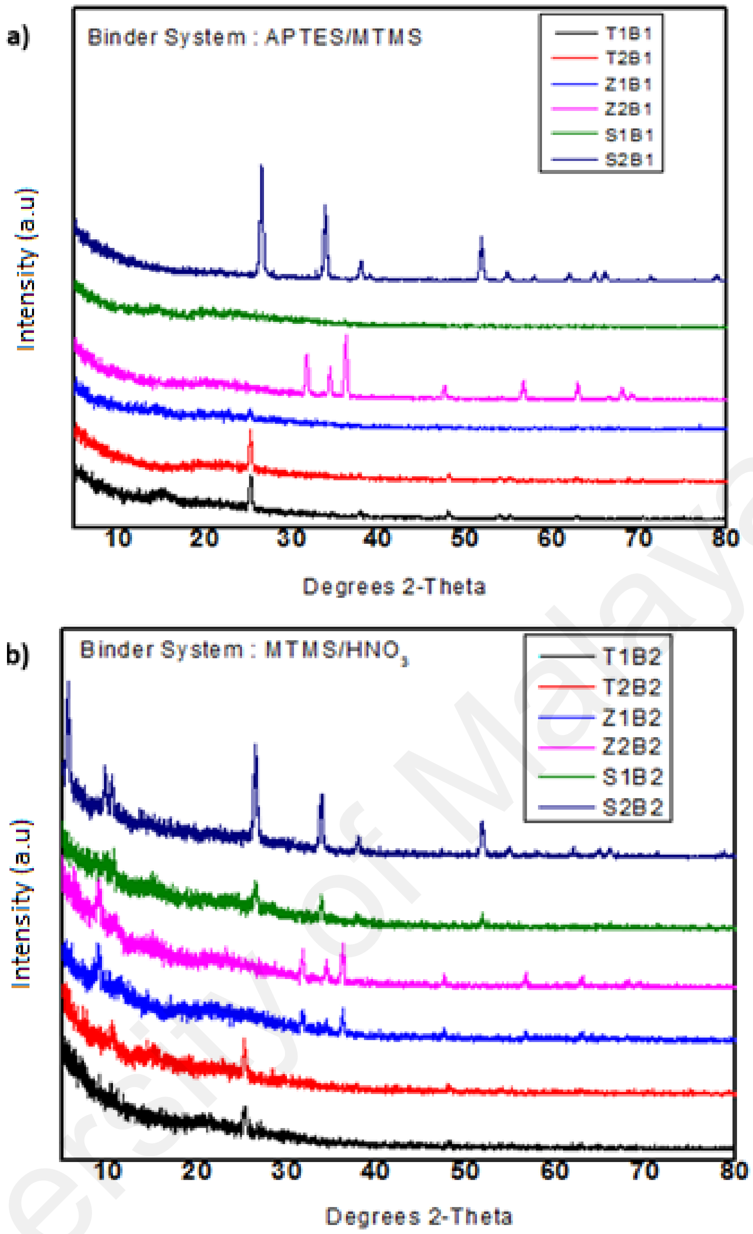

Figure 4.10: XRD diffraction peaks for nanoparticle coatings in a) B1 binder system and b) B2 binder system

University of Malaya

Compared to the peaks for nanoparticle coatings in B1 coating system in Figure 4.10 (a), the peaks for nanoparticle coatings in B2 coating system in Figure 4.10 (b) shows a stronger and higher peak intensities indicating a higher crystalline nature of the reaction products in the MTMS/HNO_3 matrix (B2 binder system) (Mekla, Juisuwannathat, & Tipparach, 2015). It is also observed that when there is an increase in nanoparticles concentration in the precursor solutions (B1 and B2 binder systems), the peak intensities are further amplified due to corresponding increase in film thickness and decrease in transparency of coatings as proven in the ‘Transparency of nanoparticle coating’ section (Van Heerden & Swanepoel, 1997). With addition of more nanoparticles, SnO_2 (JCPDS No. 41-1445) (H. Gu, Zhao, Zhang, & Shao, 2018; Patil, Kajale, Gaikwad, & Jain, 2012; Zhou et al., 2013) nanoparticle coatings (S1B1, S2B1, S1B2 and S2B2 coatings) give the highest difference in peak intensities in both binder solutions (B1 and B2), followed by ZnO (JCPDS No. 36-1451) (Dinesh et al., 2014; Kumar et al., 2017) nanoparticle coatings (Z1B1, Z2B1, Z1B2 and Z2B2 coatings) and lastly TiO_2 Anatase (JCPDS No. 21-1272) (Chang et al., 2015) nanoparticle coatings (T1B1, T2B1, T1B2 and T2B2 coatings) which gives the lowest peak intensities. This shows that addition of more TiO_2 nanoparticles inside both binder coating systems does not affect much in the crystallinity of the coating systems.

For nanoparticle coatings in the B1 coating systems, the highest diffraction peak intensities are observed in S2B1 samples with appearing peaks at $2\theta = 26.53^\circ$, 33.81°, 38.00°, 51.74°, 54.88°, 57.89°, 62.06°, 64.91°, 65.99°, 71.29°, and 78.99° which corresponds to (110), (101), (200), (211), (220), (002), (310), (112), (301), (202) and (321) reflection planes (h, k, l) respectively as shown in Table 4.4. Similarly, for nanoparticle coatings in the B2 coating systems, the highest diffraction peak intensities are observed in S2B2 samples with appearing peaks at $2\theta = 26.57^\circ$, 33.81°, 38.05°, 51.79°, 54.90°, 61.95°, 64.78° and 66.08° which corresponds to (110), (101), (200), (211), (220), (310), (112), and (301) reflection planes respectively. These intense peak intensities of SnO_2 nanoparticles in both binder coating systems (B1 and B2 coating systems) confirm their high crystallinity and regular alignment of the crystal lattice. A well-crystalline structure promotes more pore volumes, leading to an improved porosity of the coating films and therefore resulting in high hydrophobicity as confirmed in contact

University of Malaya

angle measurement (Fang, Yan, Tan, Liu, & Wang, 2005; Ji et al., 2018; S. S. Kim & Lee, 2004).

Table 4.4: A detailed XRD characterization for TiO_2 Anatase (JCPDS No. 21-1272), ZnO (JCPDS No. 36-1451), and SnO_2 (JCPDS No. 41-1445) nanoparticle coating systems

Binder System	Nanoparticles (wt%)	Coating system	2θ (°)	Phase ID	Coating's Phase	(h k l)
Binder 1 (B1) APTES/ MTMS	20	T1B1	15.22	-	Amorphous	-
			25.26	TiO_2	Crystalline	(101)
			47.97	TiO_2	Crystalline	(200)
	60	T2B1	25.22	TiO_2	Crystalline	(101)
			47.98	TiO_2	Crystalline	(200)
	20	Z1B1	25.14	-	Amorphous	-
	60	Z2B1	31.76	ZnO	Crystalline	(100)
			34.37	ZnO	Crystalline	(002)
			36.2	ZnO	Crystalline	(101)
			47.46	ZnO	Crystalline	(102)
			56.64	ZnO	Crystalline	(110)
			62.84	ZnO	Crystalline	(103)
			67.98	ZnO	Crystalline	(112)
	20	S1B1	14.21	-	Amorphous	-
			21.19	-	Amorphous	-
	60	S2B1	26.53	SnO_2	Crystalline	(110)
			33.81	SnO_2	Crystalline	(101)
			38	SnO_2	Crystalline	(200)
			51.74	SnO_2	Crystalline	(211)
			54.88	SnO_2	Crystalline	(220)
			57.89	SnO_2	Crystalline	(002)
			62.06	SnO_2	Crystalline	(310)
			64.91	SnO_2	Crystalline	(112)
			65.99	SnO_2	Crystalline	(301)
			71.29	SnO_2	Crystalline	(202)
			78.99	SnO_2	Crystalline	(321)
Binder 2 (B2) MTMS/ HNO_3	20	T1B2	21.44	-	Amorphous	-
			25.29	TiO_2	Crystalline	(101)
			48.48	-	Amorphous	-
	60	T2B2	10.48	-	Amorphous	-
			14.48	-	Amorphous	-
			25.2	TiO_2	Crystalline	(101)

University of Malaya

			48.09	TiO_2	Crystalline	(200)
	20	Z1B2	9	-	Amorphous	-
			21.49	-	Amorphous	-
			31.7	ZnO	Crystalline	(100)
			36.2	ZnO	Crystalline	(101)
			47.53	ZnO	Crystalline	(102)
			56.42	ZnO	Crystalline	(110)
			63.01	ZnO	Crystalline	(103)
	60	Z2B2	8.95	-	Amorphous	-
			23.1	-	Amorphous	-
			31.74	ZnO	Crystalline	(100)
			34.37	ZnO	Crystalline	(002)
			36.2	ZnO	Crystalline	(101)
			47.54	ZnO	Crystalline	(102)
			56.64	ZnO	Crystalline	(110)
			62.8	ZnO	Crystalline	(103)
			68.2	ZnO	Crystalline	(112)
	20	S1B2	10.66	-	Amorphous	-
			15.44	-	Amorphous	-
			26.56	SnO_2	Crystalline	(110)
			33.7	SnO_2	Crystalline	(101)
			37.75	-	Amorphous	-
			51.79	SnO_2	Crystalline	(211)
	60	S2B2	5.53	SnO_2	Amorphous	-
			9.71	SnO_2	Amorphous	-
			26.57	SnO_2	Crystalline	(110)
			33.81	SnO_2	Crystalline	(101)
			38.05	SnO_2	Crystalline	(200)
			51.79	SnO_2	Crystalline	(211)
			54.9	SnO_2	Crystalline	(220)
			61.95	SnO_2	Crystalline	(310)
			64.78	SnO_2	Crystalline	(112)
			66.08	SnO_2	Crystalline	(301)

University of Malaya

4.4 Electrical Properties

4.4.1 I-V Curves

Table 4.4 depicts the fill factor for solar cells with binder coating systems, B1 and B2, which are improved by approximately 0.1 or 16.67%, compared with the non-coated solar cell. This might due to the presence of modified alkoxide precursor, MTMS, which has been intensively used in many previous projects for filtering unwanted wavelengths from the light source and widely used in optical filters (Ichimura, Hayashi, & Morii, 2007;

King, 1971; Llobera et al., 2011). MTMS, which has one non-hydrolysable organic radical may leads to good filtering properties as it managed to produce exceptional electrical properties for many types of films (Meera, Yang, & Choi, 2006; Nadargi, Latthe, & Rao, 2009).

Table 4.5: Fill factor for all coating systems

	Nanoparticles (wt%)	**Coating system**	**Fill Factor**
No Coating	0	-	0.6277
Binder 1 (B1): APTES/ MTMS	0	B1	0.7211
	20	T1B1	0.802
	60	T2B1	0.8005
	20	Z1B1	0.8015
	60	Z2B1	0.8013
	20	S1B1	0.8027
	60	S2B1	0.8028
Binder 2 (B2): MTMS/ HNO_3	0	B2	0.7151
	20	T1B2	0.8022
	60	T2B2	0.8033
	20	Z1B2	0.8007
	60	Z2B2	0.8014
	20	S1B2	0.8027
	60	S2B2	0.8029

University of Malaya

Table 4.4 also records that the fill factor for the solar cells is further enhanced with addition of nanoparticles into the binder coating system by another 0.1 which makes an overall improvement of approximately 0.2 or 33.33% compared with the solar cells without any coating. S2B1 nanoparticle coating system produces the highest fill factor of 0.8028 in B1 binder coating system because the SnO_2 nanoparticles in S2B1 coating system may lead to low electron transport time for solar cells (Gubbala, Chakrapani, Kumar, & Sunkara, 2008). SnO_2 has been widely used as electron transport layer in previous studies due to its properties such as having a wide band gap (3.6–3.8 eV) (Mohamadkhani, Javadpour, & Taghavinia, 2019) and high electron mobility (Roose, Baena, et al., 2016) which made SnO_2 as an attractive choice for the nanoparticle coating to gain more photoelectron for crystalline solar cells in this study. Similarly, T2B2 produces the highest fill factor of 0.8033 in B2 binder coating system as TiO_2 nanoparticles in T2B2 coating system may fastens the electron transport rates for solar cells (Tan & Wu, 2006).

In addition, the loading of nanoparticles in the coating systems generally does not affect much to the fill factor of solar cells as only small unsteady difference in fill factor values are found between each nanoparticle coating system. Overall, the nanoparticle coating systems managed to enhance the efficiency of solar cells as a higher fill factor results in a better squareness of I-V characteristic curve as seen in Figure 4.11 and Figure 4.12, indicating a better quality of a solar cell (Sharma & Purohit, 2013). The optimization of this parameter ensures a maximized efficiency of a solar device system (Sharma & Purohit, 2013). However, there are clear reductions in the short circuit currents (I_{sc}) for solar cells using nanoparticle coating systems as seen in Figure 4.13 and Figure 4.14. This may relate with the decrease in transparency of coatings since the parameter affect the wavelength absorption of the solar cells, leading to a decrease in I_{sc} and this is in the agreement with the result obtained by UV-Vis characterization (J. Huang, Li, & Yang, 2008). Nonetheless, although S1B1 has the highest transparency, it gives out the lowest I_{sc} value which is most probably due the low number of photons absorbed by the coating system for the photon-to-electron conversion of the solar cell. The low amount of SnO_2 inside S1B1 coating system leads to the probability of having low absorption of photons from the light as the amount of nanoparticles is also a crucial factor for the light harvesting of solar cells (Banik, Ansari, & Qureshi, 2018; Snaith & Ducati, 2010).

University of Malaya

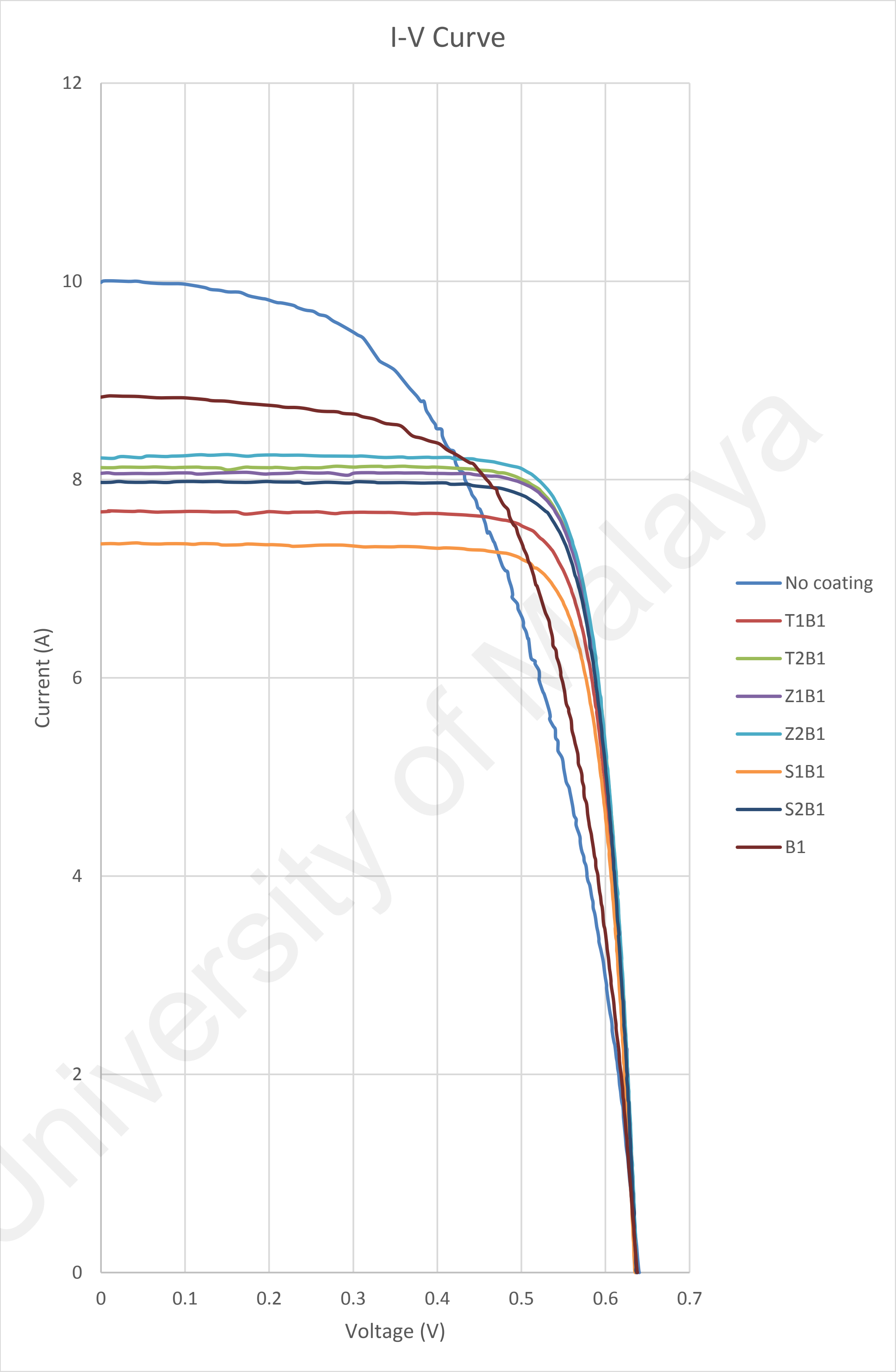

Figure 4.11: I-V curve of coating systems in B1 binder

University of Malaya

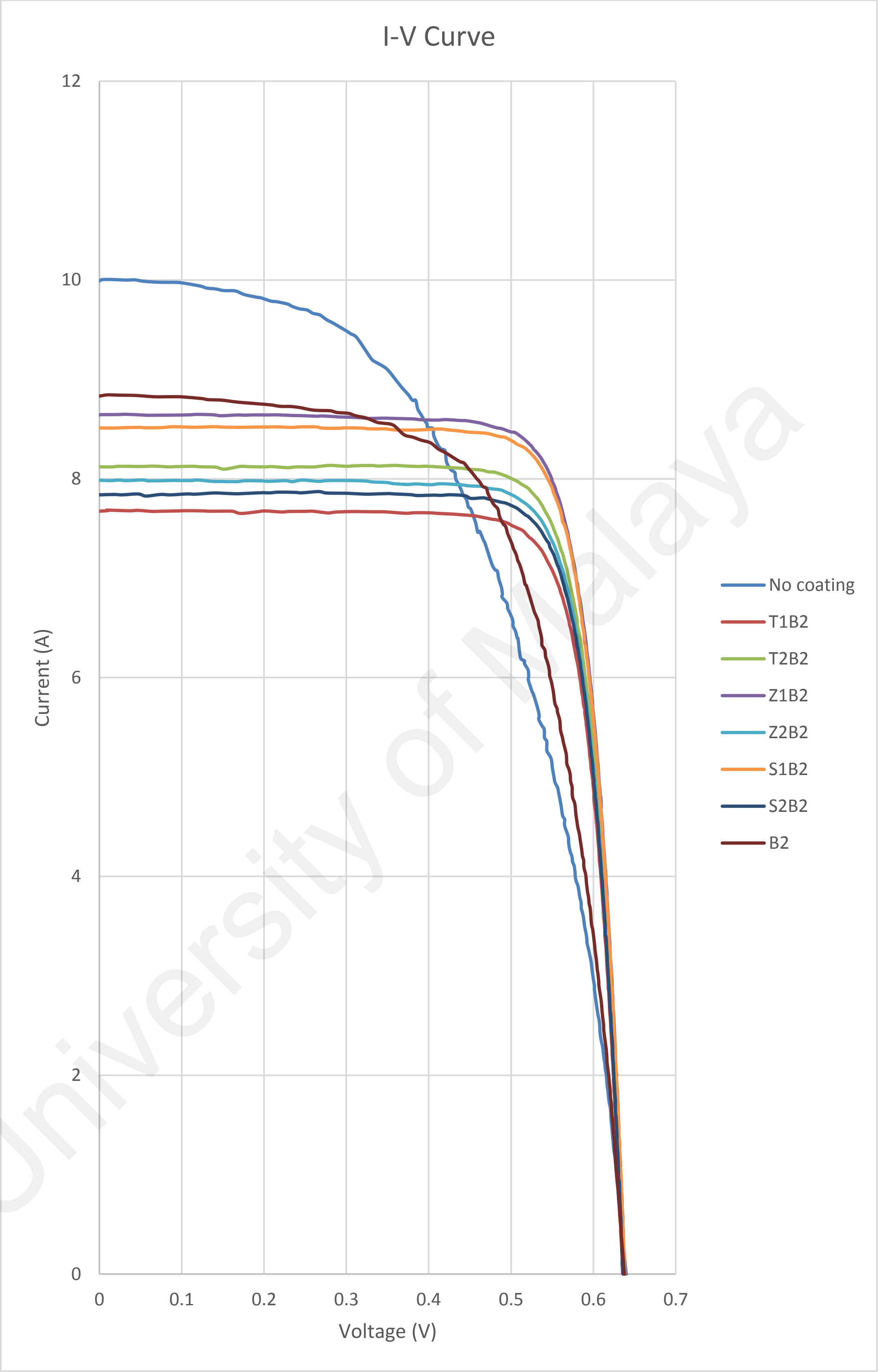

University of Malaya

Figure 4.12: I-V curve of nanoparticle coating systems in B2 binder

4.5 Thermal Properties

4.5.1 Thermal Analysis

Figure 4.13 and Figure 4.14 shows the changes in surface temperature of solar cells when exposed under 1000W/m^2 irradiation at standard room temperature of 25°C for one-hour. Surface temperature for all solar cells are about the same initially, which is approximately 27°C.

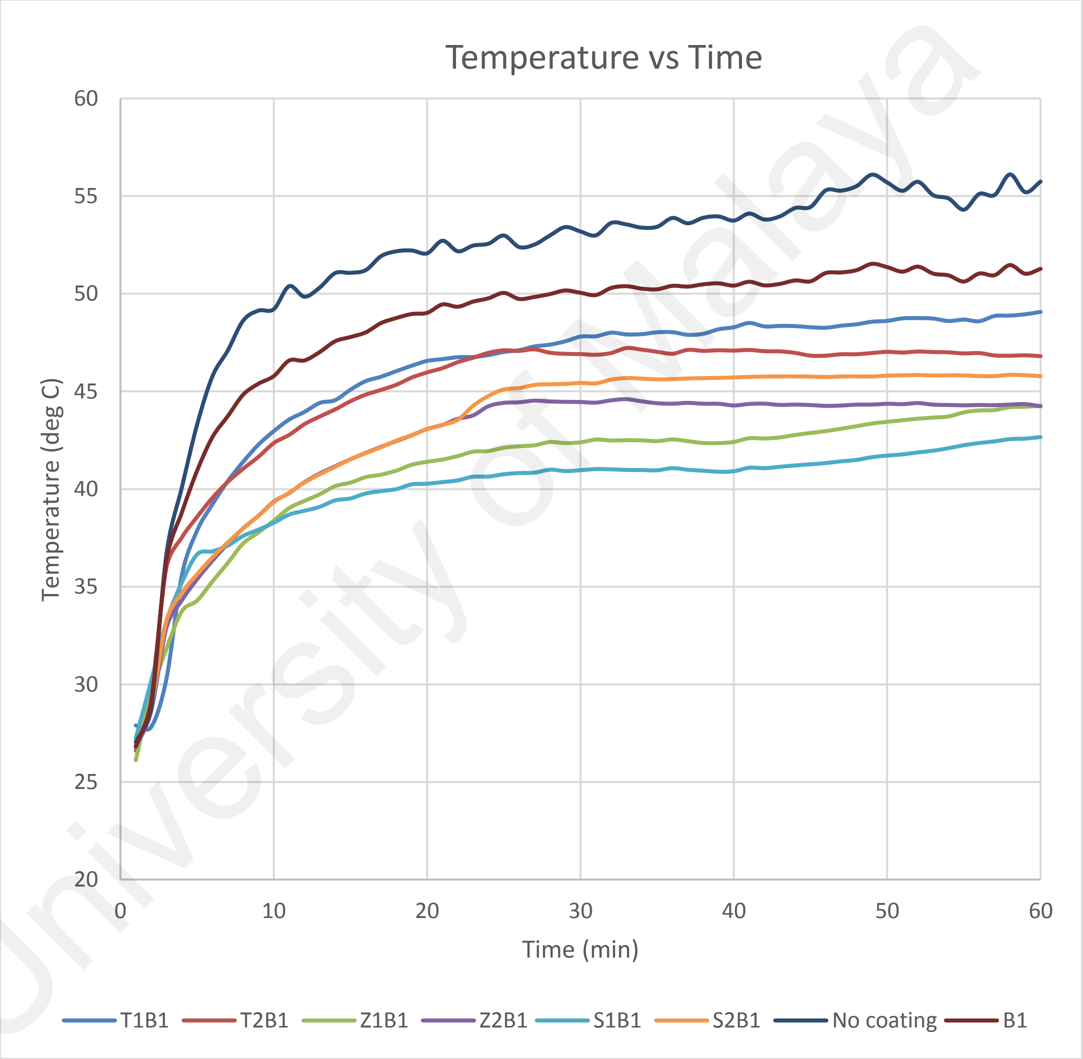

Figure 4.13: Temperature graph for nanoparticle coating systems in B1 binder

University of Malaya

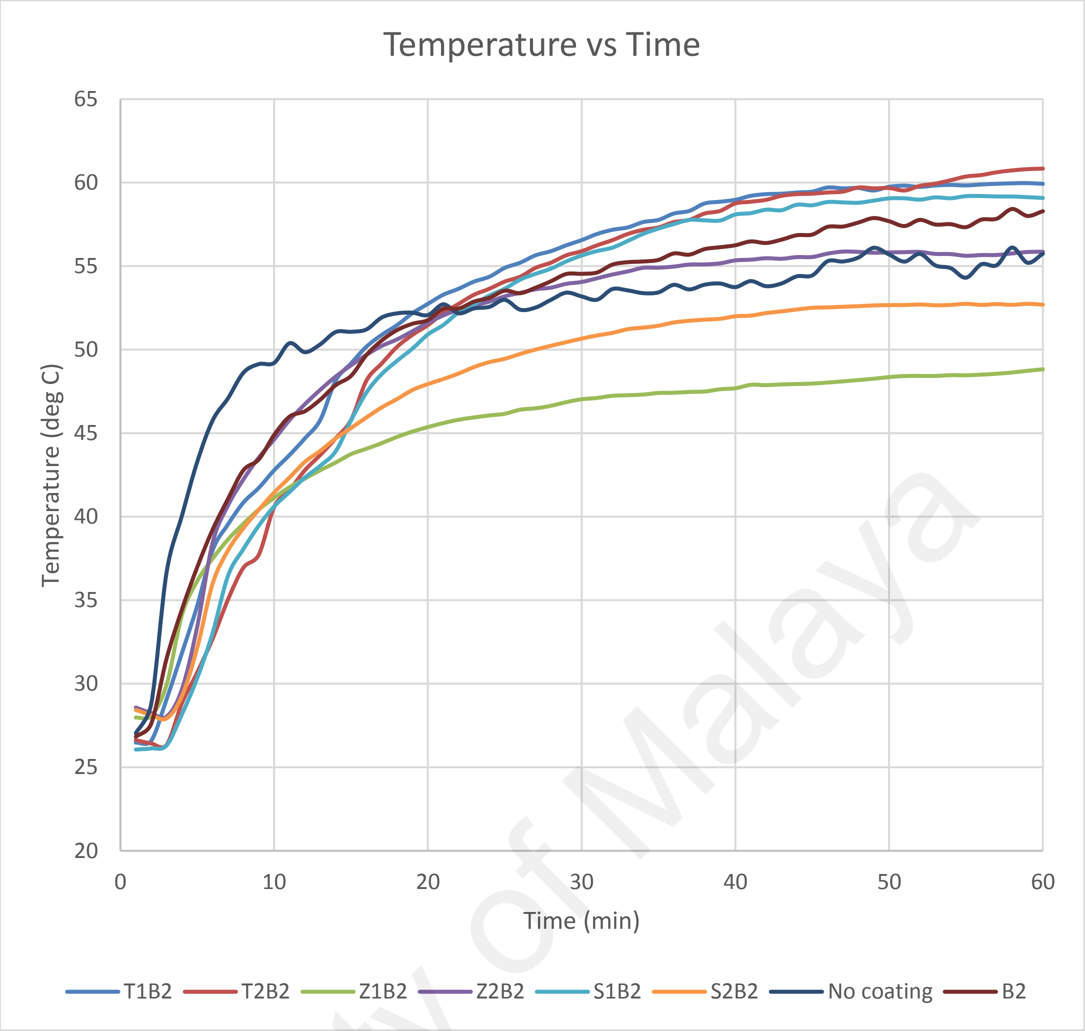

Figure 4.14: Temperature graph for nanoparticle coating systems in B2 binder

University of Malaya

For all solar cells, the temperature increases over time and eventually stabilizes at various steady state temperatures by the end of the 60-minute test. In comparison with solar cells without coating, it is observed that B1 binder coating system managed to decrease the temperature of solar cell by 4.47°C.The decrease in temperature in B1 binder coating system is due to the presence of APTES which has been employed as precursors to produce thermal control coatings with high thermal emittance that can radiates heat back into the atmosphere (Mhd Haniffa, Ching, Chuah, Ching, & Liou, 2019; Razavi, Barekat, Kiomarsipour, Ghani, & Bastani, 2012). On the other hand, B2 binder coating system is found to heat up the non-coated solar cell by 2.54°C. The presence of nitric acid, which is a strong oxidant may increase the thermal conductivity of the B2 binder coating system, causing an increase in surface temperature of the solar cell.

After the addition of nanoparticles into the binder system, S1B1 nanoparticle coating record the lowest temperature of 42.66°C for B1 binder system at 60th minute. SnO_2 nanoparticles in S1B1 coating system have a high bandgap (E_g = 3.62 eV at 300 K) (H. Kim & Shim, 2007), whereby the materials are stable at high working temperatures and gives good thermal insulation property to the coating system (F. Gu et al., 2004; Mei et al., 2012). Despite having a good thermal insulation, apparently, this property of SnO_2 degrades upon combination with HNO_3 as seen in the high temperatures of S1B2 (59.08°C) and S2B2 (52.70°C). For B2 binder system, although the MTMS/HNO_3 binder solution increases the surface temperature of solar cell, the addition of small amount of ZnO nanoparticles, which has good solar reflectance, in Z1B2 coating system manage to reduce the surface temperature of solar cells which records a temperature of 48.82°C on 60th minute. However, the temperature rises abruptly by 7°C as the loading of ZnO nanoparticles increases. The incorporation of more ZnO nanoparticles with metallic structures appears to conduct more heat with the combination of nitric acid as a strong oxidizer inside the coating system. The details on temperature of solar cells 60th minute are displayed in Table 4.5.

Most of the research studies have demonstrated that some nanoparticles can filter wavelengths that leads to degradation of solar cells due to heat such as ultraviolet (UV) or infrared (IR) radiation effectively in many cases in solar cell industry (H. Huang, Ng, Wu, & Kong, 2015; Roose, Gödel, et al., 2016; H. Zhang et al., 2015). Since the nanoparticle coating system in this work uses the concept of solar filter that filters unwanted wavelength from solar cell, the results lead to discussions on factor that might involve in the process which causes the degradation of solar cells due to heat. Hence,

University of Malaya

compared to other research studies, this current work highlights the binder system which play a crucial role in the enhancement of nanoparticles on the surface temperature of solar cells. The obtained results showed that S1B1 nanoparticle coating in B1 binder system and Z1B2 nanoparticle in B2 binder system exhibit the best filtrations against the degrading radiations among the prepared nanoparticle coating systems.

Table 4.6: Temperatures at 60th minute for all coating systems

	Nanoparticles (wt%)	Coating system	Temperature at 60th minute (°C)
No Coating	0	-	55.75
Binder 1 (B1): APTES/ MTMS	0	B1	51.28
	20	T1B1	49.07
	60	T2B1	46.8
	20	Z1B1	44.27
	60	Z2B1	44.23
	20	S1B1	42.66
	60	S2B1	45.78
Binder 2 (B2): MTMS/ HNO_3	0	B2	58.29
	20	T1B2	59.93
	60	T2B2	60.84
	20	Z1B2	48.82
	60	Z2B2	55.86
	20	S1B2	59.08
	60	S2B2	52.7

University of Malaya

CHAPTER 5: CONCLUSIONS AND SUGGESTIONS

This chapter concludes the overall work for the synthesis and characterization of hybrid nanoparticle coating system towards thermal-decreasing feature of solar cells. This section is divided by three parts, namely; conclusions, recommendation for future work and recent research trends for

5.1 Conclusions

The overall discussion was divided into four parts, namely, physical, structural, electrical and thermal properties. For physical characterization, it is observed that the presence of MTMS in both binder systems act as a hydrophobic agent which increases the contact angle value from the non-coated glass slides (30 ± 0.27°) by approximately 40° for B1 binder coating system and 48° for B2 binder coating system. Surface roughness of the coating samples was further increased as nanoparticles were introduced into the coating systems, which leads to better hydrophobicity of the coatings as S2B1 from B1 binder system and S2B2 from B2 binder system record the highest readings of 125.00 ± 0.50° and 105.20 ± 0.20° respectively. However, transparency of the coatings reduces as when compared with the glass sample with no coating (average transmittance of 91.2%), both binder coating systems decrease the transmittance percentage with values of 88.9% (B1 binder coating system) and 83.77% (B2 binder coating system) at wavelength range of 600 – 800 nm. On top of that, the overall result proves that as the amount of nanoparticle in the system increases, the transparency of the nanoparticle coating sample decreases because the light absorption by nanoparticles increases. S1B1 coating from B1 binder coating system shows the highest transmittance of 85.06% compared to all nanoparticle coating systems.

For structural studies, FESEM images shows that the nanoparticles in T1B1, T2B1, S1B1, S2B1 T1B2, T2B2, S1B2 and S2B2 are distributed uniformly throughout their

University of Malaya

respective binder systems, indicating that the TiO_2 and SnO_2 are well-blended in APTES/MTMS matrix (B1 binder system) and the MTMS/HNO_3 (B2 binder system). In Z1B1, Z2B1, Z1B2 and Z2B2 coating systems, deterioration of the uniformity is observed since ZnO nanoparticles does not mix well in both B1 and B2 binder networks. EDX study further confirms the presence of nanoparticles in the binder network whereby as the amount of TiO_2/ZnO/SnO_2 nanoparticles in the both binders (B1 and B2 binder systems) increases, the percentage of Ti/Zn/Sn elements which are detected on the coated samples also increases. From FTIR spectra, it is observed that all coating systems contained sharp peaks at Si-C band and the strongest peaks at Si-OH bending. High density of methyl group in all coatings can be observed from the peaks at wavenumber around 900 – 960 cm^{-1}, causing the surface of the coatings to be hydrophobic. This is proven whereby S2B1 nanoparticle coating system produces the sharpest peak at 921.22 cm^{-1} and has the most hydrophobic surface as seen in contact angle measurement. In XRD study, compared to the peaks for nanoparticle coatings in B1 coating system, the peaks for nanoparticle coatings in B2 coating system shows stronger and higher peak intensities indicating a higher crystalline nature of the reaction products in the MTMS/HNO_3 matrix (B2 binder system). It is also observed that an increase in nanoparticles concentration in the precursor solutions (B1 and B2 binder systems), the peak intensities are further amplified due to corresponding increase in film thickness and decrease in transparency of coatings.

In electrical characterization studies, the nanoparticle coating systems managed to enhance the efficiency of solar cells as a higher fill factor results in a better squareness of I-V characteristic curve, indicating a better quality of a solar cell. The fill factor for solar cells with binder coating systems, B1 and B2 are improved by approximately 0.1 or 16.67%, compared with the non-coated solar cell. fill factor for the solar cells is further enhanced with addition of nanoparticles into the binder coating system by another 0.1 which makes an overall improvement of approximately 0.2 or 33.33% compared with the

University of Malaya

solar cells without any coating. S2B1 nanoparticle coating system produces the highest fill factor of 0.8028 in B1 coating system and T2B2 nanoparticle coating system produces the highest fill factor of 0.8033 in B2 coating system. However, there are clear reductions in the short circuit currents (I_{sc}) for solar cells using nanoparticle coating systems and this may relate with the decrease in transparency of coatings.

Thermal analysis of this work shows that for all solar cells, the temperature increases over time and eventually stabilizes at various steady state temperatures by the end of the 60-minute test under 1000W/m^2 irradiation at standard room temperature of 25°C. In comparison with solar cells without coating, it is observed that B1 binder system managed to decrease the temperature of solar cell by 4.47°C while B2 binder coating system is found to heat up the non-coated solar cell by 2.54°C. After the addition of nanoparticles into the binder system, S1B1 nanoparticle coating record the lowest temperature of 42.66°C for B1 binder system at 60th minute. For B2 binder coating system, Z1B2 coating system manage to reduce the surface temperature of solar cells which records a temperature of 48.82°C despite having the binder system that increases the temperature of the solar cells. Overall, the obtained results showed that S1B1 nanoparticle coating in B1 binder system and Z1B2 nanoparticle in B2 binder system exhibit the best filtrations against the degrading radiations among the prepared nanoparticle coating systems.

University of Malaya

5.2 Recommendations

There are numerous issues that need to be addressed while maximizing the performance of the crystalline solar cells by using nanoparticle coatings as filters to reduce thermal degradations of the cells in this work. The solutions to these problems might bring solar technologies closer to replacing the conventional energy uses. Hence, from this work, there are several recommendations for further improvements which can be done in future as listed below:

- A more promising and cost-effective method of coating can be introduced whereby the layers and thickness can be more even and controlled upon deposition on a large-sized glass which can be conveniently installed in laboratories for research purposes.
- The combination of binder matrices can be further extended to various other combinations of suitable precursors with good thermal stability.
- Introduction of dispersing agent into the coating solutions can be done to improve the dispersion of nanoparticles and prevent agglomeration of particles inside the precursors.
- This work can be combined with other developed solar technologies such as solar concentrator or encapsulations for better architecture designs which can potentially be used for outdoor applications to produce remarkable electrical and thermal performances.

University of Malaya

5.3 Recent trends

A year-wise trend for publications that are related to this study is shown in Figure 5.1. With the keyword “thermal degradation of solar cell”, which is the main focus of this work, there is increments in number of studies that have been published in the last ten years from well-known data sources; Scopus (783 publications) and Web of Science (1083 publications). From both search engines, the total publications went up from 47 (Year 2009) to 400 (Year 2018 and 2019), showing the increase in awareness among scientists regarding the importance of the study to keep developing new designs and methods to reduce thermal degradation of solar cells. Interestingly, their works were diversified into various concepts such as doping of active layer (Paci et al., 2012), volumetric absorbers (Oliveira et al., 2019), encapsulations (Han et al., 2015) and they were implemented on different types of solar cells such as plasmonic solar cells, dye-sensitized solar cells, quantum dots solar cells and many more. Nonetheless, those ideas are streamed down and led into this work which uses the concept of coatings to filter unwanted wavelengths from sunlight in order to minimize thermal degradation of crystalline solar cells on top of maintaining their efficiencies or better, improving them.

University of Malaya

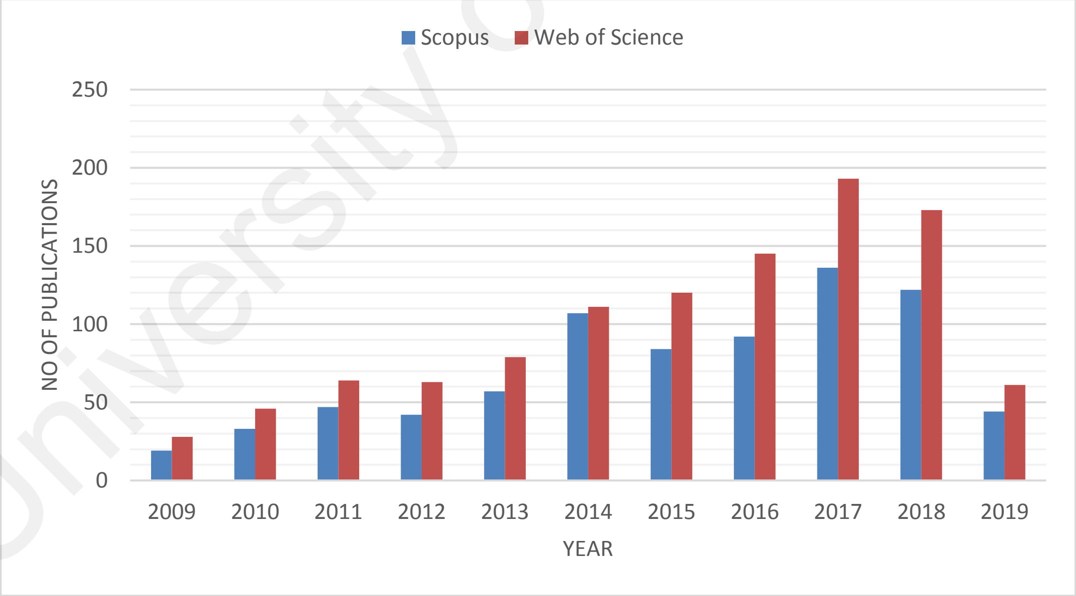

Figure 5.1: Related year-wise publications which are published in Scopus and Web of Science data sources

REFERENCES

Ã–zisik, M. N., Özısık, M. N., & Özışık, M. N. (1993). *Heat conduction*: John Wiley & Sons.

Abudula, A., Gao, F., Liu, T., Zhang, Y., Song, M., Li, N., . . . Tuersun, P. (2014). Effect of Ag Film Thickness on the Morphology and Light Scattering Properties of Ag Nanoparticles. *Nanoscience and Nanotechnology Letters, 6*(5), 392-397.

Adamczyk, A., & Długoń, E. (2012). The FTIR studies of gels and thin films of Al2O3–TiO2 and Al2O3–TiO2–SiO2 systems. *Spectrochimica Acta Part A: Molecular and Biomolecular Spectroscopy, 89*, 11-17.

Adhyaksa, G. W., Johlin, E., & Garnett, E. C. (2017). Nanoscale back contact perovskite solar cell design for improved tandem efficiency. *Nano letters, 17*(9), 5206-5212.

Adjallah, Y. G. (2010). Electronic transport in mixed-phase hydrogenated amorphous/nanocrystalline silicon thin films.

Adnadjević, B., Vukićević, J., Filipović-Rojka, Z., & Marković, V. (1990). The influence of NaX zeolite particle size on crystallinity measured by the XRD method. *Zeolites, 10*(7), 699-702.

Agbo, S., & Okoroigwe, E. (2007). Analysis of thermal losses in the flat-plate collector of a Thermosyphon Solar water Heater. *Research Journal of Physics, 1*(1), 35-41.

Ahmad, M. S., Pandey, A., & Rahim, N. A. (2017). Advancements in the development of TiO 2 photoanodes and its fabrication methods for dye sensitized solar cell (DSSC) applications. A review. *Renewable and Sustainable Energy Reviews, 77*, 89-108.

Ahmad, N., Ota, Y., & Nishioka, K. (2017). Temperature reduction of solar cells in a concentrator photovoltaic system using a long wavelength cut filter. *Japanese Journal of Applied Physics, 56*(3), 032301.

Ahmmed, S., Aktar, A., Kuddus, A., & Ismail, A. B. M. (2018). *Fabrication of Thin-Film Solar Cell using Spin Coated Zinc Oxide and Silicon Nanoparticles Doped Cupric Oxide Heterojunction.* Paper presented at the 2018 International Conference on Computer, Communication, Chemical, Material and Electronic Engineering (IC4ME2).

Ali, K., Khan, S. A., & Jafri, M. M. (2014). Effect of double layer (SiO 2/TiO 2) anti-reflective coating on silicon solar cells. *Int. J. Electrochem. Sci, 9*, 7865-7874.

Amelia, A., Irwan, Y., Leow, W., Irwanto, M., Safwati, I., & Zhafarina, M. (2016). Investigation of the Effect Temperature on Photovoltaic (PV) Panel Output Performance. *International Journal on Advanced Science Enginering, Information Technology (IJASEIT), 6*(5).

University of Malaya

Ananthoju, B., Mohapatra, J., Bahadur, D., Medhekar, N. V., & Aslam, M. (2019). Influence of the Cu2ZnSnS4 nanoparticles size on solar cell performance. *Solar energy materials and solar cells, 189*, 125-132.

Bahro, D., Koppitz, M., Mertens, A., Glaser, K., Mescher, J., & Colsmann, A. (2015). Understanding the External Quantum Efficiency of Organic Homo‐Tandem Solar Cells Utilizing a Three‐Terminal Device Architecture. *Advanced Energy Materials, 5*(22).

Banik, A., Ansari, M. S., & Qureshi, M. (2018). Efficient Energy Harvesting in SnO2-Based Dye-Sensitized Solar Cells Utilizing Nano-Amassed Mesoporous Zinc Oxide Hollow Microspheres as Synergy Boosters. *ACS omega, 3*(10), 14482-14493.

Barnes, R., Dhanoa, M. S., & Lister, S. J. (1989). Standard normal variate transformation and de-trending of near-infrared diffuse reflectance spectra. *Applied spectroscopy, 43*(5), 772-777.

Bejan, A. (2013). *Convection heat transfer*: John wiley & sons.

Bell, T. J., & Ikeda, Y. (2011). The application of novel hydrophobic ionic liquids to the extraction of uranium (VI) from nitric acid medium and a determination of the uranyl complexes formed. *Dalton Transactions, 40*(39), 10125-10130.

Belogorokhov, A., Gavrilov, S., Kashkarov, P., & Belogorokhov, I. (2005). FTIR investigation of porous silicon formed in deutrofluoric acid based solutions. *physica status solidi (a), 202*(8), 1581-1585.

Bi, Y., Pradhan, S., Gupta, S., Akgul, M. Z., Stavrinadis, A., & Konstantatos, G. (2018). Infrared Solution‐Processed Quantum Dot Solar Cells Reaching External Quantum Efficiency of 80% at 1.35 µm and Jsc in Excess of 34 mA cm− 2. *Advanced Materials*.

Bicer, Y., Sprotte, A. F. V., & Dincer, I. (2017). Concentrated solar light splitting using cold mirrors for photovoltaics and photonic hydrogen production applications. *Applied Energy, 197*, 169-182.

Blanker, A. J., Berendsen, P., Phung, N., Vroon, Z. E. A. P., Zeman, M., & Smets, A. H. M. (2018). Advanced light management techniques for two-terminal hybrid tandem solar cells. *Solar energy materials and solar cells, 181*, 77-82.

Born, M., & Wolf, E. (2013). *Principles of optics: electromagnetic theory of propagation, interference and diffraction of light*: Elsevier.

Bradshaw, L. R., Knowles, K. E., McDowall, S., & Gamelin, D. R. (2015). Nanocrystals for luminescent solar concentrators. *Nano letters, 15*(2), 1315-1323.

Bryant, D., Aristidou, N., Pont, S., Sanchez-Molina, I., Chotchunangatchaval, T., Wheeler, S., . . . Haque, S. A. (2016). Light and oxygen induced degradation limits the operational stability of methylammonium lead triiodide perovskite solar cells. *Energy & Environmental Science, 9*(5), 1655-1660.

University of Malaya

Burgos, M., & Langlet, M. (1999). The sol-gel transformation of TIPT coatings: a FTIR study. *Thin Solid Films, 349*(1-2), 19-23.

Bush, K. A., Bailie, C. D., Chen, Y., Bowring, A. R., Wang, W., Ma, W., . . . McGehee, M. D. (2016). Thermal and Environmental Stability of Semi‐Transparent Perovskite Solar Cells for Tandems Enabled by a Solution‐Processed Nanoparticle Buffer Layer and Sputtered ITO Electrode. *Advanced Materials, 28*(20), 3937-3943.

Caron, J. R., & Littmann, B. (2012). *Direct monitoring of energy lost due to soiling on first solar modules in California.* Paper presented at the Photovoltaic Specialists Conference (PVSC), Volume 2, 2012 IEEE 38th.

Cassie, A. (1948). Contact angles. *Discussions of the Faraday society, 3*, 11-16.

Chandran, S., Begam, N., Padmanabhan, V., & Basu, J. (2014). Confinement enhances dispersion in nanoparticle–polymer blend films. *Nature communications, 5*, 3697.

Chang, M., Song, Y., Zhang, H., Sheng, Y., Zheng, K., Zhou, X., & Zou, H. (2015). Hydrothermal assisted sol–gel synthesis and multisite luminescent properties of anatase TiO 2: Eu 3+ nanorods. *RSC Advances, 5*(73), 59314-59319.

Cheacharoen, R., Rolston, N., Harwood, D., Bush, K. A., Dauskardt, R. H., & McGehee, M. D. (2018). Design and understanding of encapsulated perovskite solar cells to withstand temperature cycling. *Energy & Environmental Science*.

Chemisana, D., Fernandez, E. F., Riverola, A., & Moreno, A. (2018). Fluid-based spectrally selective filters for direct immersed PVT solar systems in building applications. *Renewable Energy*.

Chou, C.-Y., Lee, C.-P., Vittal, R., & Ho, K.-C. (2011). Efficient quantum dot-sensitized solar cell with polystyrene-modified TiO2 photoanode and with guanidine thiocyanate in its polysulfide electrolyte. *Journal of Power Sources, 196*(15), 6595-6602.

Chowdhury, S. R., & Saha, H. (2010). Maximum power point tracking of partially shaded solar photovoltaic arrays. *Solar energy materials and solar cells, 94*(9), 1441-1447.

Cimmino, M., Miranda, R., Sicignano, E., Ferreira, A., Skelton, R., & Fraternali, F. (2017). Composite solar façades and wind generators with tensegrity architecture. *Composites Part B: Engineering, 115*, 275-281.

Currie, M. J., Mapel, J. K., Heidel, T. D., Goffri, S., & Baldo, M. A. (2008). High-efficiency organic solar concentrators for photovoltaics. *science, 321*(5886), 226-228.

DeJarnette, D., Tunkara, E., Brekke, N., Otanicar, T., Roberts, K., Gao, B., & Saunders, A. E. (2016). Nanoparticle enhanced spectral filtration of insolation from trough concentrators. *Solar energy materials and solar cells, 149*, 145-153.

University of Malaya

Dennler, G., Lungenschmied, C., Neugebauer, H., Sariciftci, N., Latreche, M., Czeremuszkin, G., & Wertheimer, M. (2006). A new encapsulation solution for flexible organic solar cells. *Thin Solid Films, 511*, 349-353.

Depan, D., Shah, J., & Misra, R. (2011). Controlled release of drug from folate-decorated and graphene mediated drug delivery system: synthesis, loading efficiency, and drug release response. *Materials Science and Engineering: C, 31*(7), 1305-1312.

Dinesh, V., Biji, P., Ashok, A., Dhara, S., Kamruddin, M., Tyagi, A., & Raj, B. (2014). Plasmon-mediated, highly enhanced photocatalytic degradation of industrial textile dyes using hybrid ZnO@ Ag core–shell nanorods. *RSC Advances, 4*(103), 58930-58940.

Dong, Q., Liu, F., Wong, M. K., Tam, H. W., Djurišić, A. B., Ng, A., . . . Ng, A. M. C. (2016). Encapsulation of Perovskite Solar Cells for High Humidity Conditions. *ChemSusChem, 9*(18), 2597-2603.

Dong, S., Jiao, H., Zhang, J., Zhao, Y., Li, J., Wang, Z., & Cheng, X. (2018). *Optimal design and fabrication of multilayer antireflection coating for III-V quadruple-junction solar cells.* Paper presented at the Advances in Optical Thin Films VI.

Drelich, J., Chibowski, E., Meng, D. D., & Terpilowski, K. (2011). Hydrophilic and superhydrophilic surfaces and materials. *Soft Matter, 7*(21), 9804-9828.

Duan, Z., Li, M., Mwenya, T., Li, Y., & Song, D. (2017). Morphology Optimization of Silver Nanoparticles Used to Improve the Light Absorption in Thin-Film Silicon Solar Cells. *Plasmonics*, 1-7.

Ebnesajjad, S. (2011). Surface and material characterization techniques *Handbook of Adhesives and Surface Preparation* (pp. 31-48): Elsevier.

Elshorbagy, M., Abdel-Hady, K., Kamal, H., & Alda, J. (2017). Broadband anti-reflection coating using dielectric Si 3 N 4 nanostructures. Application to amorphous-Si-H solar cells. *Optics Communications, 390*, 130-136.

Fang, Z., Yan, Z., Tan, Y., Liu, X., & Wang, Y. (2005). Influence of post-annealing treatment on the structure properties of ZnO films. *Applied Surface Science, 241*(3-4), 303-308.

Fonash, S. (2012). *Solar cell device physics*: Elsevier.

Forrest, E., Williamson, E., Buongiorno, J., Hu, L.-W., Rubner, M., & Cohen, R. (2010). Augmentation of nucleate boiling heat transfer and critical heat flux using nanoparticle thin-film coatings. *International Journal of Heat and Mass Transfer, 53*(1-3), 58-67.

Gao, L., & McCarthy, T. J. (2006). A perfectly hydrophobic surface (θA/θR= 180/180). *Journal of the American Chemical Society, 128*(28), 9052-9053.

García, M., Marroyo, L., Lorenzo, E., & Pérez, M. (2011). Soiling and other optical losses in solar‐tracking PV plants in navarra. *Progress in Photovoltaics: Research and Applications, 19*(2), 211-217.

University of Malaya

Ghasemi-Kahrizsangi, A., Neshati, J., Shariatpanahi, H., & Akbarinezhad, E. (2015). Improving the UV degradation resistance of epoxy coatings using modified carbon black nanoparticles. *Progress in Organic Coatings, 85*, 199-207.

Ghosh, H., Mitra, S., Saha, H., Datta, S. K., & Banerjee, C. (2017). Argon plasma treatment of silicon nitride (SiN) for improved antireflection coating on c-Si solar cells. *Materials Science and Engineering: B, 215*, 29-36.

Ghosh, S. K. (2006). *Functional coatings: by polymer microencapsulation*: John Wiley & Sons.

Goldberg, M. W. (2008). Immunolabeling for scanning electron microscopy (SEM) and field emission SEM. *Methods in cell biology, 88*, 109-130.

Goldstein, J. I., Newbury, D. E., Michael, J. R., Ritchie, N. W., Scott, J. H. J., & Joy, D. C. (2017). *Scanning electron microscopy and X-ray microanalysis*: Springer.

Good, P., Cooper, T., Querci, M., Wiik, N., Ambrosetti, G., & Steinfeld, A. (2016). Spectral reflectance, transmittance, and angular scattering of materials for solar concentrators. *Solar energy materials and solar cells, 144*, 509-522.

Goossens, D., & Van Kerschaever, E. (1999). Aeolian dust deposition on photovoltaic solar cells: the effects of wind velocity and airborne dust concentration on cell performance. *Solar energy, 66*(4), 277-289.

Green, M. A. (1982). Solar cells: operating principles, technology, and system applications.

Green, M. A. (1984). Limits on the open-circuit voltage and efficiency of silicon solar cells imposed by intrinsic Auger processes. *IEEE Transactions on electron devices, 31*(5), 671-678.

Green, M. A., Emery, K., Hishikawa, Y., Warta, W., & Dunlop, E. D. (2015a). Solar cell efficiency tables (Version 45). *Progress in photovoltaics: research and applications, 23*(1), 1-9.

Green, M. A., Emery, K., Hishikawa, Y., Warta, W., & Dunlop, E. D. (2015b). Solar cell efficiency tables (version 46). *Progress in Photovoltaics: Research and Applications, 23*(7), 805-812.

Green, M. A., Hishikawa, Y., Warta, W., Dunlop, E. D., Levi, D. H., Hohl‐Ebinger, J., & Ho‐Baillie, A. W. (2017). Solar cell efficiency tables (version 50). *Progress in Photovoltaics: Research and Applications, 25*(7), 668-676.

Griffini, G., & Turri, S. (2016). Polymeric materials for long‐term durability of photovoltaic systems. *Journal of Applied Polymer Science, 133*(11).

Gu, F., Wang, S. F., Lü, M. K., Zhou, G. J., Xu, D., & Yuan, D. R. (2004). Photoluminescence properties of SnO2 nanoparticles synthesized by sol− gel method. *The Journal of Physical Chemistry B, 108*(24), 8119-8123.

University of Malaya

Gu, H., Zhao, C., Zhang, Y., & Shao, G. (2018). Stable high-performance perovskite solar cells based on inorganic electron transporting bi-layers. *Nanotechnology, 29*(38), 385401.

Gubbala, S., Chakrapani, V., Kumar, V., & Sunkara, M. K. (2008). Band‐edge engineered hybrid structures for dye‐sensitized solar cells based on SnO2 nanowires. *Advanced Functional Materials, 18*(16), 2411-2418.

Gueymard, C. A. (2009). Spectral effects on the transmittance, solar heat gain, and performance rating of glazing systems. *Solar energy, 83*(6), 940-953.

Gunawan, O., & Lei, B. (2017). Solar cell characterization system with an automated continuous neutral density filter: Google Patents.

Gupta, A., Ingham, J. D., & Yavrouian, A. H. (1983). Solar cell encapsulation: Google Patents.

H Aberlin, H., & Eppel, H. (2012). *Photovoltaics*: Wiley.

Hafeez, H., Choi, D. K., Lee, C. M., Jesuraj, P. J., Kim, D. H., Song, A., . . . Kim, C.-S. (2019). Replacement of n-type layers with a non-toxic APTES interfacial layer to improve the performance of amorphous Si thin-film solar cells. *RSC Advances, 9*(13), 7536-7542.

Han, Y., Meyer, S., Dkhissi, Y., Weber, K., Pringle, J. M., Bach, U., . . . Cheng, Y.-B. (2015). Degradation observations of encapsulated planar CH 3 NH 3 PbI 3 perovskite solar cells at high temperatures and humidity. *Journal of Materials Chemistry A, 3*(15), 8139-8147.

Harris, J. A., & Lenz, T. G. (1985). Thermal performance of solar concentrator/cavity receiver systems. *Solar energy, 34*(2), 135-142.

He, Z., Zhong, C., Su, S., Xu, M., Wu, H., & Cao, Y. (2012). Enhanced power-conversion efficiency in polymer solar cells using an inverted device structure. *Nature Photonics, 6*(9), 591.

Hecht, E. (2002). Optics, 4th. *International edition, Addison-Wesley, San Francisco, 3*.

Hirose, M., Zhou, J., & Nagai, K. (2000). The structure and properties of acrylic-polyurethane hybrid emulsions. *Progress in Organic Coatings, 38*(1), 27-34.

Hong, W., Xu, Y., Lu, G., Li, C., & Shi, G. (2008). Transparent graphene/PEDOT–PSS composite films as counter electrodes of dye-sensitized solar cells. *Electrochemistry Communications, 10*(10), 1555-1558.

Hou, C., Jia, X., Wang, J., Tan, Y., Zhang, Y., & Li, C. (2017). Efficient Preparation and Performance Characterization of the HMX/F2602 Microspheres by One-Step Granulation Process. *Journal of Nanomaterials, 2017*, 7.

Huang, H., Ng, M., Wu, Y., & Kong, L. (2015). Solvothermal synthesis of Sb: SnO2 nanoparticles and IR shielding coating for smart window. *Materials & Design, 88*, 384-389.

University of Malaya

Huang, J.-J., & Lee, Y.-T. (2013). Self-cleaning and antireflection properties of titanium oxide film by liquid phase deposition. *Surface and Coatings Technology, 231*, 257-260.

Huang, J., Li, G., & Yang, Y. (2008). A semi‐transparent plastic solar cell fabricated by a lamination process. *Advanced Materials, 20*(3), 415-419.

Huang, X., Lin, Y., & Fang, G. (2018). Thermal properties of polyvinyl butyral/graphene composites as encapsulation materials for solar cells. *Solar energy, 161*, 187-193.

Huang, Z., Cai, C., Kuai, L., Li, T., Huttula, M., & Cao, W. (2018). Leaf-structure patterning for antireflective and self-cleaning surfaces on Si-based solar cells. *Solar energy, 159*, 733-741.

Huhtamäki, T., Tian, X., Korhonen, J. T., & Ras, R. H. (2018). Surface-wetting characterization using contact-angle measurements. *Nature protocols, 13*(7), 1521.

Ichihara, E., Kato, S., Akaishi, R., Gotoh, K., Kurokawa, Y., Kishi, N., & Soga, T. (2018). *Improving Intrinsic Silicon Nanoparticle Film by Press Treatment for use in p–i–n Solar Cells.* Paper presented at the 2018 IEEE 7th World Conference on Photovoltaic Energy Conversion (WCPEC)(A Joint Conference of 45th IEEE PVSC, 28th PVSEC & 34th EU PVSEC).

Ichimura, K., Hayashi, K., & Morii, H. (2007). Transparent coloring composition and color filter: Google Patents.

Inoue, M., & Hirasawa, I. (2013). The relationship between crystal morphology and XRD peak intensity on CaSO4· 2H2O. *Journal of Crystal Growth, 380*, 169-175.

Iqbal, M. (2012). *An introduction to solar radiation*: Elsevier.

Ismail, B. I. (2011). Power Generation Using Nonconventional Renewable Geothermal & Alternative Clean Energy Technologies *Planet Earth 2011-Global Warming Challenges and Opportunities for Policy and Practice*: InTech.

Ito, S., Kitamura, T., Wada, Y., & Yanagida, S. (2003). Facile fabrication of mesoporous TiO2 electrodes for dye solar cells: chemical modification and repetitive coating. *Solar energy materials and solar cells, 76*(1), 3-13.

Jang, B. N., & Wilkie, C. A. (2004). A TGA/FTIR and mass spectral study on the thermal degradation of bisphenol A polycarbonate. *Polymer Degradation and Stability, 86*(3), 419-430.

Jenkins, M., & Mills, N. (2005). *Plastics: Microstructure and Engineering Applications*: Elsevier.

Jentsch, A., Eichhorn, K.-J., & Voit, B. (2015). Influence of typical stabilizers on the aging behavior of EVA foils for photovoltaic applications during artificial UV-weathering. *Polymer Testing, 44*, 242-247.

University of Malaya

Ji, H., Lee, S., Park, J., Kim, T., Choi, S., & Oh, M. (2018). Improvement in Crystallinity and Porosity of Poorly Crystalline Metal–Organic Frameworks (MOFs) through Their Induced Growth on a Well-Crystalline MOF Template. *Inorganic chemistry, 57*(15), 9048-9054.

Jiang, Y.-C., Liu, S.-B., Zhang, H.-F., & Kong, X.-K. (2015). Realization of all optical half-adder based on self-collimated beams by two-dimensional photonic crystals. *Optics Communications, 348*, 90-94.

Jiang, Y., Luo, B., Jiang, F., Jiang, F., Fuentes-Hernandez, C., Liu, T., . . . Wang, T. (2016). Efficient colorful perovskite solar cells using a top polymer electrode simultaneously as spectrally selective antireflection coating. *Nano letters, 16*(12), 7829-7835.

Jiao, J., Seraphin, S., Wang, X., & Withers, J. C. (1996). Preparation and properties of ferromagnetic carbon‐coated Fe, Co, and Ni nanoparticles. *Journal of Applied Physics, 80*(1), 103-108.

Jiji, L. M., & Jiji, L. M. (2006). *Heat convection*: Springer.

Joshi, S. S., & Dhoble, A. S. (2017). Experimental investigation of solar photovoltaic thermal system using water, coconut oil and silicone oil as spectrum filters. *Journal of the Brazilian Society of Mechanical Sciences and Engineering, 39*(8), 3227-3236.

Ju, X., Xu, C., Han, X., Du, X., Wei, G., & Yang, Y. (2017). A review of the concentrated photovoltaic/thermal (CPVT) hybrid solar systems based on the spectral beam splitting technology. *Applied Energy, 187*, 534-563.

K. Colladet, M. N., L. Goris, L. Lutsen, D. Vanderzande,. (2004). *Thin Solid Films, 451*, 7.

Kahraman Döğüşcü, D., Kızıl, Ç., Biçer, A., Sarı, A., & Alkan, C. (2018). Microencapsulated n-alkane eutectics in polystyrene for solar thermal applications. *Solar energy, 160*, 32-42.

Kandilli, C., & Külahlı, G. (2017). Performance analysis of a concentrated solar energy for lighting-power generation combined system based on spectral beam splitting. *Renewable Energy, 101*, 713-727.

Kanemitsu, Y., & Okamoto, S. (1997). Resonantly excited photoluminescence from porous silicon: Effects of surface oxidation on resonant luminescence spectra. *Physical review B, 56*(4), R1696.

Karki, I. B. (2016). Effect of Temperature on the IV Characteristics of a Polycrystalline Solar Cell. *Journal of Nepal Physical Society, 3*(1), 35-40.

Karthik, D., Pendse, S., Sakthivel, S., Ramasamy, E., & Joshi, S. V. (2017). High performance broad band antireflective coatings using a facile synthesis of ink-bottle mesoporous MgF 2 nanoparticles for solar applications. *Solar energy materials and solar cells, 159*, 204-211.

University of Malaya

Kazem, H. A., & Chaichan, M. T. (2016). The impact of using solar colored filters to cover the PV panel on its outcomes. *Bulletin Journal, 2*(7), 464-469.

Kim, H., & Shim, S. (2007). Temperature-controlled fabrication of SnO 2 nanoparticles via thermal heating of Sn powders. *Applied Physics A, 88*(4), 769-773.

Kim, S. S., & Lee, B.-T. (2004). Effects of oxygen pressure on the growth of pulsed laser deposited ZnO films on Si (0 0 1). *Thin Solid Films, 446*(2), 307-312.

King, F. T. (1971). Methods of making filters and products made therefrom: Google Patents.

Kumar, S., E, N., Palanisamy Alamelu, P., Das, S., Vimalan, M., & Potheher, I. (2017). *Synthesis, Anti-bacterial, Anti-arthritic, Anti-oxidant and In-vitro Cytotoxicity Activities of ZnO Nanoparticles Using Leaf Extract of Tectona Grandis(L.)* (Vol. 41).

le Reinders, A., Verlinden, P., & Freundlich, A. (2017). *Photovoltaic Solar Energy: From Fundamentals to Applications*: John Wiley & Sons.

Lee, Y.-J., Ruby, D. S., Peters, D. W., McKenzie, B. B., & Hsu, J. W. (2008). ZnO nanostructures as efficient antireflection layers in solar cells. *Nano letters, 8*(5), 1501-1505.

Leem, J. W., Yu, J. S., Heo, J., Park, W.-K., Park, J.-H., Cho, W. J., & Kim, D. E. (2014). Nanostructured encapsulation coverglasses with wide-angle broadband antireflection and self-cleaning properties for III–V multi-junction solar cell applications. *Solar Energy Materials and Solar Cells, 120*, 555-560.

Li, Y., Liu, F., & Sun, J. (2009). A facile layer-by-layer deposition process for the fabrication of highly transparent superhydrophobic coatings. *Chemical communications*(19), 2730-2732.

Liang, Y., Xu, Z., Xia, J., Tsai, S. T., Wu, Y., Li, G., . . . Yu, L. (2010). For the bright future—bulk heterojunction polymer solar cells with power conversion efficiency of 7.4%. *Advanced Materials, 22*(20).

Lien, S.-Y., Wuu, D.-S., Yeh, W.-C., & Liu, J.-C. (2006). Tri-layer antireflection coatings (SiO 2/SiO 2–TiO 2/TiO 2) for silicon solar cells using a sol–gel technique. *Solar energy materials and solar cells, 90*(16), 2710-2719.

Lisbona, E. F. (2012). Chapter IID-3 - Calibration, Testing, and Monitoring of Space Solar Cells. In A. McEvoy, T. Markvart & L. Castañer (Eds.), *Practical Handbook of Photovoltaics (Second Edition)* (pp. 881-913). Boston: Academic Press.

Liu, T., Zhou, Y., Li, Z., Zhang, L., Ju, M. G., Luo, D., . . . Yang, W. (2018). Stable Formamidinium ‐ Based Perovskite Solar Cells via In Situ Grain Encapsulation. *Advanced Energy Materials*, 1800232.

Llobera, A., Cadarso, V., Carregal-Romero, E., Brugger, J., Domínguez, C., & Fernández-Sánchez, C. (2011). Fluorophore-doped xerogel antiresonant reflecting optical waveguides. *Optics express, 19*(6), 5026-5039.

University of Malaya

Lue, S. J., Lo, P. W., Hung, L.-Y., & Tung, Y. L. (2010). Application of micro-porous polycarbonate membranes in dye-sensitized solar cells: Cell performance and long-term stability. *Journal of Power Sources, 195*(22), 7677-7683.

Luque, A., & Hegedus, S. (2003). Handbook of photovoltaic science and technology: Wiley, Chichester.

Ma, M., Zhang, Y., Yu, W., Shen, H.-y., Zhang, H.-q., & Gu, N. (2003). Preparation and characterization of magnetite nanoparticles coated by amino silane. *Colloids and Surfaces A: physicochemical and engineering aspects, 212*(2-3), 219-226.

Macleod, H. A. (2017). *Thin-film optical filters*: CRC press.

Mailoa, J. P., Lee, M., Peters, I. M., Buonassisi, T., Panchula, A., & Weiss, D. N. (2016). Energy-yield prediction for II–VI-based thin-film tandem solar cells. *Energy & Environmental Science, 9*(8), 2644-2653.

Mansur, H. S., Oréfice, R. L., & Mansur, A. A. (2004). Characterization of poly (vinyl alcohol)/poly (ethylene glycol) hydrogels and PVA-derived hybrids by small-angle X-ray scattering and FTIR spectroscopy. *Polymer, 45*(21), 7193-7202.

Mansur, H. S., Oréfice, R. L., & Mansur, A. A. P. (2004). Characterization of poly(vinyl alcohol)/poly(ethylene glycol) hydrogels and PVA-derived hybrids by small-angle X-ray scattering and FTIR spectroscopy. *Polymer, 45*(21), 7193-7202.

Marmur, A. (2004). The lotus effect: superhydrophobicity and metastability. *Langmuir, 20*(9), 3517-3519.

Martí, A., & Luque, A. (2015). Three-terminal heterojunction bipolar transistor solar cell for high-efficiency photovoltaic conversion. *Nature communications, 6*.

Masson, D., Paquin, L., Poulin-Dandurand, S., Sacher, E., & Yelon, A. (1984). Time-dependent changes in the Si・Hn vibrational spectrum of amorphous silicon, a-Si: H. *Journal of Non-Crystalline Solids, 66*(1-2), 93-98.

Maurin, J. K., Pluciński, F., Mazurek, A. P., & Fijałek, Z. (2007). The usefulness of simple X-ray powder diffraction analysis for counterfeit control—The Viagra® example. *Journal of pharmaceutical and biomedical analysis, 43*(4), 1514-1518.

Mbakop, F. K., Djongyang, N., Ejuh, G. W., Raïdandi, D., & Woafo, P. (2017). Transmission of light through an optical filter of a one-dimensional photonic crystal: application to the solar thermophotovoltaic system. *Physica B: Condensed Matter, 516*, 92-99.

McLeod, S. M., Hages, C. J., Carter, N. J., & Agrawal, R. (2015). Synthesis and characterization of 15% efficient CIGSSe solar cells from nanoparticle inks. *Progress in Photovoltaics: Research and Applications, 23*(11), 1550-1556.

McMeekin, D. P., Sadoughi, G., Rehman, W., Eperon, G. E., Saliba, M., Hörantner, M. T., . . . Rech, B. (2016). A mixed-cation lead mixed-halide perovskite absorber for tandem solar cells. *Science, 351*(6269), 151-155.

University of Malaya

Measurement, A. C. E. o. T. (1993). *Manual on the use of thermocouples in temperature measurement* (Vol. 12): ASTM International.

Meera, K., Yang, C. S., & Choi, C. K. (2006). Bonding structure and electrical properties of SiOC (-H) films deposited with a methyltrimethoxysilane precursor by using inductively coupled plasma chemical vapor deposition. *Journal of the Korean Physical Society, 48*(6), 1713-1718.

Mei, S.-G., Ma, W.-J., Zhang, G.-L., Wang, J.-L., Yang, J.-H., & Li, Y.-Q. (2012). Transparent ATO/epoxy nanocomposite coating with excellent thermal insulation property. *Micro & Nano Letters, 7*(1), 12-14.

Meiron, T. S., Marmur, A., & Saguy, I. S. (2004). Contact angle measurement on rough surfaces. *Journal of Colloid and Interface Science, 274*(2), 637-644.

Mekhilef, S., Saidur, R., & Kamalisarvestani, M. (2012). Effect of dust, humidity and air velocity on efficiency of photovoltaic cells. *Renewable and Sustainable Energy Reviews, 16*(5), 2920-2925.

Mekla, V., Juisuwannathat, C., & Tipparach, U. (2015). *The Growth of TiO2 Nanostructures Prepared by Anodization in Combination with Hydrothermal Method on the Ti Foil.* Paper presented at the MATEC Web of Conferences.

Metz, A., Demenik, G., Richter, A., Vlasenko, T., Buchovskaya, I., Zwegers, M., . . . Stassen, A. (2015). International technology roadmap for photovoltaic. *ITRPV, Frankfurt, Rep, 1*.

Metzman, J. S., Wang, G., Morris, J. R., & Heflin, J. R. (2018). Enhanced scratch resistance of self-assembled silica nanoparticle anti-reflection coatings. *Journal of Materials Chemistry C*.

Mhaisagar, Y. S., Joshi, B. N., & Mahajan, A. (2012). Surface texture modification of spin-coated SiO 2 xerogel thin films by TMCS silylation. *Bulletin of Materials Science, 35*(2), 151-155.

Mhd Haniffa, M. A. C., Ching, Y. C., Chuah, C. H., Ching, K. Y., & Liou, N.-S. (2019). Synergistic effect of (3-Aminopropyl)Trimethoxysilane treated ZnO and corundum nanoparticles under UV-irradiation on UV-cutoff and IR-absorption spectra of acrylic polyurethane based nanocomposite coating. *Polymer Degradation and Stability, 159*, 205-216.

Michael, J. J., Iqbal, S. M., Iniyan, S., & Goic, R. (2018). Enhanced electrical performance in a solar photovoltaic module using V-trough concentrators. *Energy*.

Mihály, J., Sterkel, S., Ortner, H. M., Kocsis, L., Hajba, L., Furdyga, É., & Mink, J. (2006). FTIR and FT-Raman spectroscopic study on polymer based high pressure digestion vessels. *Croatica chemica acta, 79*(3), 497-501.

Minnaert, B., & Veelaert, P. (2014). A proposal for typical artificial light sources for the characterization of indoor photovoltaic applications. *Energies, 7*(3), 1500-1516.

University of Malaya

Mohamadkhani, F., Javadpour, S., & Taghavinia, N. (2019). Improvement of planar perovskite solar cells by using solution processed SnO2/CdS as electron transport layer. *Solar energy, 191*, 647-653.

Mojiri, A., Taylor, R., Thomsen, E., & Rosengarten, G. (2013). Spectral beam splitting for efficient conversion of solar energy—A review. *Renewable and Sustainable Energy Reviews, 28*, 654-663.

Múgica-Vidal, R., Alba-Elías, F., Sainz-García, E., & Pantoja-Ruiz, M. (2015). Hydrophobicity attainment and wear resistance enhancement on glass substrates by atmospheric plasma-polymerization of mixtures of an aminosilane and a fluorocarbon. *Applied Surface Science, 347*, 325-335.

Nadargi, D. Y., Latthe, S. S., & Rao, A. V. (2009). Effect of post-treatment (gel aging) on the properties of methyltrimethoxysilane based silica aerogels prepared by two-step sol–gel process. *Journal of Sol-Gel Science and Technology, 49*(1), 53-59.

Nakae, H., Inui, R., Hirata, Y., & Saito, H. (1998). Effects of surface roughness on wettability. *Acta Materialia, 46*(7), 2313-2318.

Nallusamy, S., & Manoj Babu, A. (2016). *X-Ray Differaction and FESEM Analysis for Mixture of Hybrid Nanoparticles in Heat Transfer Applications.* Paper presented at the Journal of Nano Research.

Nann, S., & Emery, K. (1992). Spectral effects on PV-device rating. *Solar energy materials and solar cells, 27*(3), 189-216.

Nelson, R. E. (2003). A brief history of thermophotovoltaic development. *Semiconductor Science and Technology, 18*(5), S141.

Neugebauer, H., Brabec, C., Hummelen, J. C., & Sariciftci, N. S. (2000). Stability and photodegradation mechanisms of conjugated polymer/fullerene plastic solar cells. *Solar energy materials and solar cells, 61*(1), 35-42.

Neville, R. C. (1995). *Solar energy conversion: the solar cell*: Elsevier.

Ni, J., Li, J., An, W., & Zhu, T. (2018). Performance analysis of nanofluid-based spectral splitting PV/T system in combined heating and power application. *Applied Thermal Engineering, 129*, 1160-1170.

Nikafshar, S., Zabihi, O., Ahmadi, M., Mirmohseni, A., Taseidifar, M., & Naebe, M. (2017). The Effects of UV Light on the Chemical and Mechanical Properties of a Transparent Epoxy-Diamine System in the Presence of an Organic UV Absorber. *Materials, 10*(2), 180.

Ogihara, H., Xie, J., Okagaki, J., & Saji, T. (2012). Simple method for preparing superhydrophobic paper: spray-deposited hydrophobic silica nanoparticle coatings exhibit high water-repellency and transparency. *Langmuir, 28*(10), 4605-4608.

University of Malaya

Oliveira, F. A. C., Fernandes, J. C., Galindo, J., Rodríguez, J., Canãdas, I., & Rosa, L. G. (2019). Thermal resistance of solar volumetric absorbers made of mullite, brown alumina and ceria foams under concentrated solar radiation. *Solar energy materials and solar cells, 194*, 121-129.

Osterhold, M., & Armbruster, K. (1998). Correlation between surface tension and physical paint properties. *Progress in Organic Coatings, 33*(3-4), 197-201.

Otanicar, T., DeJarnette, D., Brekke, N., Tunkara, E., Roberts, K., & Harikumar, P. (2016). Full Spectrum Collection of Concentrated Solar Energy Using PV Coupled with Selective Filtration Utilizing Nanoparticles. *MRS Advances, 1*(43), 2935-2940.

Paci, B., Generosi, A., Albertini, V. R., Spyropoulos, G. D., Stratakis, E., & Kymakis, E. (2012). Enhancement of photo/thermal stability of organic bulk heterojunction photovoltaic devices via gold nanoparticles doping of the active layer. *Nanoscale, 4*(23), 7452-7459.

Palmer, J. M. (1995). The measurement of transmission, absorption, emission, and reflection. *Handbook of optics, 2*, 251-255.

Pan, Y., He, S., Gong, L., Cheng, X., Li, C., Li, Z., . . . Zhang, H. (2017). Low thermal-conductivity and high thermal stable silica aerogel based on MTMS/Water-glass co-precursor prepared by freeze drying. *Materials & Design, 113*, 246-253.

Pandey, A., Tyagi, V., Jeyraj, A., Selvaraj, L., Rahim, N., & Tyagi, S. (2016). Recent advances in solar photovoltaic systems for emerging trends and advanced applications. *Renewable and Sustainable Energy Reviews, 53*, 859-884.

Park, N.-G., Grätzel, M., Miyasaka, T., Zhu, K., & Emery, K. (2016). Towards stable and commercially available perovskite solar cells. *Nature Energy, 1*, 16152.

Patel, H., & Agarwal, V. (2008). MATLAB-based modeling to study the effects of partial shading on PV array characteristics. *IEEE transactions on energy conversion, 23*(1), 302-310.

Patil, G. E., Kajale, D. D., Gaikwad, V. B., & Jain, G. H. (2012). Preparation and characterization of SnO2 nanoparticles by hydrothermal route. *International Nano Letters, 2*(1), 17.

Pavan, A. M., Mellit, A., & De Pieri, D. (2011). The effect of soiling on energy production for large-scale photovoltaic plants. *Solar energy, 85*(5), 1128-1136.

Pazos-Outón, L. M., Lee, J. M., Futscher, M. H., Kirch, A., Tabachnyk, M., Friend, R. H., & Ehrler, B. (2017). A Silicon–Singlet Fission Tandem Solar Cell Exceeding 100% External Quantum Efficiency with High Spectral Stability. *ACS Energy Letters, 2*(2), 476-480.

Peak, D. (2005). FOURIER TRANSFORM INFRARED SPECTROSCOPY. In D. Hillel (Ed.), *Encyclopedia of Soils in the Environment* (pp. 80-85). Oxford: Elsevier.

University of Malaya

Peet, J., Kim, J. Y., Coates, N. E., Ma, W. L., Moses, D., Heeger, A. J., & Bazan, G. C. (2007). Efficiency enhancement in low-bandgap polymer solar cells by processing with alkane dithiols. *Nature materials, 6*(7), 497.

Pereyra, I., Carreno, M., Tabacniks, M. H., Prado, R., & Fantini, M. C. d. A. (1998). The influence of “starving plasma” regime on carbon content and bonds in a-Si 1− x C x: H thin films. *Journal of Applied Physics, 84*(5), 2371-2379.

Perzon, E., Wang, X., Zhang, F., Mammo, W., Delgado, J. L., de la Cruz, P., . . . Andersson, M. R. (2005). Design, synthesis and properties of low band gap polyfluorenes for photovoltaic devices. *Synthetic metals, 154*(1-3), 53-56.

Phillips, T., Horr, T., Huson, M., Turner, P., & Shanks, R. (1995). Imaging wool fiber surfaces with a scanning force microscope. *Textile research journal, 65*(8), 445-453.

Pilotek, S., & Schmidt, H. K. (2003). Wettability of Microstructured Hydrophobic Sol-Gel Coatings. *Journal of Sol-Gel Science and Technology, 26*(1), 789-792.

Pospíšil, J., Pilař, J., Billingham, N. C., Marek, A., Horák, Z., & Nešpůrek, S. (2006). Factors affecting accelerated testing of polymer photostability. *Polymer Degradation and Stability, 91*(3), 417-422.

Prevo, B. G., Hon, E. W., & Velev, O. D. (2007). Assembly and characterization of colloid-based antireflective coatings on multicrystalline silicon solar cells. *Journal of Materials Chemistry, 17*(8), 791-799.

Pryde, C. (1985). Photoaging of polycarbonate: effects of selected variables on degradation pathways: ACS Publications.

Rabady, R. I. (2017). Optimized spectral splitting in thermo-photovoltaic system for maximum conversion efficiency. *Energy, 119*, 852-859.

Rabek, J. F. (2012). *Polymer photodegradation: mechanisms and experimental methods*: Springer Science & Business Media.

Rao, A. P., Rao, A. V., & Pajonk, G. (2007). Hydrophobic and physical properties of the ambient pressure dried silica aerogels with sodium silicate precursor using various surface modification agents. *Applied Surface Science, 253*(14), 6032-6040.

Ray, S., Okpalugo, T., Pao, C., Tsai, H., Chiou, J., Jan, J., . . . Wang, W. (2005). Electronic structure and photoluminescence study of silicon doped diamond like carbon (Si: DLC) thin films. *Materials research bulletin, 40*(10), 1757-1764.

Razavi, R. S., Barekat, S., Kiomarsipour, N., Ghani, K., & Bastani, S. (2012). Evaluation of thermo-optical and adhesion properties of thermal control coatings employed in spacecraft surfaces. *Surf. Sci. Eng, 13*, 79-89.

Reynolds, S., & Smirnov, V. (2015). Modelling performance of two-and four-terminal thin-film silicon tandem solar cells under varying spectral conditions. *Energy Procedia, 84*, 251-260.

University of Malaya

Rizzo, A., Ortolan, L., Murrone, S., Torto, L., Barbato, M., Wrachien, N., . . . Di Carlo, A. (2017). *Effects of thermal stress on hybrid perovskite solar cells with different encapsulation techniques.* Paper presented at the Reliability Physics Symposium (IRPS), 2017 IEEE International.

Roose, B., Baena, J.-P. C., Gödel, K. C., Graetzel, M., Hagfeldt, A., Steiner, U., & Abate, A. (2016). Mesoporous SnO2 electron selective contact enables UV-stable perovskite solar cells. *Nano Energy, 30*, 517-522.

Roose, B., Gödel, K. C., Pathak, S., Sadhanala, A., Baena, J. P. C., Wilts, B. D., . . . Steiner, U. (2016). Enhanced Efficiency and Stability of Perovskite Solar Cells Through Nd ‐ Doping of Mesostructured TiO2. *Advanced Energy Materials, 6*(2), 1501868.

Rowell, M. W., & McGehee, M. D. (2011). Transparent electrode requirements for thin film solar cell modules. *Energy & Environmental Science, 4*(1), 131-134.

Rubin, E. B., Chen, Y., & Chen, R. (2019). Optical properties and thermal stability of Cu spinel oxide nanoparticle solar absorber coatings. *Solar energy materials and solar cells, 195*, 81-88.

Sagdinc, S., & Bayari, S. (2004). Theoretical study of ofloxacin: geometrical parameters and vibrational wavenumbers. *Journal of Molecular Structure: THEOCHEM, 668*(2-3), 93-99.

Sahli, F., Werner, J., Kamino, B. A., Bräuninger, M., Monnard, R., Paviet-Salomon, B., . . . Ballif, C. (2018). Fully textured monolithic perovskite/silicon tandem solar cells with 25.2% power conversion efficiency. *Nature materials*.

Sarswat, P. K., Jagannathan, M., & Free, M. L. (2017). Performance of photovoltaic cells in different segments of spatial-spectral distributions. *Vacuum*.

Schittich, C. (2003). *Solar architecture: strategies, visions, concepts*: Walter de Gruyter.

Scimeca, M., Bischetti, S., Lamsira, H. K., Bonfiglio, R., & Bonanno, E. (2018). Energy Dispersive X-ray (EDX) microanalysis: A powerful tool in biomedical research and diagnosis. *European journal of histochemistry: EJH, 62*(1).

Shah, A., Torres, P., Tscharner, R., Wyrsch, N., & Keppner, H. (1999). Photovoltaic technology: the case for thin-film solar cells. *Science, 285*(5428), 692-698.

Shaheen, S. E., Brabec, C. J., Sariciftci, N. S., Padinger, F., Fromherz, T., & Hummelen, J. C. (2001). 2.5% efficient organic plastic solar cells. *Applied Physics Letters, 78*(6), 841-843.

Sharma, D., & Purohit, G. (2013). *Fill Factor Based Maximum Power Point Tracking (MPPT) for Standalone Solar PV System.* Paper presented at the IVth International Conference on Advances in Energy Research Indian Institute of Technology Bombay, Mumbai, Paper.

University of Malaya

Shewale, P. M., Rao, A. V., & Rao, A. P. (2008). Effect of different trimethyl silylating agents on the hydrophobic and physical properties of silica aerogels. *Applied Surface Science, 254*(21), 6902-6907.

Shokri, B., Firouzjah, M. A., & Hosseini, S. (2009). *FTIR analysis of silicon dioxide thin film deposited by metal organic-based PECVD.* Paper presented at the Proceedings of 19th international symposium on plasma chemistry society, Bochum, Germany.

Singh, S., Wu, C., & Williams, P. T. (2012). Pyrolysis of waste materials using TGA-MS and TGA-FTIR as complementary characterisation techniques. *Journal of Analytical and Applied Pyrolysis, 94*, 99-107.

Sivaram, V., Stranks, S. D., & Snaith, H. J. (2015). Outshining silicon. *Scientific American, 313*(1), 54-59.

Skoog, D. A., Holler, F. J., & Crouch, S. R. (2017). *Principles of instrumental analysis*: Cengage learning.

Smestad, G. P. (1998). Education and solar conversion:: demonstrating electron transfer. *Solar Energy Materials and Solar Cells, 55*(1), 157-178.

Snaith, H. J., & Ducati, C. (2010). SnO2-based dye-sensitized hybrid solar cells exhibiting near unity absorbed photon-to-electron conversion efficiency. *Nano letters, 10*(4), 1259-1265.

Sopian, K., Liu, H., Kakac, S., & Veziroglu, T. (2000). Performance of a double pass photovoltaic thermal solar collector suitable for solar drying systems. *Energy Conversion and Management, 41*(4), 353-365.

Stuckelberger, M., Biron, R., Wyrsch, N., Haug, F.-J., & Ballif, C. (2017). Review: Progress in solar cells from hydrogenated amorphous silicon. *Renewable and Sustainable Energy Reviews, 76*, 1497-1523.

Sukmanowski, J., Viguié, J.-R., Nölting, B., & Royer, F. (2005). Light absorption enhancement by nanoparticles. *Journal of Applied Physics, 97*(10), 104332.

Sun, L., Thomas, R. C., Crooks, R. M., & Ricco, A. J. (1991). Real-time analysis of chemical reactions occurring at a surface-confined organic monolayer. *Journal of the American Chemical Society, 113*(22), 8550-8552.

Tada, H., Carter Jr, J., Anspaugh, B., & Downing, R. (1982). Solar cell radiation handbook.

Tan, B., & Wu, Y. (2006). Dye-sensitized solar cells based on anatase TiO2 nanoparticle/nanowire composites. *The Journal of Physical Chemistry B, 110*(32), 15932-15938.

Tatsiankou, V., Hinzer, K., Haysom, J., Schriemer, H., Emery, K., & Beal, R. (2016). Design principles and field performance of a solar spectral irradiance meter. *Solar energy, 133*, 94-102.

University of Malaya

Tavella, F., Ampelli, C., Frusteri, L., Frusteri, F., Perathoner, S., & Centi, G. (2017). Development of photoanodes for photoelectrocatalytic solar cells based on copper-based nanoparticles on titania thin films of vertically aligned nanotubes. *Catalysis Today*.

Teo, H., Lee, P., & Hawlader, M. (2012). An active cooling system for photovoltaic modules. *Applied Energy, 90*(1), 309-315.

Thirugnanasambandan, T., Pal, K., Sidhu, A., Elkodous, M. A., Prasath, H., Kulasekarapandian, K., . . . Jeevanandam, J. (2018). Aggrandize efficiency of ultra-thin silicon solar cell via topical clustering of silver nanoparticles. *Nano-Structures & Nano-Objects, 16*, 224-233.

. Three layer anti-reflection coating. (1965): Google Patents.

Topolniak, I., Chapel, A., Gaume, J., Bussiere, P.-O., Chadeyron, G., Gardette, J.-L., & Therias, S. (2017). Applications of polymer nanocomposites as encapsulants for solar cells and LEDs: Impact of photodegradation on barrier and optical properties. *Polymer Degradation and Stability, 145*(Supplement C), 52-59.

Tsai, S. Y., Ni, C. T., & Fung, K. Z. (2017). Characterization of infrared transmittance in mixed transition metal oxides for solar cells application. *Ceramics International, 43*, S460-S463.

Ulhaq, E., Zaidi, S., Zubair, M., Abdul Karim, M. R., Kunjalukkal, S., & Licciulli, A. (2017). Hydrophobic Silica Aerogel Glass-Fibre Composite with Higher Strength and Thermal Insulation based on Methyltrimethoxysilane (MTMS) Precursor. *Energy and buildings, 151*.

Uzum, A., Kuriyama, M., Kanda, H., Kimura, Y., Tanimoto, K., Fukui, H., . . . Ito, S. (2017). Sprayed and Spin-Coated Multilayer Antireflection Coating Films for Nonvacuum Processed Crystalline Silicon Solar Cells. *International Journal of Photoenergy, 2017*.

Valenzuela, G. R. (1978). Theories for the interaction of electromagnetic and oceanic waves—A review. *Boundary-Layer Meteorology, 13*(1), 61-85.

Van Heerden, J., & Swanepoel, R. (1997). XRD analysis of ZnO thin films prepared by spray pyrolysis. *Thin Solid Films, 299*(1-2), 72-77.

Verma, L. K., Sakhuja, M., Son, J., Danner, A. J., Yang, H., Zeng, H. C., & Bhatia, C. S. (2011). Self-cleaning and antireflective packaging glass for solar modules. *Renewable Energy, 36*(9), 2489-2493.

Virtuani, A., & Fanni, L. (2014). Seasonal power fluctuations of amorphous silicon thin‐film solar modules: distinguishing between different contributions. *Progress in photovoltaics: research and applications, 22*(2), 208-217.

Virtuani, A., Lotter, E., & Powalla, M. (2006). Influence of the light source on the low-irradiance performance of Cu (In, Ga) Se 2 solar cells. *Solar energy materials and solar cells, 90*(14), 2141-2149.

University of Malaya

Visoly‐Fisher, I., Dobson, K. D., Nair, J., Bezalel, E., Hodes, G., & Cahen, D. (2003). Factors affecting the stability of CdTe/CdS solar cells deduced from stress tests at elevated temperature. *Advanced functional materials, 13*(4), 289-299.

Vorontsov, A. V., & Tsybulya, S. V. (2018). Influence of nanoparticles size on XRD patterns for small monodisperse nanoparticles of Cu0 and TiO2 anatase. *Industrial & Engineering Chemistry Research, 57*(7), 2526-2536.

Wan, Y., McIntosh, K. R., & Thomson, A. F. (2013). Characterisation and optimisation of PECVD SiNx as an antireflection coating and passivation layer for silicon solar cells. *AIP Advances, 3*(3), 032113.

Wang, L., Liu, N., Guo, Z., Wu, D., Chen, W., Chang, Z., . . . Wang, J. (2016). Nitric Acid-Treated Carbon Fibers with Enhanced Hydrophilicity for Candida tropicalis Immobilization in Xylitol Fermentation. *Materials (Basel, Switzerland), 9*(3), 206.

Wei, J., Yoshinari, M., Takemoto, S., Hattori, M., Kawada, E., Liu, B., & Oda, Y. (2007). Adhesion of mouse fibroblasts on hexamethyldisiloxane surfaces with wide range of wettability. *Journal of Biomedical Materials Research Part B: Applied Biomaterials: An Official Journal of The Society for Biomaterials, The Japanese Society for Biomaterials, and The Australian Society for Biomaterials and the Korean Society for Biomaterials, 81*(1), 66-75.

Wheeler, G., Mendez-Vivar, J., & Fleming, S. (2003). The use of modified Zr-nPropoxide in the consolidation of calcite: a preliminary study focused into the conservation of cultural heritage. *Journal of Sol-Gel Science and Technology, 26*(1-3), 1233-1237.

Widyolar, B., Jiang, L., & Winston, R. (2018). Spectral beam splitting in hybrid PV/T parabolic trough systems for power generation. *Applied Energy, 209*, 236-250.

Willson, R. C., Gulkis, S., Janssen, M., Hudson, H., & Chapman, G. (1981). Observations of solar irradiance variability. *Science, 211*(4483), 700-702.

Winston, R. (1974). Principles of solar concentrators of a novel design. *Solar energy, 16*(2), 89-95.

Witteck, R., Veith‐Wolf, B., Schulte‐Huxel, H., Morlier, A., Vogt, M. R., Köntges, M., & Brendel, R. (2017). UV‐induced degradation of PERC solar modules with UV‐transparent encapsulation materials. *Progress in Photovoltaics: Research and Applications, 25*(6), 409-416.

Woolley, J. T. (1971). Reflectance and transmittance of light by leaves. *Plant physiology, 47*(5), 656-662.

Workman Jr, J., & Springsteen, A. (1998). *Applied spectroscopy: a compact reference for practitioners*: Academic Press.

Wu, K., Li, H., & Klimov, V. I. (2018). Tandem luminescent solar concentrators based on engineered quantum dots. *Nature Photonics*, 1.

University of Malaya

X. Wang, E. P., J.L. Delgado, P. De La Cruz, F. Zhang, F. Langa, M.R. Andersson, O. Inganas. (2004). *Appl. Phy. Lett, 85*, 5081.

Xue, L., Li, J., Fu, J., & Han, Y. (2009). Super-hydrophobicity of silica nanoparticles modified with vinyl groups. *Colloids and Surfaces A: physicochemical and engineering aspects, 338*(1), 15-19.

Yang, S., Zhao, D., Zhang, H., Lu, S., Chen, L., & Yu, X. (2010). Impact of environmental conditions on the sorption behavior of Pb (II) in Na-bentonite suspensions. *Journal of Hazardous Materials, 183*(1-3), 632-640.

Yeh, P., & Yeh, N. (2018). Design and analysis of solar-tracking 2D Fresnel lens-based two staged, spectrum-splitting solar concentrators. *Renewable Energy, 120*, 1-13.

Yokogawa, H., Yokoyama, M., Takahama, K., & Uegaki, Y. (1996). Process of forming a hydrophobic aerogel: Google Patents.

Yousif, E., & Haddad, R. (2013). Photodegradation and photostabilization of polymers, especially polystyrene: review. *SpringerPlus, 2*, 398.

Zhang, H., Zou, Y., Sun, Y., Sun, L., Xu, F., Zhang, J., & Zhou, H. (2015). A novel thermal-insulating film incorporating microencapsulated phase-change materials for temperature regulation and nano-TiO2 for UV-blocking. *Solar energy materials and solar cells, 137*, 210-218.

Zhang, Z., Wang, S., & Zhang, J. (2014). Large stabilizing effect of titanium dioxide on photodegradation of PVC/α‐methylstyrene‐acrylonitrile copolymer/impact modifier‐matrix composites. *Polymer Composites, 35*(12), 2365-2375.

Zhou, X., Fu, W., Yang, H., Mu, Y., Ma, J., Tian, L., . . . Li, M. (2013). Facile fabrication of transparent SnO2 nanorod array and their photoelectrochemical properties. *Materials Letters, 93*, 95-98.

Zorrilla‐Casanova, J., Piliougine, M., Carretero, J., Bernaola‐Galván, P., Carpena, P., Mora‐López, L., & Sidrach‐de‐Cardona, M. (2013). Losses produced by soiling in the incoming radiation to photovoltaic modules. *Progress in Photovoltaics: Research and Applications, 21*(4), 790-796.

Zweibel, K., & Singh, P. (1993). Harnessing solar power: the photovoltaics challenge. *American Journal of Physics, 61*(3), 286-287.

University of Malaya

LIST OF PUBLICATIONS

ISI-publications:-

1. Synthesis of nano-TiO_2 coating systems for solar cell, Pigment & Resin Technology, 2019 (Accepted: 26th July 2019).

Conferences

1. SnO_2 and TiO_2 coatings toward decreasing the surface temperature of solar cells. 5th IET Clean Energy and Technology Conference 2018 (CEAT 2018), 5-6 Sept. 2018, Pullman Hotel, Kuala Lumpur (Published: 2018).

University of Malaya